FUNDAMENTAL STUDY FOR 2-D NUMERICAL SIMULATION OF CHANNEL CHANGES IN LARGE RIVERS DOMINATED BY FINE SEDIMENT

A Dissertation

Submitted to the National Graduate Institute for Policy Studies (GRIPS)

And the International Centre for Water Hazard and Risk Management (ICHARM),

Public Works Research Institute (PWRI)

in Partial Fulfillment of the Requirements for the Degree of

Ph.D. in Disaster Management

by

Ahmad Ali GUL

September, 2019

Declaration

Except where specific reference has been made to the work of others, the work embodied in this thesis is the result of investigation carried out by the author. No part of this thesis has been submitted or is being concurrently submitted in candidature for any degree at any other institution.

Ahmad Ali Gul

Abstract

Numerous barrage structures have been constructed on the Indus River for irrigation and water distribution. These structures affect the flow and sediment continuity of the river during high flows, and have led to channel changes and embankment failures in the past. The 2-D numerical modeling of flow and sediment is a viable tool to predict channel changes in large rivers. However, it is not easy to verify such numerical models in a large river dominated by fine sediment. In the current numerical model, e.g., the one developed by Takebayashi and Egashira (2001), sediment is transported by the flow based on the transport equation. The non-equilibrium transport of fine sediment is modelled using erosion and deposition, as source and sink terms, respectively, which control the bed elevation change in rivers dominated by fine sediment. The objectives of this study are twofold: to verify the current numerical models governing fine sediment transport based on field measurements and satellite-based observations; and to propose modifications where observed physical processes could not be adequately explained using the current model. Subsequently, the proposed numerical method can be used to predict channel changes in a large, fine sediment-dominated river, such as the Indus, which can be used propose changes in channel management or countermeasures to river managers and policy makers.

To elucidate the sediment transport processes and verify the current numerical models in a large river, field measurements are conducted in the Brahmaputra River using an Acoustic Doppler Current Profiler (ADCP), turbidity meter, water sampler and bed material sampler. Acoustic Backscatter Turbidity (ABT) is used as a surrogate for fine sediment concentrations. Furthermore, satellite-based NIR observation is employed to

obtain a spatial distribution of turbidity near the water surface. The ABT, and the satellite-based NIR are proven to be robust methods to monitor fine sediment. Boils are also observed in areas of the river where velocity differences exist due to bedform or river bed shape. It is found that the force generated by boils lifts larger particles into suspension, and that the vertical sediment concentration profile is controlled by the vertical flow velocity, in addition to the turbulent-diffusion process. Thereafter, using dense measurements by the ADCP, the transport of fine sediment is discussed for different flow conditions. ABT is used to estimate vertical profiles of non-uniform sediment concentrations implying the Rousean distribution. In an area where the flat-bed condition exists, no boils are observed, and nearly equilibrium condition is observed. In the areas where the vertical velocity exists due to influence of bedform or boils, the vertical distribution of sediment concentrations can be represented using the Rouse equation by including the influence of vertical velocity. To model boils in a 2-D numerical model, the occurrence of boils is predicted using bedform roughness.

The final part of the study outlines policy implications in light of the findings of the present study. In particular, the requirements and constraints of the proposed method for numerical modelling in large, fine sediment-dominated rivers are discussed. As a number of new methods based on the field measurements and satellite data are used to verify the current numerical model in fine sediment-dominated river. Practical applications of the present study towards improving river management and policy are also discussed.

Acknowledgements

I am deeply grateful and indebted to my supervisors Associate Professor Atsuhiro Yorozuya, and Professor Shinji Egashira for their guidance, consistent support, and encouragement throughout the period of my research. I will always be deeply indebted to them for sharing their extensive knowledge and invaluable experience with me. I am also thankful to Professor Hajime Nakagawa, Professor Takashi Tsuchiya, and Professor Hitoshi Ieda, for their careful review and positive advice regarding my work.

I owe many thanks to Dr. Shoji Okada and Hiroshi Koseki, for their help in conducting field measurements and analyzing the measurement data, which is an essential part of this research. I also owe my thanks to Dr. Tsuyoshi Hoshino for his help in analyzing and visualizing the measurement data. I am also thankful for the kind support from Dr. Daisuke Harada and for his help with the implementation of the numerical model.

I am indebted to Asif, Karina, Daniel, Khairul, Tanjir, Robin, Hemakanth and Hoang for lending their unconditional support, sharing ideas, and for providing their valuable insights. I also owe a debt of gratitude to Yukie Okawa for her immense support as a colleague and a friend, without her, this study would surely be impossible.

I would also like to thank all colleagues and staff at ICHARM for their immeasurable help and encouragement throughout this research. I would like to thank ICHARM and PWRI for the financial and institutional support, and for the opportunity to carry out this research.

Finally, I would like to thank my family for their support and understanding throughout the duration of this research. I am thankful for my parents for their

unconditional love, encouragement, and prayers, which has been instrumental for me to complete this study. Most especially, I would like to express my deepest gratitude to my beloved wife, Mariam, for her love, understanding, and unwavering support.

Table of Contents

Table of Figures

List of Symbols

a	reference level near the bed where a =0.05h
α	variable related to boil intensity, $\alpha = f(\tau_*'')$
α_s, α_w	absorption coefficients of sediment particles and water respectively
β	experimental constant in Ashida & Michiue (1970)
β_0	constant of proportionality
c	sediment concentration
d	sediment particle diameter
dB	backscatter intensity
$\overline{Dur}_{boil}$	duration of boil observed at the water surface
c_{ae}	equilibrium sediment concentration near the bed
c_s	average sediment concentration of the bedload layer
$\bar{c}$	depth-averaged sediment concentration of wash load (c_w) or suspended sediment ($\overline{c_s}$)
c_i	sediment concentration of size class *i* at level z
c_{ai}	Sediment concentration of class *i* at $z = a$.
h	total depth of flow
E_s	erosion rate of suspended sediment
e	coefficient of restitution (0.85)
ε_x, ε_y, ε_z	coefficient of diffusion in *x*, *y*, and *z* direction respectively
g	gravitational acceleration
H	water depth
h_s	thickness of sediment layer
h_t	total depth
I	channel slope, calculated using water surface slope
κ	Von Karman constant
K_1	experimental constant in the Ashida & Michiue (1970) equation

K	experimental constant in the Ashida & Michiue (1970) equation
K_s	constant related to the transducer
k_s	equivalent roughness equal to 2.5 times mean particle diameter
k_d	k_d is empirical constant (0.0828)
k_f	k_f is empirical constant (0.16)
$M(r)$	sediment concentrations at distance r from the transducer
N	number of sediment particles per unit area
t	Time
$\bar{T}_{boil}$	mean recurrence period of boil
p	fraction of fine sediment in the bed surface layer
ρ_s	density of sediment
P_{rms}	backscatter intensity
R	Hydraulic radius
R'	Hydraulic radius due to skin friction
S	backscatter coefficient
σ_p	standard deviation of the function $f(w_p)$
U	depth-averaged velocity measured by ADCP
u_*	Shear velocity or friction velocity
u_{*b}	Shear velocity estimated using ADCP bedload velocity
u_{*ghi}	Shear velocity estimated as $u_* = \sqrt{ghi}$
u, v and w	components of flow velocity in x, y and z direction respectively
$\bar{u}$ *and* $\bar{v}$	depth averaged velocity in the x and y direction respectively
U_{max}	Maximum flow velocity along the direction of the flow
w	vertical velocity which is positive in the upwards direction
τ_*	total non-dimensional bed shear stress
τ_*'	non-dimensional bed shear stress due to grain roughness
τ_*''	non-dimensional bed shear stress due to bed form roughness
θ	local bed slope

ϕ_s	internal friction angle
$\overline{v_s}$	$\overline{v_s}$ is the vertical-averaged bedload velocity
λ	Porosity of bed sediment
ρ, σ	density of water and sediment particle respectively
w_0	fall velocity of sediment particle
w_{0i}	fall velocity of sediment of class *i*
w_p	actual velocity of sediment particle near the bed
x and y	orthogonal coordinates in the horizontal plane
z	vertical coordinate
z_*	Rouse number
z_b	bed level
ξ_0	Variable in Ashida & Michiue (1970), where $\xi_0 = \frac{w_0}{\sigma_p}$
ξ	Integration variable in Ashida & Michiue (1970), where $\xi = \frac{w_p}{\sigma_p}$

1. Introduction

1.1. Background

The Indus is a large river originating from the Himalayas and the Karakoram mountain ranges. Flows in the Indus River exhibit large variation from an average of 6,600 m^3/s to peak discharges of around 35,000 m^3/s. Water from the Indus has been utilized for irrigation since as early as 3000 BC, sustaining one of the earliest civilizations of the world. Till this day, the Indus waters area heavily utilized for irrigation to sustain the agriculture based economy in a largely arid region.

Over the past few decades, six (6) barrage structures have been constructed on the Indus River, along with embankments and river training works, to divert water for irrigation. This forms a part of the Indus Basin Irrigation System, that utilizes more than 60 percent of the Indus water to sustain agriculture on 170,000 km^2, which is nearly 80 percent of all cultivable land in Pakistan (Iftikhar, 2002). The primary objective of these structures is water distribution during low to median flows. To maintain the present river course through the barrage and to prevent frequent flooding during high flows, river training structures and levees have been constructed on the upstream and downstream of the barrage structures.

Figure 1.1 shows satellite images of Guddu Barrage in the lower Indus. The satellite images were taken in the low flow season (top) and during flood period (bottom). During the low flows, the upstream channel width is proportional to the barrage width and no significant ponding is seen in the upstream of the barrage. However, during high flows, it can be seen that flow in a 10 km wide river in the upstream of the barrage converges to a 1.3km wide barrage structure. As water stage rises, sediment rich flows from the main

channel interact with the floodplains, and the lateral flux results in deposition of coarser to finer sediment as flow velocity decreases(Lewin et al., 2017)

An example of this can be seen in Figure 1.2, which shows a recently observed digital elevation model of the Guddu barrage to Sukkur barrage section of the Indus River obtained by the JAXA's ALOS satellite. Barrage locations, embankments and river training works can also be seen. The Indus can be seen as confined between embankments on both sides, floodplain is as wide as 20km and reaches bankfull discharge every 2-5 years, and at Sukkur the river converges to an approximately 1km wide channel. The digital elevations show higher elevations near the right bank, compared with the elevations immediately outside the embankments. This large scale channel aggradation can be attributed to the backwater effect due to the flow constriction at Sukkur. Such channel changes greatly increase the risk of embankment breaches which result in large-scale, prolonged flooding(Kale, 2008; Syvitski and Robert Brakenridge, 2013). In particular, the location of Tori Embankment on the right bank of the Indus River, is highlighted in blue. Embankment failure at Tori has occurred at least 8 times in the past 100 years, most recently in 2010, when it displaced 1.3 million people and claimed 97 lives (Khan et al., 2011). After each such incident, the earthen embankment was raised above the previous high flood level according to the existing river management policy. This indicates the gaps in the current river management policy and its failure to identify and address the root causes of such channel changes. In addition, bank erosion has been a particular challenge in such rivers. Channel changes cause damage to flood protection structures such as earthen levees and cause widespread flooding (Ferderal Flood Commission, 2010). As no scientific tool is employed in the lower Indus to understand channel changes on a reach scale, only local-level studies are carried out for various

purposes, e.g., construction of river training works to control bank erosion. Essentially, such approach focuses on the affected area on a local scale disregarding the impact on the channel changes in the whole river reach. It is nevertheless important for river managers to consider the impact of structural countermeasures on a larger scale. Such gaps exist mainly due to the lack of appropriate tools that can model the short-term as well as long-term effects of such channel changes, and enable informed policy-making.

Thereafter, we can see that effects of the barrage on changes in the river channel are not only on a local scale, but also on a large scale, particularly in the upstream area. Large-scale sandbar formation, channel avulsion and bank erosion are often observed (Ferderal Flood Commission, 2010; Kale, 2008). Thereafter, these changes may lead to disasters during floods such as embankment breach, bank erosion, and damage to the barrage or its associated protection structure (Kale, 2008; Syvitski and Robert Brakenridge, 2013). Such catastrophic disasters have been seen in the past, as embankment breaches occurred in the upstream of 3 out the 6 barrages on the Indus (Taunsa Barrage, Guddu Barrage and Sukkur Barrage) causing widespread damage and loss of livelihoods (Ferderal Flood Commission, 2010; Gaurav et al., 2011). Similar phenomena were observed in 2008 in Koshi River, India, where channel changes due to barrage structure caused embankment breaches that displaced in excess of 10m people and more than 400 lives were lost.

Such channel changes in large rivers can be modelled using the 2-D numerical model such as the one proposed by Takebayashi and Egashira, (2001), which has been extensively used for bedload-dominated rivers, such as the ones in Japan (Takebayashi, 2005; Takebayashi and Okabe, 2009). However, the current 2-D numerical model needs to be verified before it can be applied to large, fine sediment-dominated rivers. This is

mainly due to non-equilibrium sediment transport conditions, and lack of available data about complex sediment transport processes. It is therefore important to understand the capabilities of the existing numerical models, and verify them based on robust field measurement and satellite-based information.

Field measurements are essential for understanding river geometry, flow conditions and sediment transport characteristics. Water sampling, bed material and turbidity are used to understand the sediment concentrations and size distributions. Acoustic Doppler Current Profilers (ADCP) are widely used for measurement of flow and bathymetry. Previous research has demonstrated an effective system for simultaneous measurement of flow, bathymetry and sediment transport (Kudo et al., 2017; Okada et al., 2016; Yorozuya et al., 2017). Such a simultaneous measurement system can be used to understand flow and sediment transport mechanics in greater detail.

In this study, the author aims to provide a framework to simulate the channel changes in large, fine sediment-dominated rivers. The proposed methodology uses field measurements and satellite data to understand the dominant sediment transport processes, and to verify the current 2-D numerical model. One of the main purpose of this study is therefore to describe the sediment transport processes in large, fine sediment dominated rivers in terms of the current 2-D numerical model by utilizing advanced observation methods in different flow conditions. It is found that boils are often observed in such rivers at locations where bedform has occurred (Best et al., 2008; Coleman, 1969; Jackson, 1976). Such boils are observed to suspend large amount of sediment and therefore contribute to the river bed elevation change. This study evaluates the boil phenomena in detail and proposes a treatment to model such phenomena in the 2-D numerical model.

1.2. Characteristics of rivers dominated by fine sediment

To understand the dominant processes of bed changes and sandbar deformations, it is important to ascertain the dominant mode of sediment transport in a river. Rivers with coarse bed material may be dominated by bed load transport where sediment moves in the bedload layer by rolling, sliding and saltation. The bed load is characterized by the non-dimensional bed shear stress (τ_*) and is initiated when τ_* exceeds a threshold required for incipient motion. In suspended sediment transport, the sediment particles are lifted upwards and entrained in the main flow outside the bedload layer as suspended load. For stronger flow, or finer particles, the entrained sediment can remain suspended longer periods of time, before returning to the bed. The suspended sediment transport is characterized by the ratio of shear velocity (u_*) and particle fall velocity (w_0), and is initiated when w_0/u_* is less than unity. The entrainment rate of sediment into the main flow is a function of w_0 and u_* known as erosion. Similarly, the settling rate of the suspended sediment is a function of w_0 and the concentration near the bed, known as deposition. Both erosion and deposition directly contribute to bed elevation changes. In rivers dominated by fine sediment transport, the bed load transport rate is much smaller compared with the suspended load transport rate, therefore the bed elevation changes are governed by the erosion and deposition processes.

The Indus and Brahmaputra are both categorized as large, fine sediment dominated rivers with similar channel slope and sediment size distributions. In the present study, the methodology presented is based on field measurements dataset, which could not be obtained for the Indus River. However, based on the similarities of the dominant physical

processes in both rivers, the author intends to develop and test the methodology based on observations in Brahmaputra, which can subsequently be applied to the Indus River.

1.3. Objectives of research

The numerical modeling of channel changes is an effective scientific tool for predicting channel changes in an actual river. In particular the prediction of channel changes in a large, fine sediment-dominated rivers such as the lower Indus is considered a complex challenge that requires a comprehensive 2-D numerical model framework that can simulate the dominant physical processes of fine sediment transport.

Based on the above challenges it is important to understand the sediment transport processes and the associated changes in river morphology. Subsequently, a river management strategy may be proposed to execute appropriate countermeasures and policy changes. For this purpose, the objectives of this research are as follows: to verify the current numerical models governing fine sediment transport based on field measurements and satellite-based observations; and to propose modifications where observed physical processes could not be adequately explained using the current model. Subsequently, the proposed numerical method can be used to predict channel changes in a large fine sediment dominated river, such as the Indus, and can be used to propose changes in channel management to river managers and policy makers.

1.4. Outline of thesis

The current chapter provides the background related to river management challenges in large rivers dominated by fine sediment. Chapter 2 reviews the current 2-D numerical model in particular related to the transport of fine sediment. In addition the current

understanding of boil phenomena is summarized based on past research. The chapter 3 discusses various methods to monitor fine sediment transport in large rivers based on in-situ field measurements and satellite data. Thereafter, in Chapter 4, a combination of observation methods are used to discuss fine sediment transport in different flow areas, observed in the Brahmaputra River. The results of measurements are used to verify the current 2-D numerical model, using the interpolated results of the ADCP measurements, satellite-based NIR, and numerous in-situ sampling methods. It is also noted that the current 2-D numerical model cannot explain the sediment transport due to boil phenomena. In Chapter 5, a method is proposed to model boil phenomena using 2-D numerical model, and changes in the governing equations are also proposed by modifying the erosion and deposition terms to include the effect of boil. Numerical simulations are carried out in an experimental channel to check the validity of the proposed method. The final chapter summarizes the outcomes of the present research and draws conclusions. Furthermore, policy implications for river and water resources management are discussed.

2. Transport of fine sediment in large rivers

2.1. Introduction

In order to use numerical simulation for modeling river bed evolution, 2-D depth integrated models have been found practical for large rivers dominated by fine sediment transport, such as the Brahmaputra and Indus.

Specifically, both suspended sediment, and wash load are transported by sediment transport equation. In the case of suspended sediment, entrainment from the river bed is defined as a positive source, E_s, which is a function of shear velocity (u_*); alternatively, it sinks to the river bed as negative source, D_s, which is a function of near-bed concentration and falling velocity. Furthermore, the entrainment of wash load, E_w, is described as a function of bed degradation; and the deposition of wash load, D_w, is described as a function of its concentration and falling velocity (Takebayashi and Egashira, 2001).

Boil phenomena have been frequently observed in large rivers dominated by fine sediment(Best et al., 2008; Coleman, 1969; Gul et al., 2018). In particular boils are observed over bedform, such boils are attributed to coherent turbulent structures that form near the bed behind bedform crests and lift large amounts of sediment to the water surface. This means that boils thus control the spatial and temporal distribution of suspended sediment and are therefore important to consider in the governing equations of the current model.

This chapter discusses the current 2-D numerical model in its non-equilibrium form in light of the physical processes observed in an actual river. As boil phenomena have

been frequently observed in large rivers, the current understanding of boil phenomena is discussed and related to the field measurements in the present study.

2.2. The current 2-D numerical model

2.2.1. Mass conservation of sediment in flow body

The mass conservation of sediment entrained in flow body, in the 3-D Cartesian coordinate system can be described as follows:

$$\frac{\partial c}{\partial t}+\frac{\partial cu}{\partial x}+\frac{\partial cv}{\partial y}+\frac{\partial (cw-cw_0)}{\partial z} = \frac{\partial}{\partial x}\left(\varepsilon_x \frac{\partial c}{\partial x}\right)+\frac{\partial}{\partial y}\left(\varepsilon_y \frac{\partial c}{\partial y}\right)+\frac{\partial}{\partial z}\left(\varepsilon_z \frac{\partial c}{\partial z}\right) \quad (2.1)$$

Where c is sediment concentration, t is the time, x and y are orthogonal coordinates in the horizontal plane, z is the vertical coordinate; u, v and w are the components of flow velocity in x, y and z direction respectively, ε_x, ε_y and ε_z are coefficient of diffusion in x, y, and z direction respectively, and w_0 is the fall velocity of the sediment particle.

The 2-D depth-averaged form of equation (2.1) is obtained as follows:

$$\frac{\partial \bar{c}h}{\partial t}+\frac{\partial \overline{cu}h}{\partial x}+\frac{\partial \overline{cv}h}{\partial y}=\frac{\partial}{\partial x}\left(h\varepsilon_x \frac{\partial \bar{c}}{\partial x}\right)+\frac{\partial}{\partial y}\left(h\varepsilon_y \frac{\partial \bar{c}}{\partial y}\right)+E-D \quad (2.2)$$

Where h is water depth, t is time, x and y are horizontal directions perpendicular to each other, $\bar{u}$ and $\bar{v}$ are the depth averaged velocity in the x and y direction respectively, $\bar{c}$ is the depth-integrated concentration of wash load (c_w) or suspended sediment ($\overline{c_s}$). ε_x

and ε_y are the coefficient of diffusion in the *x* and *y* direction. The erosion and deposition terms, *E* and *D* respectively, for suspended sediment and wash load are described below.

$$E_s = w_0 c_{ae} \tag{2.3}$$

$$D_s = w_0 c_a \tag{2.4}$$

In equation (2.3) erosion rate of suspended sediment, E_s, is a function of fall velocity of sediment particle, w_0, and equilibrium sediment concentration near the bed, c_{ae}. Wherein, c_{ae} is a function of flow conditions such as shear velocity and particle size (Garcia and Parker, 1991; Itakura and Kishi, 1980; Lane and Kalinske, 1941). Similarly deposition of suspended sediment, D_s, is modelled by w_0 and the sediment concentration at the reference level, c_a, as in equation (2.4).

Wash load is considered as very fine particles of sediment which may move directly from resting state (in the bed) to suspended state, the maximum diameter for wash load particle was defined by Ashida et al., (1981) as 100μm. Egashira and Matsuki, (2000) proposed treatment for the erosion and deposition of wash load in the numerical model. The erosion and deposition of wash load are described as follows:

$$E_w = -(1-\lambda)p\frac{\partial z_b}{\partial t}, \quad (when\ \frac{\partial z_b}{\partial t} < 0); \qquad E_w = 0, \quad (when\ \frac{\partial z_b}{\partial t} \geq 0) \tag{2.5}$$

$$D_w = w_0 c_{wa} \tag{2.6}$$

Where z_b is the bed level, λ is porosity and p is the fraction of fine sediment in the bed surface layer. The erosion of wash load, E_w, takes place only when bed degradation occurs and is otherwise zero. Deposition, D_w, of wash load is a function of w_0 and the wash load concentration near the bed c_{wa}. It is pertinent to note that according to the

equation (2.5) of the current model, E_w is not a function of shear velocity, as can be seen in the case of E_s, and therefore may not be evaluated only on the basis of flow parameters such as the shear velocity.

2.2.2. **Equilibrium concentration of sediment near the bed**

Rouse (1937)

The vertical distribution of suspended sediment concentration can be evaluated under steady, homogeneous flow in horizontal plane considering isotropic turbulence. The downwards flux of particles in the water body having concentration *c* can be described as $-cw_0$. Alternatively, the upwards flux of sediment due to diffusion from near the bed can be characterized by Fick's law as $\varepsilon_z \frac{\partial c}{\partial z}$. The equation (2.1) reduces to the following

$$cw_0 + \varepsilon_z \frac{\partial c}{\partial z} = 0 \tag{2.7}$$

Where the coefficient of diffusion, ε_z, is proportional to the kinematic eddy viscosity, and can be written as:

$$\varepsilon_z = \beta_0 u_* \kappa z \left(1 - \frac{z}{h}\right) \tag{2.8}$$

In which, β_0 is the constant of proportionality, κ is the Von Karman constant. Combining and integrating equation 2.7 and 2.8, we can obtain the equation by Rouse, (1937):

$$\frac{c_s\,(z)}{c_a} = \left[\frac{h-z}{z} \cdot \frac{a}{h-a}\right]^{z_*} \tag{2.9}$$

Where:

$$z_* = \frac{w_0}{\kappa u_*} \tag{2.10}$$

Where a is the reference height near the bed taken as $a = 0.05h$, c_a is sediment concentration near the bed at level a. The exponent z_* is also known as the Rouse number. Sediment is entrained into suspension when the vertical component of turbulence exceeds the fall velocity of the sediment particles, i.e. w_0/u_* is less than unity. As $\kappa = 0.4$, $w_0/u_* \leq 1$ corresponds to $z_* \leq 2.5$.

Ashida and Michiue (1970)

Ashida and Michiue, (1970) used kinematic statistics on flow and particle motion near the river bed to understand the entrainment rate and the reference concentration near the bed. Assuming that the river bed is composed of non-cohesive sediment, the velocity distribution of sediment particles can be described by the normal distribution as follows:

$$f(w_p) = \frac{1}{\sqrt{2\pi}\sigma_p} exp\left\{-\frac{1}{2}\left(\frac{w_p}{\sigma_p}\right)^2\right\} \tag{2.11}$$

Where w_p is the actual velocity of the sediment particle near the bed, and σ_p is the standard deviation of the velocity distribution. Taking into account the effect of gravity:

$$w_{pg} = w_p - w_0 \tag{2.12}$$

Using equation (2.11) and (2.12), we can provide an expression of the average velocity of sediment particles lifted in the vertical direction:

$$\overline{w_{pg}} = \frac{\int_{w_0}^{\infty}(w_p - w_0)f(w_p)dw_p}{\int_{w_0}^{\infty}f(w_p)dw_p} \tag{2.13}$$

Based on this, the entrainment rate of suspended sediment, q_{su} (in terms of volume of sediment suspended/ time/ area), can be written as follows:

$$q_{su} = K_1 N \frac{\pi}{6} d^3 \rho_s \frac{w_{pg}}{d} \int_{w_0}^{\infty} f(w_p)dw_p \tag{2.14}$$

$$N = \frac{1}{(\pi/4)d^2} \tag{2.15}$$

Where *N* is the number of sediment particles per unit area as shown in equation (2.15), d is the particle diameter, ρ_s is the density of sediment, and K_1 is experimental constant ($K_1 = 0.0375$).

The rate of deposition, q_{sd}, can be formulated as a function of concentration near the bed, c_b, and the fall velocity of the sediment particle.

$$q_{sd} = c_b w_0 \rho_s \tag{2.16}$$

In equilibrium condition, the entrainment rate and deposition rate are equal ($q_{su} = q_{sd}$), and in this condition, c_b can be written as follows:

$$c_b = K\left[g(\xi_0)/\xi_0 - G(\xi_0)\right] \tag{2.17}$$

Where,

$$g(\xi_0) = \frac{1}{\sqrt{2\pi}} exp\left\{-\frac{1}{2}(\xi_0)^2\right\} \tag{2.18}$$

$$G(\xi_0) = \frac{1}{\sqrt{2\pi}} \int_{\xi_0}^{\infty} exp\left\{-\frac{1}{2}(\xi)^2\right\} d\xi \tag{2.19}$$

Where, $\xi = \frac{w_p}{\sigma_p}$, $\xi_0 = \frac{w_0}{\sigma_p}$ and K is an experimental constant ($K = 0.025$). The distribution of velocity of particles near the bed ($f(w_p)$) can be explained using a normal distribution as shown in equation 2.11. The spread of this distribution is governed by σ_p which is a function of shear velocity, and has been determined experimentally as follows:

$$\sigma_p = \beta u_* \tag{2.20}$$

Where β may vary based on sediment size, however it is determined experimentally as $\beta = 0.83$ for sediment size 80~350μm. Thus the equilibrium sediment concentration near the bed, which can be described as a function of shear velocity can be considered as:

$$C_{ae} = f(\sigma_p) \tag{2.21}$$

Where σ_p is described in equation 2.20 and the function f is described in equation (2.17).

2.3. Boil phenomena

In natural rivers, turbulence at different scales is linked with sediment transport and bed shape. Turbulence near the bed as an independent, random process can be described by a normal probability function which can also be used to describe sediment entrainment due to turbulent diffusion processes (e.g. Itakura and Kishi, 1980). Alternatively, 'coherent' turbulent structures are commonly observed around sudden changes of flow area, e.g., behind bedform crests, and the components of such turbulence are correlated

with each other in time and space. Various researchers have previously reported on the observations of such turbulent structures in rivers, estuaries and experimental channels (e.g. Coleman, 1969; Gul et al., 2018; Iseya and Ikeda, 1986; Jackson, 1976).

Such turbulent structures, called boils or kolk-boils, have been often observed in the developing stages of a bedform (Iseya and Ikeda, 1986) in laboratory conditions. Figure 2.1 shows flow over a dune bed with dune wavelength λ, dune height Δ, and separation zone length $a\Delta$ (where $a = 2.5 \sim 5$). Flow separation occurs over the dune crest at the lee side, separation vortices are formed behind dune crests and turbulent vortices are generated from the reattachment point of the separated flow. The strong turbulent vortices formed at the flow reattachment point near the bed lift large amounts of sediment from the bed. These turbulent vortices gradually loose energy as the rise and appear on the free surface as boils. Such phenomenon has been categorized as 'boil of first kind' by Nakagawa and Nezu, (1993).

Coleman (1969), observed intermittent kolk-boils at various scales and intensities on the water surface in Brahmaputra. Using aerial imagery, a long section of a channel was observed to be lined with boils aligned in the lateral direction, which was due to a laterally aligned dune bed. Various researchers have found the size and intensity of these boils to be proportional to form roughness, as larger dunes (with larger relative roughness, Δ/λ) produce more intense turbulent vortices (Babakaiff and Hicken, 1996; Jackson, 1976).

Several researchers have documented the size and frequency of boils in rivers and through experimental studies. Jackson, (1976) proposed the following relations based on observations in different flows:

$$D_{boil} = (0.3\sim0.6)h \tag{2.22}$$

$$\bar{T}_{boil} = {7.6\ h}/{U_{max}} \tag{2.23}$$

Where D_{boil} is the diameter of boil at the water surface, h is is water depth, $\bar{T}_{boil}$ is the mean recurrence period of boil and U_{max} is the maximum flow velocity along the direction of the flow. It is worth noting that these relations do not differentiate boils observed behind dune crests (boil of first kind) from others. Nezu et al., (1980) obtained similar relations by observations of 'boil of first kind' in a laboratory flume, and the results were $D_{boil} = 0.6h$, $\bar{T}_{boil} = {(2\sim3)\ h}/{U_{max}}$. The histogram of boil period observations by both studies fits a log normal distribution.

Gul et al., (2018) observed boil phenomenon in a section of the Brahmaputra River, where sandwave bedform existed. Figure 2.2 shows the flow magnitude (a), vertical velocity (b), and backscatter (c) measured with an ADCP along the direction of the flow where a boil is observed. In Figure 2.2 (a) flow velocity differences can be observed above bedform crests and at the lee side of the bedform due to flow convergence and expansion respectively. Higher velocity is observed at the bedform crest as flow area is constricted, flow separation occurs at downstream of bedform crest, as the velocity decreases. Figure 2.2 (b) shows a large upwards flow at the location where flow reattachment would occur, this upward flow is due to a strong turbulent structure that subsequently appears on the water surface as a boil. Figure 2.2 (c) shows ADCP backscatter as a surrogate for fine sediment concentrations. High sediment concentrations are observed during the upwards flow due to boil. The high sediment concentrations which are observed up to the water surface as shown in Figure 2.2 (c) at i), suddenly decrease around ii). This sudden

decrease in sediment concentrations is correlated with a downwards flow shown at Figure 2.2 (c) ii) which is a part of the boil flow structure (Best, 2005; Gul et al., 2018). Figure 2.2 provides a detailed insight of the flow structure and sediment concentrations due to the boil of first kind, as observed in an actual river.

3. Methodology of monitoring fine sediment

3.1. Introduction

It is important for river managers to understand the fine sediment load transported through a hydraulic structure or a section in an actual river. Traditionally, direct sampling by obtaining numerous water samples under varying flow conditions are used to create empirical relations for estimating fine sediment load as a function of stream flow. Such sediment transport curves may provide limited understanding of fine sediment load where the upstream sediment supply may vary between different tributaries, or where sediment hysteresis is observed (different sediment load observed against the same discharge during the rising or falling limb of the hydrograph). Furthermore, understanding the mechanics of fine sediment in large rivers with traditional direct sampling methods may be infeasible and poses numerous challenges. Numerical modeling of fine sediment, such as described in Chapter 2, is hard to verify in an actual river. Therefore, the need to measure fine sediment has led to the development of several surrogate measurement techniques.

The in-situ, direct sampling of water-sediment mixture provides a useful insight to the sediment concentration and size distribution of the suspended particles. Typically, a water sampler, attached with a pressure gauge, is lowered into the water and a sample is taken from the designated flow depth. The measurement is repeated at the same location if samples at other depth are also needed. These samples must then be analyzed in the laboratory for their sediment concentration (e.g using filtering, and weighing dried sediment samples) and particle size distribution (e.g using laser diffraction spectroscopy).

The methods for monitoring fine sediment can therefore be described as either a) Direct sampling, by obtaining water sample using a submersible water sampler b) Surrogate measurements for monitoring fine sediment. The surrogate measurements can further be classified into 1) in-situ measurements (e.g acoustic backscatter, turbidity meter) and 2) remotely sensed data (e.g. NIR reflectance by aerial or satellite platforms). This chapter discusses the methods used to monitor the transport of fine sediment, in particular the surrogate measurement of fine sediment using optical-NIR scattering, acoustic backscattering, and NIR reflectance.

3.2. Optical-NIR scattering

Turbidity is generally considered as a measure of 'optical clarity' of a fluid, and is used in various disciplines in different contexts. However, in the context of fluvial, coastal and marine hydrology, turbidity typically refers to presence of fine sediment and other particulate matter in water. Therefore, turbidity has often been used as a surrogate measure for Suspended Sediment Concentration (SSC) or Total Suspended Matter (TSM) (Gao et al., 2008; Okada et al., 2016; Teixeira et al., 2016; Wood and Teasdale, 2012).

Modern turbidity meters operate by illuminating the sample by a directed source of light (usually 700-900nm). The scattered light is then measured at an angle θ from the direction of the light source, where θ may range between 0-180˚. A measurement angle of where $0^\circ < \theta < 90^\circ$ is known as forward-scattering, $\theta = 90^\circ$ is known as side-scattering, and $90^\circ < \theta < 180^\circ$ is known as backscattering. Since 1926, a stable synthetic material known as Formazin, having uniform particle size is used as a standard for calibration, with Formazin Turbidity Units (FTU). Thereby, FTU is the most commonly used unit for turbidity, while other units of turbidity are NTU (USEPA, 1993), FNU (ISO, 2016) etc.,

which have specific provisions for light source wavelength, measurement angle θ, and geometric properties of measurement apparatus.

Direct sampling of water and sediment mixture in an actual river is a challenging task especially during rough flow conditions or when conducting measurements in a large river. The availability of compact field-deployable turbidity meters to obtain concentration of fine sediments has provided a more efficient alternative to obtain sample concentrations using standard methods. The standard method is comprised of directly obtaining water samples during field measurements and then processing samples in a lab to obtain sample concentrations. Alternatively, a submersible turbidity meter attached with a pressure gauge for simultaneous depth measurement can be lowered into water at a sampling location to obtain turbidity measurements at various depths. A few sediment samples may be used to obtain a relationship between turbidity (FTU) and sediment concentration e.g., Gul et al., (2018). Such measurement set up can be used to obtain a vertical profile of sediment concentrations at various sampling locations e.g., Okada et al., (2016).

3.3. Acoustic Backscatter

3.3.1. Acoustic Backscatter Turbidity

The ADCP is a hydroacoustic current measurement instrument which is commonly used to provide accurate measurement flow velocity and bathymetry. Recent advances in ADCP measurements have enabled non-contact measurement of vertical concentration profile by using ADCP acoustic backscatter (Kitsuda et al., 2006, 2011; Wood and Teasdale, 2012). These techniques provide advantages over use of optical/NIR scattering

instruments which require submerging the instrument at various depths, subject to favorable flow conditions, and other limitations. Kitsuda et al., (2006) proposed the following relation to calculate sediment concentrations from ADCP acoustic backscatter intensity:

$$\log M(r) = S\big(dB + 2r(\alpha_w + \alpha_s)\big) + K_s \tag{3.1}$$

$$\mathrm{dB} = log_e^{\left(\frac{ra_s}{f} P_{rms}\right)} \tag{3.2}$$

Where *M(r)* is sediment concentrations at distance *r* from the transducer, *S* is backscatter coefficient, dB is backscatter intensity, α_s and α_w are absorption coefficients of sediment particles and water respectively, K_s is a constant related to the transducer, a_s is particle size, f is a function of particle and P_{rms} is backscatter intensity. Figure 3.1 illustrated how equation (3.1) is used to estimate sediment concentrations using ADCP backscatter. The value of coefficients K_s, α_w, S can be determined based on calibration with observed sediment concentration (or turbidity meter) data. As a result, equation (3.1) can be used to obtain a continuous observation of vertical turbidity profiles along the ADCP track.

3.3.2. **Using ADCP Bottom Track velocity to estimate shear velocity and bedload discharge**

ADCP bottom track capability enables measurement of the instrument displacement and velocity with respect to the bottom of the river. This observation, with simultaneous observation of displacement using DGPS, provides a way to calculate the velocity of the near-bed sediment, or u_b. Several previous researchers have previously linked u_b to

bedload discharge (Jamieson et al., 2011; Latosinski et al., 2017; Rennie et al., 2002; Yorozuya et al., 2010, 2017).

Okada et al., (2016) proposed using equation (3.3) by Egashira et al., 1997, to calculate shear velocity, as follows:

$$\frac{\overline{v_s}}{u_*} = \frac{4}{15}\frac{K_1 K_2}{\sqrt{f_d + f_f}}\tau_* \tag{3.3}$$

$$K_1 = \frac{1}{cos\,\theta\,.\,(tan\,\phi_s - tan\,\theta)} \tag{3.4}$$

$$K_2 = \frac{1}{c_s}\left[1 - \frac{h_s}{h_t}\right]^{1/2} \tag{3.5}$$

$$h_s = \frac{K_1}{c_s} d\tau_* \tag{3.6}$$

$$f_d = k_d(1 - e^2)(\sigma/\rho){c_s}^{1/3} \tag{3.7}$$

$$f_f = k_f(1 - c_s)^{5/3}(\sigma/\rho){c_s}^{-2/3} \tag{3.8}$$

Where $\overline{v_s}$ is the vertical-averaged bedload velocity, equal to nearly half of bedload surface velocity measured by the ADCP (u_b). u_* is shear velocity, τ_* is non-dimensional shear stress as a function of shear velocity, θ is local bed slope which can be measured using ADCP 4-beam bathymetry, ϕ_s is the internal friction angle, k_d is empirical constant (0.0828), k_f is empirical constant (0.16), e is the coefficient of restitution (0.85), c_s is the average sediment concentration of the bedload layer, h_s is the thickness of sediment layer, h_t is the total depth, ρ is density of water, and σ is density of sediment. The equation (3.3) can therefore be used to calculate shear velocity.

Additionally, the unit bedload discharge, q_b, can be calculated using equation proposed by Egashira, (2005; 1997) as follows:

$$q_b = c_s h_s \overline{v_s} \tag{3.9}$$

Therefore, the ADCP measurement can be used to simultaneously calculate shear velocity, bedload discharge and the suspended sediment discharge in actual rivers.

3.4. NIR reflectance

The previous sections outline methods to obtain fine sediment concentrations by in-situ measurements. However, in-situ observations methods may provide limited understanding of the sediment transport processes in a large river, particularly due to varying temporal and spatial resolutions of those processes.

Multispectral satellite information has been used in the past to understand plan-view distribution of turbidity, as a surrogate for suspended sediment and wash load concentrations near the water surface (Quang et al., 2017; Dogliotti et al., 2015; Nechad et al., 2009). NIR reflectance has been used to estimate turbidity in the range of 100-1000 FTU (Dogliotti et al., 2015). Figure 3.2 shows a section of the Brahmaputra River near Bahadurabad at the confluence with the Teesta River (top-left), as observed using Sentinel-2 satellite on 12 September 2017. The figure shows two views of the same section, RGB true-color on the left, and NIR reflectance in pseudo-color on the right, with cloud and land appearing red. The NIR reflectance over the water clearly indicates the difference in characteristics of different channels. The channels near the right bank around the confluence point show a lower turbidity as opposed to the channels near the left bank.

It can be inferred that the tributary has a less concentration of finer particles as in Brahmaputra. Subsequently it can be seen that this difference continues downstream, similar to observations in other rivers.

Furthermore, the utility of the NIR satellite imagery can be explained further based on a closer look at the NIR reflectance over a sandbar, in a wash load-dominated part of the Brahmaputra River, as shown in Figure 3.3. The NIR reflectance shows a higher turbidity around the banks, possibly due to bank erosion. This region of high concentration extends downstream along the streamline of the flow. Moreover, low turbidity can be seen inside the bar and its immediately downstream region possibly due to low shear stresses and the deposition of fine sediments.

3.4.1. **Case study: Brahmaputra River near Jamuna Bridge**

A Sentinel-2 satellite image around Jamuna Bridge of the Brahmaptura River, was acquired on 29 September 2018, nearly one month after the measurements were conducted in the field using turbidity meter. The Top Of Atmosphere (TOA) reflectance was processed using ESA Sentinel-2 Toolbox and Sen2Cor (Muller-Wilm, 2016) for atmospheric corrections and cirrus cloud removal. The resulting NIR (band 8, 842nm) Bottom Of Atmosphere (BOA) reflectance was tuned up using 45 turbidity meter observations to obtain turbidity. Based on this process, a relation of BOA NIR reflectance, R, and turbidity (FTU), T, was obtained with R^2 =0.767, as shown in Figure 3.4. The relation shows that BOA NIR reflectance can be used as a surrogate for estimating turbidity. The outliers are shown in red, which correspond to satellite observation over cloud cover, or where land surface became exposed due to changes in river stage over

time. Based on this relation the BOA NIR reflectance over the water surface can be used to create turbidity, hereafter referred to as Turbidity-NIR, as shown in Figure 3.5. Land area, clouds, and water having turbidity below or above the range shown in Figure 3.4(~150-400 FTU) is masked as white to avoid extrapolation. The turbidity observations are located in the region downstream of the sandbar, where flow is approaching from two different directions (Channel A and B). The lowest and highest turbidity meter observations have been highlighted in Figure 3.4 and 3.5, the highest turbidity measurement is along the direction of the flow of the main channel. A high turbidity is observed in the flow from channel A and in the flow near sandbar bank i.e. where flow velocities are high and erosion process is dominant. Similarly, low-turbidity areas can be seen inside and immediately downstream of the sandbar where a low flow velocity exists, and deposition is dominant. The results show that NIR reflectance is a robust measure of fine sediment and can be used to understand fine sediment mechanics over a large area.

4. Characteristics of fine sediment based on monitoring in different flow areas

4.1. Introduction

In order to understand the mechanics of wash load and suspended sediment and to verify the current 2-D numerical model (discussed in Chapter 2) in an actual river, measurements were conducted in a large, fine sediment-dominated river in different flow conditions. During field measurements, it is found that boils occur in areas where flow velocity differences exist due to bed shape. Such boils are characterized by large vertical velocities, which influence the vertical sediment concentration profile (Gul et al., 2018). Similarly, a vertical flow was also observed over bed form crests.

This chapter discusses the characteristics of fine sediment transport in four different kinds of flow, based on observations conducted in the Brahmaputra River. These flow conditions are:

1. Flow in flatbed conditions where sediment transport is close to equilibrium
2. Flow conditions where sand wave bedform exists and boils are observed
3. Flow conditions where boils are generated due to river bed shape
4. Flow conditions near the bank where bank erosion is observed

Dense measurements were carried out in each flow area using the ADCP, turbidity meter, water sampler and bed material sampler. The methodology of such simultaneous measurement system has been outlined in previous studies (Gul et al., 2018; Okada et al., 2016; Yorozuya et al., 2010 & 2014).

4.2. Study areas and observation methods

In this study we use observed data based on measurements in the Brahmaputra River, Bangladesh. Brahmaputra is a large river dominated by fine sediment transport, with average flood and 10-year flood discharges equal to 65,000m^3/s and 90,000m^3/s respectively. The suspended sediment load to the bedload ratio was found to be between 10 and 24, which indicates the dominance of suspended sediment transport (Biswas, 2016). Measurements were conducted in two separate years, to discuss fine sediment transport in four different kinds of flows. Figure 4.1 shows the locations of the measurements along the Brahmaputra River.

Firstly, measurements were carried out in an area located in a braided reach of the Brahmaputra River near Bahadurabad in Bangladesh, during 21-24 August 2017, when the discharge was around 60,000 m^3/s. The location was around 200km upstream of the Ganges-Brahmaputra confluence where the width of the river was 10km with multiple channels separated by sandbars. Figure 4.2 shows the locations of bed material and water sampling points. The boat path and the locations of two dense measurement areas are also shown. Dense measurements were conducted in a flow area, referred as area B, where boils were observed and a sand-wave existed on the river bed. For comparison dense measurements were also carried out in an adjacent flow area, referred as area A, where no boils were observed.

Secondly, measurements were carried out near Kazipur, located 40km upstream of the Jamuna Bridge, when discharge was around 40,000 m^3/s. Large scale boils were observed on the water surface.

Lastly, measurements were carried out around Sirajganj, located immediately upstream of the Jamuna Bridge, between 28-30 August, 2018, when the discharge was around 40,000 m^3/s. Figure 4.3 shows the map of the study area, which is located near the Jamuna Bridge. The width of the river was around 15km in the upstream of the bridge, with multiple channels separated by sandbars. Channel A is the main channel and is separated from Channel B by a sandbar. Subsequently the river width narrows to around 4.6km at the Jamuna Bridge.

Figure 4.4 shows the equipment used to carry out the field measurements. The measurement was conducted using a Teledyne RDI RiverRay ADCP operating at 600 kHz and a STARFIRE WDGPS mounted on a tethered boat which was towed by a manned control-boat. Dense measurements along the direction of the flow were performed by many longitudinal passes over the target area. The boats were allowed to move along the flow with zero relative velocity in order to obtain longitudinal flow profile. The details of such a measurement are described by Yorozuya et al., (2014). During measurements, water sampler attached with a pressure gauge is used to obtain samples at various depths, these samples are subsequently analyzed for their concentrations and particle size distributions. Similarly, a submersible turbidity meter, attached with a pressure gauge, is used to obtain vertical turbidity profiles.

Acoustic backscatter from the ADCP is used to obtain Acoustic Backscatter Turbidity (ABT) using the method described by Kitsuda et al., (2006). Using this method, the coefficients in equation (3.1) are determined using in-situ turbidity meter measurements acquired during observations.

In order to obtain spatial features from dense measurements, the Inverse Distance Weighted (IDW) method is implemented. The ADCP data from the dense measurements, such as river depth, flow velocity and ABT, are interpolated to create 3-dimensional features of flow and sediment transport characteristics of the river.

4.3. Vertical sediment concentrations profile

In the 2-D numerical model, the transport of depth-averaged sediment concentrations, $\overline{c_s}$, is computed using equation (2.2). However, since the vertical profile of sediment concentrations is different from the depth averaged value, treatment is required for the relation between the depth averaged sediment concentration and the concentration near the bed. Such methods assume that the sediment concentrations decrease exponentially in the vertical direction above the bed, based on the fall velocity of the entrained particles (Lane and Kalinske, 1941). Such treatment is derived based on the assumption of uniform and steady flow where sediment are suspended based on homogenous and isotropic turbulence. However, this assumption may not hold true in non-uniform flow, as is later discussed based on the results of measurements in different flow conditions.

The current model to evaluate the vertical sediment concentrations, as proposed by Rouse in equation (2.9), assumes that the vertical flow velocity is negligible, and that the vertical profile of sediment concentration is governed only by turbulent diffusion. To analyze local sediment concentrations, ABT is used as a surrogate for vertical concentration profile, water depth is measured using ADCP, and shear velocity is measured using bedload velocity (u_b) measured by the ADCP as shown in equation (3.3).

Furthermore, to evaluate vertical sediment concentrations using equation (2.9) and understand the erosion and deposition processes, it is important to first evaluate the reference sediment concentration (at $z = a$) near the bed, c_a. The total sediment concentration at the reference level is estimated using up to 3 ABT samples near the bed, using equation (2.9). z_* is determined using the fall velocity of sediment sizes obtained using water samples, and $u_*$is calculated as $u_{*ghi} = \sqrt{ghi}$.

Figure 4.5 shows two vertical sediment concentration profiles observed in different flow areas : a) from an area where no bed form is observed and b) from an area where boil is observed. Figures 4.5 shows the observed concentration profile using ABT, as well as the one estimated using equation (2.9). It can be seen that using the current model as shown in equation (2.9) the vertical concentration profile from flat-bed area can be modelled, however, the concentration profile from an area where boil exists cannot be modelled. This may be due to the reason that the flow in a flatbed area is closer to the derivation process of the equation, i.e. uniform flow conditions. However the flow in the area with bedform is non-uniform and the vertical flow structure is observed due to the bed shape. In addition, the boil phenomena is essentially large coherent turbulent vortices that carry sediment from bed to the surface and is non-uniform flow. The turbulence due to boils that entrains sediment particles near the bed is also not represented by the shear velocity ($u_{*ghi} = \sqrt{ghi}$).

Vertical flow exists due to boil and the influence of bed form (Gul et al., 2018) and controls the vertical sediment concentration profile. In view of the derivation process, the treatment of w velocity in the Rouse equation can therefore be done with hesitation to deal with vertical sediment concentrations observed in the boil area. Such observed

concentration profiles, as shown in Figure 4.5 b), do not follow the Rousean distribution due to vertical flow structures. In order to model such vertical sediment concentrations such treatment is carried out. Equation (2.9) may be modified as follows:

$$\frac{c_i\,(z)}{c_{ai}} = \left[\frac{h-z}{z}.\frac{a}{h-a}\right]^{z_{*i}} \tag{4.1}$$

$$z_{*i} = \frac{w_{0i} - w}{\kappa u_*} \tag{4.2}$$

Where c_i is the concentration of sediment size class *i* at level z, h is the total depth of flow, a is the reference level near the bed where a =0.05 h. c_{ai} is the sediment concentration of class *i* at a. Similarly, w_{0i} is the fall velocity of sediment of class *i*, *w* is the vertical velocity which is positive in the upwards direction, K is the Von Karman constant and u_* is shear velocity.

Non-uniform sediment concentration is assumed to consist of five (5) evenly spaced sediment size classes based on water samples collected in each flow area. To create a vertical distribution considering non-uniform sediment, it is important to consider the sediment concentration at the reference level for each size class, as a ratio of the total. The ratio for each sediment size class at the reference level is determined by assuming the size distribution of the observed water sample at the corresponding relative depth. Subsequently, at each vertical level the w velocity in equation (4.2) is determined to match the observed ABT profile using least squares fit. Therefore, using this method a single value of w velocity at each z is obtained such that $\sum c_i\,(z) = c_{obs}\,(z)$, where $c_{obs}\,(z)$ is the observed concentration at level z by the ADCP.

4.4. Results

4.4.1. Flat-bed conditions

In this section the flow and sediment transport characteristics are discussed using dense measurements carried out in a flatbed area. The location of the measurements is marked as Area A in Figure 4.2. Figure 4.6 a) shows vertical velocity contours and river depth measured by the ADCP. The results of IDW interpolation of bed elevations and near surface sediment concentrations are shown in Figure 4.6 b) and c), respectively, and the ADCP boat track shown in a) is also highlighted in b).

In Figure 4.6 a), a very small amplitude wave appears to be present with a wavelength around 100m and a crest height between 0.2m-0.4m. With no sand waves observed these were considered as flatbed conditions. No discernable structures were detected in the vertical flow in relation to the river bed shape. Bed elevations in this area, shown in Figure 4.6 b), show a widely distributed and low amplitude sand wave which is a characteristic similar to flatbed conditions. The spatial distribution of sediment concentrations near the surface in Figure 4.6 c) show a nearly uniform concentration. This indicates that the flow is homogeneous in the lateral plane and it would be reasonable to assume that the sediment transport is in equilibrium.

Details of flow and sediment transport characteristics can be obtained by looking at a longitudinal profile marked as A-A'. Figure 4.7 shows the longitudinal profile along A-A' including: a) depth averaged sediment concentration $\overline{c_s}$, total concentration near the bed, c_{b_total}, and flow depth; b) depth average flow velocity U, shear velocity calculated using ADCP bedload velocity (equation 3.3) u_{*b}, shear velocity calculated as $u_{*ghi} =$

$\sqrt{ghi}$; and the c) the maximum and minimum vertical velocity calculated using equation (4.1-4.2) along with c_{b_total} and flow depth. The vertical profiles of sediment concentrations estimated using equation (4.1-4.2) at two different points along streamline at 460m and 480m are shown in d) and e), respectively.

Figure 4.7 a) shows a nearly flat bed condition with a nearly constant depth of around 8m, similar to the one seen in plan-view in Figure 4.6. The depth-averaged sediment concentration and the concentration near the bed also does not show considerable variation along the streamline. Based on this figure, we can assume that the sediment transport in area A may be close to the equilibrium condition. Figure 4.7 b) shows that the flow velocity is nearly constant along the streamline, between 1.0 and 1.2 m/s, which indicates that the flow resistance does not change along the streamline. The difference between shear velocity u_{*b} and u_{*ghi} is considerable, with u_{*ghi} being larger than u_{*b}. It may be noted that in the case of the uniform flow, the relationship $u_{*ghi} > u_{*b}$ holds as discussed by Yorozuya et al., (2017) based on observations in similar conditions in the Jamuna River.

Figure 4.7 c) indicates that the vertical velocity calculated using equation (4.1-4.2) is nearly constant, and that mild undulations in the bed can be correlated with vertical velocity.

4.4.2. **Sand-wave bedform**

At Bahadurabad, boils were observed on the surface of the water in an area located adjacent to the flat bed area. Dense measurements were carried out to investigate this phenomena in detail. It is found that sand waves existed on the river bed in the area where boils were observed. The location of the dense measurements is shown in Figure 4.a as

Area B. Figure 4.8 a) shows vertical velocity contours and river depth measured by the ADCP in the area where sand-wave bedform is observed. The results of the IDW interpolation of bed elevations and near-surface sediment concentrations are shown in Figure 4.8 b) and c) respectively. The ADCP boat track shown in a) is also highlighted in b). The locations of boils using geo-tagged photographs and videos are marked by blue mark in Figure 4.6 c), and the ADCP boat pass of Figure 2.2 showing observation of boil is also highlighted in the same figure.

The bed shape along the boat path shown in Figure 4.8 a) shows that a sand wave pattern exists with the height ranging from 1.4m - 4.2m and the wavelength between 50m - 62m. The wavelength is the horizontal distance between two successive crests, and the height is the vertical distance between the crest and the trough. The flow pattern in Figure 4.8 a) shows a distinct pattern of upwards velocity at the stoss side of the sand waves. Subsequently, a sudden downwards velocity over the crests can be seen, highlighted at points (i), (ii), (iii) and (iv). This vertical flow structure is observed due to the bed shape, and is smaller in magnitude compared with the downwards flow observed due to boil shown in Figure 2.2 b) at ii).

Based on Figure 4.8 b), it is reasonable to assume that a sand wave pattern exists over the entire area, not just along a single boat path. Furthermore, zones of superimposed bedform are also identified, diagonally aligned to the general flow direction. Figure 4.8 c) also shows numerous patches of extremely high sediment concentrations of around 2000 mg/l, which is caused by boils, and low sediment concentrations of around 1000 mg/l which are similar with concentrations found in the area with flat-bed conditions. The locations of the boils and high concentrations do not necessarily match, as the timing of

the ADCP measurement and photographs is not the same and sediment concentrations decrease rapidly in the absence of boils. In particular, at locations marked as i) and ii) where boils existed, sediment concentrations became remarkably high, and then became low shortly after that.

Figure 4.8 b) shows that even though the direct observation of boil by the ADCP is obtained in one boat pass along the direction of flow, the location of geo-tagged pictures indicates that the boils can be visually observed over the entire area where the bedform occurs.

The B1-B1' and B2-B2' in Figure 4.8 show the longitudinal profiles along the flow direction where boils were directly observed by the ADCP and where boils were not directly observed, respectively. Figure 4.9 and 4.10 show the following along B1-B1' and B2-B2' respectively a) depth averaged sediment concentration $\overline{c_s}$, total concentration near the bed, c_{b_total}, and flow depth, b) depth average flow velocity *U*, shear velocity calculated using ADCP bedload velocity (equation (3.3)) u_{*b}, shear velocity calculated as $u_{*ghi} = \sqrt{ghi}$, and the c) the maximum and minimum vertical velocity calculated using equation (4.1-4.2) along with c_{b_total} and flow depth. Vertical profiles of sediment concentrations estimated using equation (4.1-4.2) at two different points along streamline at 140m and 180m are shown in Figure 4.9 d) and e) respectively.

Figure 4.9 and Figure 4.10 a) show a bed form consisting of superimposed dunes with depths varying from 6m-14m, similarly the depth averaged sediment concentration, $\overline{c_s}$, and sediment concentration near the bed, c_{b_total}, show a pattern that can be correlated with the bed shape. In Figure 4.9 a) a sharp increase in bed c_{b_total} is observed along with an increase in $\overline{c_s}$, around 150m distance along streamline due to boil. Subsequently, this

high concentration decreases suddenly around 230m-280m. This is due to the vertical flow structure of boil, as observed in Figure 2.2.

Figures 4.9 and 4.10 b) show the difference in flow velocity due to the bed shape. Velocity, *U*, varies between 2.3 m/s and 1.0 m/s at the bedform crests and at the lee side of the bedform respectively. The effective shear velocity u_{*b} shows higher value than the one calculated as $u_{*ghi} = \sqrt{ghi}$. This difference is most prominent at bed form crests and at flow reattachment points downstream of the crests.

Figure 4.9 c) shows a large upward flow where boil was observed, this can be correlated with the location where high depth averaged sediment concentrations were observed in Figure 4.9 a). In Figure 4.9 and Figure 4.10 c) vertical flow structure due to bed shape can be seen. An upward flow is observed at the stoss side of the bedform, whereas downwards flow is observed over the crests and on the lee side of the bed form. Higher concentrations near the bed is also observed where a downward flow exists.

Figure 4.9 d) and e) show the vertical profiles of sediment concentrations before and during the occurrence of boil. Figure 4.9 e) shows high upwards velocities near the water surface corresponding with an increasing sediment concentration observed towards the water surface. The observation of high sediment concentrations near the water surface and high upward velocities are in agreement with the observations of boil in previous research (Best, 2009; Best et al., 2008; Coleman, 1969; Jackson, 1976; Nakagawa and Nezu, 1993).

4.4.3. **Boils due to bed shape and velocity differences**

The ‘boils of first kind’ appear behind bed form crests, manmade backwards facing steps and other areas where sudden velocity differences occur due to river bed shape (Biswas and Eswaran, 2002; Nakagawa and Nezu, 1993). Large scale boils were observed on the surface of the water during observations near Kazipur. The results of the dense measurements carried out near Kazipur are shown in Figure 4.11. Figure 4.11 a) shows vertical velocity contours and river depths measured by the ADCP in the area where sand-wave bedform was observed. The results of IDW interpolation of bed elevations and near-surface sediment concentrations are shown in Figure 4.11 b) and c), respectively, and the ADCP boat track shown in a) is also highlighted in b).

The ADCP boat track shown in a) indicates that the depth varies from around 14m at the crest to nearly 40m downstream of the crest. The vertical velocity contours indicate very large vertical velocities, observed immediately downstream of the crest. Figure 4.11 b) shows flow over a submerged bed form, similar to a ridge and a large depression immediately downstream of the ridge. Figure 4.11 c) shows sediment concentrations of around 1000mg/l in the upstream of the crest. Patches of high concentration, around 3500mg/l are observed downstream of the crest. These high concentrations are caused by boils observed downstream of the crest. The flow over the bedform can be categorized as similar to the flow over a backward facing step. Therefore flow convergence at the bedform crest and sudden expansion can explain the occurrence of ‘boil of first kind’ in this area. The intensity of boils observed at Kazipur is larger than the ones observed at Bahadurabad. This may be due to the difference in form roughness (related to shape of the bed form) between the two areas.

4.4.4. **Sandbars and banks**

During the field measurements near a sandbar, two kinds of flows were observed. In an area near the sandbar, flow velocity was high and active bank erosion was observed. In an area, immediately downstream of the sandbar, the flow velocities were low and erosion was not observed. Based on equation (3.3) it can be understood that the bedload velocity and non-dimensional bed shear stress are directly related to each other as shown by Egashira (2005) and Yorozuya et al. (2017). Therefore, bedload velocity, turbidity meter samples, Turbidity-NIR, and Acoustic Backscatter Turbidity (ABT) are used to discuss the behavior of fine sediment in an area where deposition may be dominated. Figure 4.3 shows the location of the measurements carried out immediately upstream of Jamuna Bridge, near Sirajganj.

Figure 4.12 shows three views of the ADCP dense measurement data, a) Turbidity-NIR and bedload velocity vectors, b) bed elevations (interpolated using the Inverse Distance Weighted method) and flow velocity vectors, and c) ABT measured by the ADCP. The bed elevations show the shape of the river bed representing the submerged part of the sandbar which gradually narrows downstream. Various points are highlighted in all three views of Figure 4.12 for discussion. Point 1, located in Channel A, shows the deepest location and a high flow velocity, although the Turbidity-NIR and ABT indicate low turbidity. Point 2 lies inside Channel B where the depth is large however flow velocity is lower than the one in Channel A at point 1, and turbidity is low. Point 3 shows a ridge-like feature and represents the shallowest point in this figure. Point 4 shows the shallow region immediately downstream of the sandbar, where the flow velocity and bedload velocity is low. Low flow velocity at Point 3 and around area D indicates that the

flow from the Channel A (Figure 3.5) does not get into area D. Furthermore, low turbidity is observed in this area based on Turbidity-NIR and ABT. This can be due to low shear stresses as a result of which, erosion is much smaller compared with deposition. The sediment transport in this area is therefore dominated by deposition as described by equation (2.2), (2.4) and (2.6). A submerged ridge exists where the flow from channel A flows over the submerged part of the sandbar as shown around Point 5. Higher shear stresses indicated by higher bedload velocities can be seen at this place, where higher Turbidity-NIR and ABT are also observed indicating sediment entrainment based on equations (2.3) and (2.5). At the Point 6, we can observe low bedload velocity, yet flow velocity is high. At this point the Turbidity-NIR and the ABT indicate higher turbidity. Based on low shear stresses and the observation of turbidity at this location, it is reasonable to infer that the sediment concentrations at this location are a result of sediment transportation by the flow, as described by equation (2.2).

4.5. Discussion

Figure 4.13 a) shows the particle size distribution of water samples and bed material from W1, W2, and B1 where no bedform or boils were observed. These locations e.g. W1 and B1 are shown in Figure 4.2. Figure 4.13 b) shows the particle size distribution regarding W15-W20, where boils were observed. Since no bed material samples were obtained within flow area of with boil and bedform, size distribution of the closest associated samples B4 and B6 are shown in Figure 4.13 b) and their location is illustrated in Figure 4.2 (Right). We observe that wash load (particle size <100μm) compose 60-90% of sediment in water samples. Similarly, the vertical sediment concentration from

area where flat-bed is observed (Figure 4.7) shows a large amount of finer particles (having small Rouse number) compared to suspended sediment.

In area with flat-bed conditions the depth averaged sediment concentration does not vary considerably in the longitudinal direction, as shown in Figure 4.7 a). However, in the area where bed form exists, the depth averaged sediment concentration varies in the longitudinal direction, even when boil is not directly observed. This variation, as shown in 4.10 a), can be correlated with the bed form shape and can be caused by variation in effective shear velocity over the bed form and the vertical flow structure as shown in Figure 4.8 a).

It is observed that despite low values of C_{ae}, very high sediment concentrations (~2000mg/l) exist in area where boils are observed. This high sediment concentration is believed to be contributed by boil phenomenon. The water samples from boil area (Figure 4.13 b)) show that particles larger than 100μm comprise between 20-40% of total composition. Whereas in samples from no-boil area (Figure 4.13 a)) particles larger than 100 μm are <10% of the total composition. This shows that the force generated by the boil lifts the larger particles, and this strength is larger than the one estimated as τ^*. The Figure 2.2 and Figure 4.8 c) show that large sediment concentrations exists due to boil which rapidly decreases in the absence of boil. Therefore, discussion based on these figures also indicates that the lift force of boil is larger than τ^*.

Equation (4.1- 4.2) are used to calculated the sediment concentration near the bed and the vertical sediment concentration profile for non-uniform sediment size classes. For this purpose, five equal sediment size classes are derived from water samples obtained from each flow area. Figure 4.7 d) and e) show the vertical sediment concentration profile in

area where flat-bed conditions exist and sediment transport is assumed to be in equilibrium. From Figure 4.7 d) and e) it can be observed that the vertical profile of d_{10}, d_{30}, d_{50}, and d_{70} (particle size 5.5μm~88μm) show a nearly vertical concentration profile, whereas d_{90} (particle size 155μm) shows a much larger concentration near the bed which decreases to nearly zero near to the free surface. This observation is consistent with Rouse (1937), where finer particles have nearly vertical sediment concentration, whereas concentration of the larger particles is nearly zero at the free surface and increases exponentially near to the bed.

Figure 4.14 shows the equilibrium concentration near the bed for each non uniform sediment class, against w_0/u_*, based on the observations in flat bed conditions where equilibrium sediment transport conditions can be supposed. The results of c_{ae} - w_0/u_* relation based on studies by Garcia and Parker (1991), Lane and Kalinske (1941), Itakura and Kishi (1980), and Ashida and Michiue (1970) are also shown for comparison. The figure shows that the c_{ae} of d_{10}, d_{30}, d_{50}, and d_{70} (particle size 5.5μm~88μm) is nearly the same whereas the c_{ae} of d_{90} (particle size 155μm) is much larger and is close to the results from previous studies. The results of the four smaller sediment size classes appear in contrast to the relations proposed by previous studies, according to which c_{ae} should increase as relative fall velocity, w_0/u_* decreases. The difference between the observed result and the results of the previous studies can be understood by the sediment size distribution of the water samples and bed samples shown in Figure 4.13 a). The four finer size classes d_{10} ~ d_{70}, comprising 80% of the water sample, are not present in the bed material in considerable quantity. Whereas the d_{90} size class is present in the bed. In contrast, the studies carried out by Garcia and Parker (1991), Lane and Kalinske (1941),

Itakura and Kishi (1980), and Ashida and Michiue (1970) are based on results from laboratory or field data where sediment size is between 80-350μm and is well represented in the bed.

In the current model, the erosion term for very fine particles is described by equation (2.5) and is a function of bed deformation and does not depend upon shear velocity. Very fine sediment (<100 μm) is found in large quantities in the flow body even in areas where boil is observed. We would like to consider the concentration of such very fine sediment as a function of shear velocity. In the Figure 4.14, equation (2.17) proposed by Ashida and Michiue is used to fit the observation results where $K = 0.004$ and $\beta = f(w_0) = 25.2\, w_{0i}^{1.03}$.

To understand the boil phenomena in further detail particularly to understand sediment transport due to boil, Figure 4.15 shows 100m to 340m distance along streamline B1-B1' where boil is observed. Figure 4.15 a) shows total concentration observed near the bed, $c_{b\_observed}$, shear velocity calculated as $u_{*ghi} = \sqrt{ghi}$, and C_{ae} calculated using the relation (2.17) (Ashida and Michiue, 1970). The distance along streamline from point B1 (Figure 4.8) is shown along the x-axis. For the purpose of discussion, few selected vertical sediment concentration profiles along the streamline are also shown. Point b) shows the location at 140m along the streamline, this point is located at the bed form crest, the vertical velocity is minimal and the concentration profile is similar to the one observed in flat bed conditions. The point c) is located at 154m where large concentration is observed near the bed. At this location the shear velocity ($u_{*ghi} = \sqrt{ghi}$) shows an increase, and the sediment concentration near the bed, $c_{b\_observed}$ is much higher than at point b). A large upwards velocity is also observed near the bed due

to boil vortex. The point d) is located at 170m along streamline, as the boil vortex rises from point c) to d), the high concentrations and upwards vertical velocity are observed near the bed and also near the water surface. The point e) is located at 225m, at this high concentration near the bed due to boil decreases compared with point c) and d), high concentration near the water surface due to boil is a result of transportation. Subsequently, after around 220m the high concentration due to boil shows a sudden decrease, this is can be related to the downwards flow observed in Figure 2.2 b) at ii).

The observation by the ADCP can be used to calculate the relationship between total non-dimensional bed shear stress, τ_*, and non-dimensional bed shear stress due to grain roughness, τ_*'. Using the equation proposed by (Einstein and Barbarossa, 1952):

$$\frac{U}{\sqrt{gR'I}} = 6.0 + 2.5ln\frac{R'}{k_s} \tag{4.3}$$

Where U is the depth-averaged velocity measured by ADCP, ks is the equivalent roughness equal to 2.5 times mean particle diameter, g is the gravitational acceleration, I is the average slope and R' is hydraulic radius due to skin friction. Using this method, the τ_*' and the bed shear stress due to form drag, τ_*'' can be calculated as follows.

$$\tau_*' = R'I/sd \tag{4.4}$$

$$\tau_*'' = \tau_* - \tau_*' \tag{4.5}$$

Several researchers have proposed methods to predict the occurrence of bedform using the relationship between τ_* and τ_*' (Engelund and Hansen, 1967; Kishi and Kuroki, 1973; Kudo et al., 2017). Figure 4.16 shows the relation between τ_* and τ_*' showing observation results from area where bedform is observed. The τ_* is calculated as $\tau_* =$

RI/sd, and τ_*' is calculated using three different methods 1) using observed velocity by the ADCP and using equation (4.3) and (4.4), 2) using the Kuroki & Kishi (1973) method, and 3) using the Kudo et al. (2017) method. The results indicate that the method proposed by Kudo et al. (2017) provides a more reasonable agreement with the results obtained using equation (4.3) and (4.4). This may be reasonable because the observed *R/d* is large, ranging from 28000 to 39000 and in such cases Kudo et al (2017) may be more appropriate compared with Kishi & Kuroki (1973).

5. Modeling the effect of Boils in a 2-D numerical model

5.1. Introduction

Various researchers have observed ‘boils of first kind’ during observations in natural rivers (Best et al., 2008; Coleman, 1969; Gul et al., 2018; Jackson, 1976) where bedform occurred, and linked it with a sudden increase in sediment suspension. In particular boils are observed where bedform exists, such boils are attributed to coherent turbulent structures that form near the bed behind bedform crests and are able to lift large amounts of sediment to the water surface. Boils thus control the spatial and temporal distribution of suspended sediment in addition to the turbulent diffusion processes; therefore they are important to consider in the governing equations of the current 2-D numerical model.

Despite its significance in sediment transport, the current 2-D numerical model (as described in Chapter 2) cannot model the occurrence, or the sediment transport due to ‘boil of first kind’. Although qualitative descriptions of such phenomena and their flow structure have been well documented (Best, 2005; Coleman, 1969; Lapointe, 1992; Nakagawa and Nezu, 1993; Noguchi, K. Nezu, I. Sanjou, 2008), their discussion has fallen short of creating a method to model sediment suspension due to boils.

Due to the importance of ‘boils of first kind’ to the sediment transport processes in large rivers, it is important to devise a method to model the sediment entrainment due to boil in the current 2-D numerical model. In this chapter, the existing model for sediment entrainment, as described by Ashida and Michiue (1970) is used to describe erosion and deposition due to boils. The proposed treatment of the erosion and deposition term can be used to simulate sediment transport due to boil in the 2-D numerical model.

5.2. Conceptual model of sediment transport due to boils

The occurrence of 'boils of first kind' over a dune bedform has been discussed in Chapter 2 in view of past research, and in detail based on measurements conducted in the field in Chapter 4, in particular the discussion based on Figure 2.2 and Figure 4.15 allows us to understand the sediment transport due to boil along a stream-pass. Therefore, to understand the effect of boils on the suspended sediment transport, at first we can develop a conceptual model considering mass conservation of suspended sediment in a 1-D model by neglecting the terms associated with transverse and temporal changes in equation (2.2)..

Figure 5.1 shows the conceptual model showing depth averaged concentration, $\overline{c_s}$, erosion and deposition as E_s and D_s respectively, along a stream-pass where boil is observed. Several vertical sections are highlighted for discussion at various distances. It assumed that hydraulic parameters (such as $u_* = \sqrt{ghi}$) are constant along the stream-pass. It can therefore be assumed that, equilibrium condition exists before the occurrence of boil at the point a). At this location the vertical sediment concentration profile is controlled only by turbulent diffusion processes, e.g. as described by Rouse (1937).

Point b) identifies the place where a boil vortex is generated near the river bed. At this point large turbulent shear forces exist near the bed, and locally, the shear velocities increase to a much higher number than that estimated using $u_* = \sqrt{ghi}$. Because of the higher shear velocities due to boil, the equilibrium concentration near the bed increases, and therefore the erosion increases. The increase in the equilibrium concentration near the bed due to boil is highlighted in Figure 5.1 b) as c_{aeb}. Thereby, due to the erosion caused by boil, the vertical sediment concentration profile at b) changes in reference to the one observed at a), this change is subsequently highlighted by a red line.

The turbulent vortex extends and rises vertically to the surface as a boil and dissipates, the depth averaged concentration reaches its maximum. At this point, shown as c), the turbulence near the bed due to boil does not exist, and therefore $c_{aeb} = 0$, the concentration near the bed can be modelled as under equilibrium condition (as shown in vertical profile at a).

Subsequently, a downwards flow structure is observed due to boil at point d) which acts as a downwards force on the suspended sediment particles. This can also be explained using equation (4.2), where a downwards flow (negative *w* velocity) increases the Rouse number, therefore the sediment concentration increases near the bed. It therefore means, such flow structure increases the sediment concentration near the bed in addition to the equilibrium concentration that exists due to the local shear velocity, consequently causing an increase in deposition of sediment particles. This increase in sediment concentration near the bed due to boil flow structure is shown in vertical profile d) as c_{bb}.

The last point is highlighted as e) where the erosion and deposition become equally active and therefore equilibrium conditions exist. The vertical sediment concentration profile at this location is expected to be the same as the one at point a).

5.3. 2-D numerical modeling of boil phenomena

5.3.1. Equilibrium concentration near the bed due to boil

Ashida and Michiue, (1970) used kinematic statistics on flow and particle motion near the river bed to understand the entrainment rate and the reference concentration near the bed, as described in equation (2.17).

The distribution of velocity of particles near the bed ($f(w_p)$) can be explained using a normal distribution as shown in equation (2.11). The spread of this distribution is governed by σ_p which is a function of shear velocity, and is determined experimentally as follows:

$$\sigma_p = \beta u_* \tag{5.1}$$

Where β may vary based on sediment size, however it is determined experimentally as $\beta = 0.83$ for sediment size 80~350μm (Ashida and Michiue, 1970). Such experimental conditions imply modeling of normal turbulent diffusion process and have no consideration for velocity of particles near the bed during occurrence of boil. During boil, much larger turbulence exists near the bed, therefore it can be considered that during boil:

$$\sigma_p = \alpha\beta u_*, \text{ where } (\alpha > 1) \tag{5.2}$$

The value of α is proportional to the intensity of boil, $\alpha > 1$ would mean larger particles may be entrained. To illustrate this, Figure 5.2 shows the standard normal distribution curve with highlighting the probability of entrainment based on equation (2.19). Where $\xi_0 = \frac{w_0}{\alpha u_*}$, and $\alpha = 1$ for the case where boil does not exist, and it is assumed that $\alpha = 2$ in the case when boil occurs. It can be seen that probability of entrainment would be significantly larger in the case of boil.

Subsequently, the equilibrium sediment concentration near the bed, which can be described as a function of shear velocity can be considered as:

$$c_{ae} = f(\sigma_p = \beta u_*) \tag{5.3}$$

Where f is the function defined by Ashida & Michiue (1970) as shown in equation (2.17). The conceptual model of boil which is based on the results of field measurements shows that larger shear velocities would exist due to boil. Due to this, a larger equilibrium concentration exists near the bed, which is referred to as C_{aeb}. Based on equation (2.17), a relation for C_{aeb} can be given as follows:

$$c_{aeb} = f\left(\sigma_p = \alpha\beta u_*\right) \tag{5.4}$$

Where f is the function defined by Ashida & Michiue (1970) as shown in equation (2.17). The equation (5.4) should be employed when boil occurs. The value α can be determined using the results of measurements in area where boil is observed and is related to the intensity of the boil. Figure 5.3 shows the relation between the bed shear stress due to form roughness (τ_*'') and the α. The τ_*'' is calculated using equation (4.3)-(4.5) using ADCP observations in flat bed conditions as well as in flow area where bedform and boil is observed. Equation (5.4) is used to calculate α as the unknown, while u* is calculated as $u_* = \sqrt{ghi}$ and C_{aeb} is the observed sediment concentration near the bed.

$$\alpha = e^{0.135\tau_*''} \tag{5.5}$$

The relation indicates that the increasing intensity of boils, indicated here by α, can be modelled as a function of form roughness, τ_*''. In Figure 5.3, the lowest value of τ_*'' which is calculated in an area where boils are observed is highlighted. More elaborate studies may be required to understand the boil of first kind in the initial stages of bedform development to determine the critical value of τ_*'', above which boils may be observed. However, in this study, the minimum value of τ_*'' observed in the boil area ($\tau_*'' = 0.4$), is used as the critical threshold for boil generation.

5.3.2. **Concentration near the bed due to boil flow structure**

Equation (2.9) can be written in the depth integrated form as follows:

$$\int_a^h c_{si}\,(z)\,.\,dz = c_{ai}\int_a^h \left[\frac{h-z}{z}.\frac{a}{h-a}\right]^{z_{*i}}.dz \tag{5.6}$$

$$c_{ai} = \frac{\overline{c_{si}}.h}{\int_a^h \left[\frac{h-z}{z}.\frac{a}{h-a}\right]^{z_{*i}}.dz} \tag{5.7}$$

Where $z_{*i} = {}^{w_0}/_{\kappa u_*}$ is given as in the equation (2.10), therefore for a known depth-averaged sediment concentration $\overline{c_{si}}$, depth h, and z_{*i}, the concentration near the bed can be calculated using equation (5.7).

A downwards flow due to boil is observed as part of the boil flow structure which causes an increase in sediment deposition, resulting in a sudden decrease in the concentrations. This increase in deposition as a result of a downward flow due to the boil flow structure therefore also needs to be modelled in the 2-D numerical model.

Equation (5.7) may be used to model such concentration near the bed due to boil, by using the following treatment:

$$c_{bb} = \frac{\overline{c_s}.h}{\int_a^h \left[\frac{h-z}{z}.\frac{a}{h-a}\right]^{z_*}.dz} \tag{5.8}$$

$$z_* = \frac{w_0 - w}{\kappa u_*} \tag{5.9}$$

Where c_{bb} is the concentration near the bed due to boil flow structure, and the rouse number, z_*, is calculated using the equation (5.9). As w is modelled as a part of boil flow structure, increasing intensity of boil is expected to have a larger magnitude of w.

Negative w velocity (downwards flow) increases the rouse number, and can therefore model the larger concentration near the bed due to boil. It is worth to be noted here that considering the derivation process of the rouse equation as discussed in Section 2.2, such treatment is used with apprehension and for lack of better alternatives to model the vertical distribution of concentrations during boil.

The *w* velocity can be observed downstream of the boil observation near the crest of the bed form, e.g. as shown in Figure 2.2 (b) at location (ii), and shown in the conceptual model in Figure 5.1 at point (d). Figure 5.4 shows the relation between the bed shear stress due to form roughness (τ_*'') and the w velocity. The equation 5.8 is used to calculate w as the unknown, while u* is calculated as $u_* = \sqrt{ghi}$ and C_{bb} is the observed sediment concentration near the bed. The relation indicates that the downwards flow, w, can be modelled as a function of form roughness, τ_*'' as follows:

$$w = -0.007\tau_*'' \tag{5.10}$$

The above relation is obtained with an $R^2 = 0.74$ where the τ_*'' is calculated using the equation 4.3-4.5 using 31 ADCP observations along the direction of flow, in flat bed conditions as well as in flow area where bedform and boil is observed.

5.3.3. **Timing and occurrence of boils**

Boils of first kind are commonly observed in large rivers where bedform exists. Based on the results of measurements of boil in Bahadurabad and Kazipur, it can be concluded that larger boils are observed where bed shape is steeper and large differences exist in velocity over dune crests and over the flow separation zone. Similarly, the size and

intensity of these boils is found to be proportional to bed shear stress due to form roughness (τ_*'') (Babakaiff and Hicken, 1996; Jackson, 1976).

Several researchers have proposed methods to predict the occurrence of bedform using the relationship between total non-dimensional bed shear stress (τ_*) and non-dimensional bed shear stress due to grain roughness (τ_*') (Engelund and Hansen, 1967; Kishi and Kuroki, 1973; Kudo et al., 2017).

Furthermore, discussion based on Figure 4.8 c) shows that boil is an intermittent phenomena. The mean period between boils is given by equation (2.23), as proposed by Jackson (1976). However, Nezu et al. (1980) obtained a similar relation by observations of 'boil of first kind' in a laboratory flume, where , $\bar{T}_{boil} = {(2\sim3)\ h}/{U_{max}}$. Similarly, the mean duration of boil observed at the water surface is given as $\overline{Dur}_{boil} = {1.75\ h}/{U_{max}}$ by (Jackson, 1976). Therefore the mean time period of boil of first kind and its duration can be described as:

$$\bar{T}_{boil} = {2.5\ h}/{U_{max}} \tag{5.11}$$

$$\overline{Dur}_{boil} = 0.7\ \bar{T}_{boil} \tag{5.12}$$

The boil phenomena can therefore be modelled under the following conditions, 1) bedform exists based on $\tau_* - \tau_*'$ relation (as described by Kudo et al. (2017)), and 2) the frequency of boil occurrence is determined a function of flow velocity and depth as shown in equation (2.12).

5.3.4. **Governing equations in treatment of boil phenomena**

The governing equations of 2-D numerical model can be modified based on the above discussion. The boil influence the erosion term due to existence of high turbulent near the bed, which is able to entrain larger particles, this increased equilibrium concentration near the bed is described earlier as c_{aeb} in equation (5.4). Similarly, a downwards flow observed downstream of boil, is part of the boil flow structure. This downwards flow, causes an increase in the concentration near the bed, which is modeled as c_{bb}, as shown in equation (5.8).

The expression of mass conservation of sediment entrained in flow body is given in equation (2.2), subsequently the mass conservation of bed sediment is given by equation (2.10) where the erosion and deposition terms are described as follows:

$$E_s = c_{aeb}.w_0 \tag{5.13}$$

$$D_s = c_{bb}.w_0 \tag{5.14}$$

Figure 5.3 illustrates a flow chart showing how sediment transport due to boil of first kind may be modelled using the treatment proposed above. First, the $\tau_* - \tau_*'$ relation proposed by Kudo et al. (2017) is used to determine whether bedform exists. In the case where τ_*'' is larger than the critical value for boil occurrence, τ_{*bc}'' , mean period of boil is calculated based on equation (5.11) and α is determined as shown in equation (5.5). Based on the timing of the boil (periodicity, and active boil duration), equation (5.13) and (5.14) are employed at the time when boil occurs, otherwise the erosion and deposition terms are calculated without any treatment of boil as follows:

$$E_s = c_{ae}.w_0 \tag{5.15}$$

$$D_s = c_b.w_0 \tag{5.16}$$

Where c_{ae} is calculated by the equation (5.3) using the Ashida & Michiue (1970) equation, and c_b is calculated by the equation (5.7).

Based on the conceptual understanding of the erosion and deposition due to boil as discussed based on Figure 5.1, the treatment for the boils may be spatially disaggregated at the bedform scale. A single wavelength of the bedform, defined from crest to crest, may be further divided into 4 regions R1, R2, R3 and R4. R1 comprises of the region where flow detachment at the bedform crest and the bed shear stress and erosion are nearly zero. R2 is the region where flow reattachment occurs, and erosion due to boil is observed. Similarly, R3 is the region where sediment is transported and the erosion and deposition is not affected by the boil. Finally, R4 is the region where higher deposition is observed due to the flow structure of boil. For an area where boil occurs based on the $\tau_* - \tau_*'$ relation, the erosion and deposition terms in each of these regions is summarized in Table 5.1. The table also shows the percentage area within a single wavelength of the bedform for each of these regions based on observation results. This proposed method to treat the erosion and deposition due to boil for different regions of the bedform is currently not implemented in numerical model. However this may be used in the future for a comprehensive modeling of erosion and deposition terms for the treatment of boils.

5.4. Numerical simulation of channel changes using the proposed treatment

5.4.1. Governing equations

2-D numerical simulation of channel changes is conducted in order to check the validity of the proposed treatment. The governing equations comprise of the mass and momentum conservation of flow, and the mass conservation of bed sediment and the sediment entrained in flow body as described in Takebayashi and Egashira, (2001); Takebayashi and Okabe, (2009). The equations for 2-D mass conservation and momentum conservation of flow are:

$$\frac{\partial h}{\partial t}+\frac{\partial}{\partial x}(\bar{u}h)+\frac{\partial}{\partial y}(\bar{v}h)=0 \tag{5.17}$$

$$\frac{\partial \bar{u}h}{\partial t}+\frac{\partial \overline{uu}h}{\partial x}+\frac{\partial \overline{uv}h}{\partial y} = -gh\frac{\partial}{\partial x}(h+z_b)-\frac{\tau_x}{\rho}+\frac{1}{\rho}\left(\frac{\partial}{\partial x}(h\sigma_{xx})+\frac{\partial}{\partial y}\left(h\tau_{yx}\right)\right) \tag{5.18}$$

$$\frac{\partial \bar{v}h}{\partial t}+\frac{\partial \overline{vu}h}{\partial x}+\frac{\partial \overline{vv}h}{\partial y} = -gh\frac{\partial}{\partial y}(h+z_b)-\frac{\tau_y}{\rho}+\frac{1}{\rho}\left(\frac{\partial}{\partial y}\left(h\sigma_{yy}\right)+\frac{\partial}{\partial x}\left(h\tau_{xy}\right)\right) \tag{5.19}$$

Where h is water depth, t is time, x and y are horizontal directions perpendicular to each other, $\bar{u}$ and $\bar{v}$ are the depth averaged velocity in the x and y direction respectively, z_b is bed elevation, g is acceleration due to gravity, ρ is the density of water σ_{xx}, σ_{yy} , τ_{xy} and τ_{yx} are the depth-averaged Reynold's shear stresses and τ_x and τ_y are the x and y components of the bed shear stress.

The 2-D mass conservation of sediment entrained in flow body is described as:

$$\frac{\partial \bar{c}h}{\partial t} + \frac{\partial \overline{cu}h}{\partial x} + \frac{\partial \overline{cv}h}{\partial y} = \frac{\partial}{\partial x}(h\varepsilon_x \frac{\partial \bar{c}}{\partial x}) + \frac{\partial}{\partial y}(h\varepsilon_y \frac{\partial \bar{c}}{\partial y}) + E - D \quad (5.20)$$

Where $\bar{c}$ is the depth-integrated concentration of suspended sediment ($\overline{c_s}$). ε_x and ε_y are the coefficient of diffusion in the *x* and *y* direction. E and D are the erosion and deposition terms.

The equation of mass conservation of bed sediment is described for calculating the temporal change in river bed elevation given as follows:

$$\frac{\partial z_b}{\partial t} + \frac{1}{1-\lambda}\left(\frac{\partial q_{bx}}{\partial x} + \frac{\partial q_{by}}{\partial y} + E - D\right) = 0 \quad (5.21)$$

Where λ is porosity, q_{bx} and q_{by} is the x and y components of bedload transport rate respectively, which is calculated using the method by Ashida and Michiue, (1972).

Two different cases are calculated. In the first case the model is run using conventional method without the proposed treatment of boil described in Section 5.3. The relation (2.17) (Ashida and Michiue, 1970), is used to calculate equilibrium concentration near the bed in which $\sigma_p = \beta u_*$ as described in equation (5.3).

The second case is run using the treatment of boil explained in the Section 5.3 and in Figure 5.5. The occurrence of boil is determined using the mean boil period and duration calculated using equation (5.5) and (5.6). Similarly, the τ_*'' is calculated using the equation (4.5) where the τ_*' is calculated using the method proposed by Kudo et al. (2017). The occurrence of boil therefore depends upon the τ_*'' where the $\tau_*'' > 0.4$, and the timing and duration of the boil. When boil occurs, the Ashida and Michiue (1970) equation (2.17) is used to calculate equilibrium concentration near the bed using the treatment shown in equation (5.4), where α is determined using the equation (5.5). Similarly, where the $\tau_*'' <$

0.4 or the criteria for the timing of the boil is not met, the erosion and deposition terms are treated the same as in the case without boil.

5.4.2. **Calculation conditions and boundary conditions**

In order to check the validity of the proposed treatment, a 500m wide and 10km long experimental channel is set up. The purpose of the numerical simulation is to compare the bed deformation and sediment transport characteristics in a domain with and without the treatment for boil. The channel is divided into 14,028 grid cells, each 20m by 20m. Initially, the channel has a flatbed where the bed slope is 1/7200. Non-uniform sediment size is implemented with 2 sediment size classes which are 0.00019m and 0.00008m composing 90% and 10% of the sediment by weight. The angle of repose of sediment is set as 34˚. Both the bedload and suspended load are considered for calculating the variation of the bed elevation. A steady flow discharge of 2280m^3/s is used as the discharge boundary condition, The initial channel water depth is around 4.5m, and non-dimensional bed shear stress, $\tau_* = 2.0$. The duration of the simulation is 5 days, whereas the time-step of the calculation is set as 0.2s.

5.4.3. **Results**

Figure 5.6 shows the channel shape in both boil and no-boil cases after 5 days of computation. It can be seen that a channel has formed in both cases; however the channel planform is different for each case. In addition, in the boil case, the channel depths (m) are larger than in the no- boil case, with a difference of 2-4 meters in the main channels.

The $q_s/(q_s + q_b)$ ratio calculated for both cases is nearly equal to one; therefore in both cases, the mode of sediment transport is dominated by suspended sediment. Figure 5.7 shows the distribution of unit suspended sediment discharge, q_s, in a plan view. It can be seen that q_s is significantly large in the boil case, particularly in the main channel (close to the right bank).

In order to understand the temporal change in sediment transport rate in both cases, the cross-sectional shape and sediment transport rate are calculated in the middle of the reach highlighted as A-A' and B-B' for both no-boil and boil cases, respectively. Figure 5.8 shows the suspended sediment discharge, Q_s (m^3/s), obtained in the highlighted section for both cases. It can be seen that Q_s is around 40~45 percent larger in the boil case. Q_s for both cases follows a similar pattern with respect to time, as the sediment discharge peaks around 30~45 hours and subsequently decreases and becomes stable. However, note that although the pattern of events is similar for both cases, the time of these events is sooner for the boil case.

To investigate further, with respect to the channel shape and planform in these events, a few notable points are highlighted in time in Figure 5.8 as a1, a2, b1, and b2, which are the local minimum and maximum before a sharp decrease in sediment transport rate occurs. Subsequently, a3 and b3 can be identified as a high sediment transport rate after the sharp decrease, and finally the last points are at the end of the 5 day computation shown as a4 and b4.

In order to highlight the difference in sediment transport rate and channel shape in relation to the boil and no-boil cases, how these characteristics change in a cross-section with time should be examined. Figures 5.9 and 5.10 show the channel shape and unit

suspended sediment discharge in cross-sections A-A' and B-B' at the time of events highlighted in Figure 5.8. Figure 5.9 shows that the channel shape is nearly flat at a1, which indicates that the channel has not formed at this stage. q_s is also lower at a1 than at a2. Similarly, at a3, sandbars have developed (where the depth is close to 0), and a channel has formed at the center. Similarly, Figure 5.10 shows that the channel is still forming at b1 and b2, where sediment is being transported across the whole cross-section. During the short time between b2 and b3, sandbars have formed and a deep channel exists near the middle. However, at b4, the channel near the left bank has a remarkably smaller q_s compared with time b3, and a large q_s is observed near the right bank. The channel depths in the boil and no-boil cases appear to be much larger, and the unit sediment discharge also appears to be larger. Based on Figures 5.8 -5.10, it can be concluded that the suspended sediment discharge and the bed form migration rate in the boil case is larger.

The results also indicate that the suspended sediment transport rate is significantly larger in the boil case, which corresponds to the observations in an boil area where larger sediment concentrations are observed due to boils (as discussed in Chapter 4). This increased sediment transport rate is linked with faster channel and bar formation compared with the no-boil case as shown in Figures 5.8 – 5.10. It can also be seen that once the channel and bars are formed in the boil case (after 60hrs), a small-scale variation in Q_s is observed, which cannot be seen for the no-boil case. This variation in the sediment transport rate is indicative of the simulated intermittence of boil phenomena in the upstream area, based on equations (5.11) and (5.12).

6. Conclusions and policy implications

6.1. Conclusions

The present research creates a fundamental understanding of sediment transport processes in a large, fine sediment-dominated river. To verify the current model in an actual river, measurements were conducted in a large, fine sediment-dominated river in different flow conditions. It was found that the current model cannot represent the boil phenomena, which is a common occurrence in large rivers. Subsequently, a method is proposed to treat boils of first kind by modifying the 2-D numerical model.

Chapter 1 provides an overview of the river management challenges in the Indus River. In particular, it is highlighted that the channel changes caused by various barrage structures posed an increasing risk of flooding due to embankment breaches upstream and bank erosion downstream of the barrage. It was identified that such channel changes in large rivers such as the Indus could be modelled using the 2-D depth integrated numerical model. However, it was necessary to verify the current 2-D numerical model before it can be applied for modeling channel changes in large rivers dominated by fine sediment transport.

In Chapter 2, the current 2-D numerical model is discussed in relation to the transport of fine sediment as suspended sediment and wash load. Boils are also discussed as an important phenomenon often observed in large rivers, which is known to lift large amounts of sediment into suspension. The current understanding of boil phenomena is therefore discussed in relation to flow structure, sediment transport and frequency of occurrence.

The current numerical model, described in Chapter 2, requires rigorous verification before it can be implemented in large, fine sediment-dominated rivers. A comprehensive methodology to conduct measurements is discussed in Chapter 3. In addition to in-situ sampling of water and sediment, various surrogate measures of sediment concentrations are discussed. In particular simultaneous measurement of flow, shear velocity, suspended load and bedload can be determined using the ADCP to provide a complete picture of flow and sediment transport based on field measurements. Additionally, NIR data is shown to have a robust linear relationship with turbidity from field measurements. The resulting Turbidity-NIR can therefore be used as a surrogate measure to observe sediment concentrations over a large area. This has invaluable potential to be used in numerical modeling of large rivers for initial conditions and verification of results.

Measurements are conducted in different flow areas of a large, fine sediment-dominated river to verify the current numerical model. Chapter 4, discusses the results of these measurements in relation to the current numerical model. The results of the measurements show that the flow and sediment concentrations are largely influenced by the shape of the riverbed. It is shown that boil phenomenon, which is commonly observed in large rivers, cannot be described using the current model. It is observed that high concentrations near the bed exist where boils are generated, and sediment is carried to the water surface by the boil vortex. The vertical profile of sediment concentrations due to boils or due to flow structure over the bedform, may be modelled by considering a vertical velocity term in the existing model. Furthermore, the results indicate that boil intensity increases as bedform roughness increases.

In Chapter 5, based on a conceptual model of the sediment transport due to boils of first kind, a treatment is proposed to model boils in the 2-D numerical model. The occurrence and timing of boils are subject to bed-form roughness and flow conditions respectively. The governing equations for the treatment of boils in the 2-D numerical model are also described where the erosion and deposition terms are modified to model the boil phenomena. The numerical simulation of channel changes with and without the proposed treatment of boils is conducted in an experimental channel. The results show an increase in the suspended sediment transport rate, increase in channel depths and more active channel changes in the case where the treatment for boil is used. The simulated results confirm the observations in a flow area where larger suspended sediment transport is observed due to boil. It is therefore believed that the new treatment for boils proposed in this study may provide a reliable tool for flood managers to predict channel changes in large, fine sediment dominated rivers where such boils also occur. Based on the results, it is proposed that further studies should be carried out to conduct numerical simulations of channel changes in an actual river. The results of the simulation for channel changes as well as the suspended sediment concentrations can be verified based on the various methods outlined in Chapter 3.

6.2. Policy implications

6.2.1. Implications for river management in large fine sediment-dominated rivers

Channel changes in the Indus River have long affected the lives and livelihoods of people since as early as the Indus valley civilization. In more recent history, since the

confinement of the river between embankments and the construction of a cascade of barrages and river training works, the lower Indus River has experienced various sediment transport related challenges. Some of the actual problems pertaining to channel changes in large, fine sediment-dominated rivers have been highlighted in detail in the beginning of this study. However, there is a need for a scientific tool to model channel changes. This study aims to address these challenges by providing a scientific tool which can be used to predict channel changes in large fine-sediment dominated rivers.

The 2-D numerical modeling of channel changes is an effective scientific tool for predicting channel changes in an actual river. During field observations conducted in this study in a large, fine sediment-dominated river, boils are observed at various locations where a large increase in suspended sediment transport is observed. As the suspended sediment due to boil phenomena affects the sediment transport rate and channel changes, it is discussed in detail in this study. This study proposes modifications to the current 2-D numerical model to better represent the sediment transport processes, such as boils. The results of this study, therefore, improve the representation of observed physical processes in the numerical model and may improve the reliability of the model being applied to rivers where boils are observed. Furthermore, practical requirements and constraints for the prediction of channel changes using the 2-D numerical model are discussed in detail below.

6.2.2. **Requirements of initial conditions for numerical modeling of channel changes in large rivers**

It is imperative to consider the practical requirements to conduct the numerical modelling in actual rivers in terms of the initial conditions, boundary conditions, and the required human and computational resources.

It is also critical to obtain reliable initial conditions for numerical simulation, e.g., initial topography, sediment size distribution, and channel bathymetry. Table 6.1 shows the practical requirements related to initial conditions for the 2-D numerical model. Initial topography is usually obtained from satellite or aerial-based Digital Terrain Model (DTM). Increasingly better quality DTMs are now available to be used free of cost, such as the ALOS World 3D-30m (AW3D30) by JAXA at a 30m spatial resolution. Validation and correction of DTM may be done by obtaining GPS Ground Control Points (GCPs) during field measurements. Field measurements are also required to obtain the sediment size distribution of bed sediment at representative locations across the river reach. Such sampling is easy to conduct in a low flow regime using a standard shovel (to obtain samples from a bank or bar), or using dredge samplers (for channel bed material). Similarly, initial channel bathymetry can be obtained using the ADCP or Multi-Beam Sonar with considerations of feasibility and operational requirements.

6.2.3. **Requirements of boundary conditions for numerical modeling of channel changes in large rivers**

Table 6.2 shows requirements for the boundary conditions of discharge and water level for the 2-D numerical modelling of channel changes in large rivers. As it may not

be important to measure discharge during low flows when sediment transport is minimal, the discharge observation should be conducted at least at 3 hourly intervals during 'high flows'. 'High flows' here means discharge larger than a threshold value which is based on the flow and transport characteristics of the river. For numerical simulations at a reach scale, the observation at fixed measurement sites (e.g. barrage, weir, bridge) may be used, provided that the uncertainty in the observation is known. Similarly, discharge boundary conditions can also be observed using an ADCP with higher accuracy, although this may have operational or logistic constraints for continuous 3-hourly monitoring.

Uncertainty in observation of boundary conditions

The availability of reliable discharge and water level as boundary condition plays an important role in the numerical modelling of channel changes. The reliability and precision of the results of the numerical model would in turn be affected by the uncertainty in the initial and boundary conditions.

To understand how the uncertainty in the observation, e.g., discharge, is reflected in the uncertainty in the prediction of the target phenomena (e.g. suspended sediment concentration, bank erosion and bed deformation), the numerical model can be used to conduct Monte Carlo type simulations. Knowing the probability density function of the boundary condition such as the discharge, Monte Carlo type simulations can be conducted to map the uncertainty of upstream boundary to the uncertainty in the prediction of the target phenomena such as sediment concentrations or bank erosion.

6.2.4. **Requirements of validation for numerical modeling of channel changes in large rivers**

Robust methods for the validation of the results of numerical simulation are needed to understand the difference between observed and predicted results. Table 6.2 shows various methods to observe channel changes such as bank erosion and sandbar formation. Verification of channel changes can be carried out using satellite data, where satellite imagery at various resolutions can be used to identify bank shifting and sandbar formation. Similarly it is important to verify the results of sediment concentrations. This can be done using various methods discussed in Chapter 3. Satellite-based NIR (Chapter 3.4) information can be used to provide a spatial distribution of sediment concentrations and can be an extremely useful tools for river managers to investigate the spatial distribution of non-equilibrium erosion and deposition processes over a large area. Similarly, the ADCP can be used in conjunction with turbidity meter and water sampler for bathymetry, flow and sediment concentration using the field measurement system discussed in Chapter 3.2 and Chapter 3.3 and using a setup similar to the one illustrated in Figure 4.4.

In addition to the above mentioned requirements it may be important to mention the computational requirements and constraints for the 2D numerical modeling for large rivers. The computation time for the numerical modeling largely depends upon the size of the grid (number of cells) and the time step. For example the Guddu-Sukkur reach of the Indus, which is 110km long and approximately 20km wide, can be divided into 0.84million grid cells of 50m x 50m size (or finer). Mainstream consumer-grade workstations are able to compute as many as 1~2 million grid for a reasonable computation time without use of other specialized hardware. It is therefore feasible to use

2-D numerical simulation for prediction of channel changes in large rivers based on the present computational requirements.

Modeling of complex physical processes with limited data availability in time and space may increase model uncertainty. However, there is an increasing availability of low cost input dataset and improvement in observation techniques, some of which are discussed in detail in Chapter 3 of this study. Each requirement, therefore, may be fulfilled with the input with least constraints (as shown in Table 6.1 and 6.2).

7. References

Ashida K. and Michiue M. (1970) Study on the suspended sediment (1) Concentration of the suspended sediment near the bed surface. *Annuals No. 13B, Disaster Prevention Reserach Institute,*: 233–242.

Ashida K. and Michiue M. (1972) Study on hydraulic resistance and bed-load transport rate in alluvial streams. In: *Proceedings of the Japan society of civil engineers*, 1972, pp. 59–69.

Ashida K., Egashira S. and Kanayashiki T. (1981) Model for the Prediction Drainage of Wash Basins Load in Mountainous By Kazuo ASHIDA , Shinji EGASHIRA and Tadayoshi KANAYASHIKI. *Bulletin of the Disaster Prevention Research Institute* 31(3): 171–209.

Babakaiff C.S. and Hicken E.J. (1996) Coherent flow structures in Squamish River Estuary, British Columbia, Canada. In: Ashworth PJ et al. (ed.) *Coherent Flow Structures in Open Channels*. Hoboken, N. J, pp. 321–342.

Best J. (2005) The fluid dynamics of river dunes : A review and some future research directions. *Journal of Geophysical Research* 110: 1–21. DOI: 10.1029/2004JF000218.

Best J. (2009) Kinematics, Topology and Significance of Dune-Related Macroturbulence: Some Observations from the Laboratory and Field. *Fluvial Sedimentology VII*: 41–60. DOI: 10.1002/9781444304350.ch3.

Best J.L., Ashworth P.J., Sarker M.H., et al. (2008) *The Brahmaputra-Jamuna River,*

Bangladesh. *Large Rivers: Geomorphology and Management*. DOI: 10.1002/9780470723722.ch19.

Biswas G. and Eswaran V. (2002) *Turbulent Flows: Fundamentals, Experiments and Modeling*. IIT Kanpur series of advanced texts. CRC Press. Available at: https://books.google.co.jp/books?id=BBsdQPhrXugC.

Biswas R.K. (2016) *NUMERICAL PREDICTION OF CHANNEL CHANGES IN LARGE, BRAIDED RIVERS DOMINATED BY SUSPENDED SEDIMENT*.

Coleman J.M. (1969) BRAHMAPUTRA RIVER: CHANNEL PROCESSES AND SEDIMENTATION. *Sediment Geology* 3: 129–239.

Dogliotti A.I., Ruddick K.G., Nechad B., et al. (2015) Remote Sensing of Environment A single algorithm to retrieve turbidity from remotely-sensed data in all coastal and estuarine waters. In: *Remote Sensing of Environment*, 2015, pp. 157–168. Elsevier B.V. DOI: 10.1016/j.rse.2014.09.020.

Egashira S. (2005) Importance of Sediment in Rivers, and Issues in Sediment Transport Mechanics. *Nagare, The Japan Society of Fluid Mechanics* 24: 581–592.

Egashira S. and Matsuki K. (2000) A method for predicting sediment runoff caused by erosion of stream channel bed. *Proceedings of Hydraulic Engineering* 44: 735–740. DOI: https://doi.org/10.2208/prohe.44.735.

Egashira S., Miyamoto K. and Ito T. (1997) Bed-load rate in view of two phase flow dynamics. *Proceedings of Hydraulic Engineering* 41: 789–794.

Einstein H.A. and Barbarossa N.L. (1952) River Channel Roughness. In: *Trans. ASCE*, 1952, pp. 1121–1132.

Engelund F. and Hansen E. (1967) A monograph on sediment transport in alluvial streams. *Teknisk Forlag*. DOI: 10.1007/s13398-014-0173-7.2.

Ferderal Flood Commission (2010) *Annual Flood Report 2010*.

Gao P., Pasternack G.B., Bali K.M., et al. (2008) Estimating Suspended Sediment Concentration Using Turbidity in an Irrigation-Dominated Southeastern California Watershed. *Journal of Irrigation and Drainage Engineering* 134(2): 250–259. DOI: 10.1061/(asce)0733-9437(2008)134:2(250).

Garcia M. and Parker G. (1991) Entrainment of Bed Sediment into Suspension. *Journal of Hydraulic Engineering, ASCE* 117(4): 414–435.

Gaurav K., Sinha R. and Panda P.K. (2011) The Indus flood of 2010 in Pakistan: A perspective analysis using remote sensing data. *Natural Hazards* 59(3): 1815–1826. DOI: 10.1007/s11069-011-9869-6.

Gul A.A., Yorozuya A., Koseki H., et al. (2018) Analysis of bedform and boil based on observations in Brahmaputra River. In: *Journal of Japan Society of Civil Engineers, Ser. B1 (Hydraulic Engineering)*, 2018, pp. 925–930.

Iftikhar U. (2002) *Valuing the Economic Costs of Environmental Degradation Due to Sea Intrusion in the Indus Delta*. *IUCN, Sea Intrusion in the Coastal and Riverine Tracts of the Indus Delta-A Case Study.* IUCN-The World Conservation Union Pakistan Country Office, Karachi.

Iseya F. and Ikeda H. (1986) Effect of dune development on sediment suspension under unsteady flow conditions. *Proceedings Of Hydraulic Engineering*.

ISO (2016) *Water quality - Determination of turbidity. ISO, 7027-1*.

Itakura T. and Kishi T. (1980) Open channel flow with suspended sediments. *Journal of the Hydraulics Division, ASCE* 106: 1325–1343.

Jackson R.G. (1976) Sedimentological and fluid-dynamic implications of the turbulent bursting phenomenon in geophysical flows. *Journal of Fluid Mechanics* 77(3): 531–560.

Jamieson E.C., Rennie C.D., Jacobson R.B., et al. (2011) Evaluation of ADCP Apparent Bed Load Velocity in a Large Sand-Bed River: Moving versus Stationary Boat Conditions. *Journal of Hydraulic Engineering* 137(9): 1064–1071. DOI: 10.1061/(asce)hy.1943-7900.0000373.

Kale V.S. (2008) Himalayan catastrophe that engulfed North Bihar. *Journal Geological Society of India* 72(6): 713–719. Available at: http://www.scopus.com/inward/record.url?eid=2-s2.0-60549113383&partnerID=tZOtx3y1.

Khan M.A., Khajjak F.K., Kazi A.W., et al. (2011) *Report of the Flood Inquiry Commission*. Available at: http://www.pakissan.com/english/watercrisis/flood/report.of.flood.inquiry.commission.shtml.

Kishi T. and Kuroki M. (1973) Bed Forms and Resistance to Flow in Erodible-Bed Channels (I) : Hydraulic Relations for Flow over Sand Waves. *Bulletin of the Faculty of Engineering, Hokkaido University* 67. Hokkaido University: 1–23.

Kitsuda T., Okada S., Arai R., et al. (2006) Issues of River flow measurement method and Applied observation result using acoustic Dop- pler current profiler. *Advances in River Engineering, JSCE* 12: 133–138.

Kitsuda T., Yokoyama H., Hashiba M., et al. (2011) Technology for turbidity measurement using acoustic backscatter. *河川流量観測の新時代,第2巻* 2.

Kudo S., Yorozuya A., Koseki H., et al. (2017) Analysis of hydraulic resistance with field observation data. *Journal of Japan Society of Civil Engineers, Ser. B1 (Hydraulic Engineering)* 73(4): 769–774.

Lane E.W. and Kalinske A.A. (1941) Engineering calculations of suspended sediment. *Transactions, American Geophysical Union* 22: 603–607. DOI: 10.1029/TR022i003p00603.

Lapointe M. (1992) Burst-like sediment suspension events in a sand bed river. *Earth Processes and Landforms* 17: 253–270.

Latosinski F.G., Szupiany R.N., Guerrero M., et al. (2017) The ADCP's bottom track capability for bedload prediction: Evidence on method reliability from sandy river applications. *Flow Measurement and Instrumentation* 54(June 2016). Elsevier: 124–135. DOI: 10.1016/j.flowmeasinst.2017.01.005.

Lewin J., Ashworth P.J. and Strick R.J.P. (2017) Spillage sedimentation on large river floodplains. *Earth Surface Processes and Landforms* 42(2): 290–305. DOI: 10.1002/esp.3996.

Muller-Wilm U. (2016) Sentinel-2 MSI – Level-2A Prototype Processor Installation and User Manual. Available at: http://step.esa.int/thirdparties/sen2cor/2.2.1/S2PAD-VEGA-SUM-0001-2.2.pdf.

Nakagawa H. and Nezu I. (1993) *Turbulence in Open Channel Flows*. IAHR Monographs. Taylor & Francis.

Nechad B., Ruddick K.G. and Neukermans G. (2009) Calibration and validation of a generic multisensor algorithm for mapping of turbidity in coastal waters. In: *SPIE 9998, Remote Sensing for Agriculture, Ecosystems, and Hydrology XVIII*, 2009, pp. 1–11. DOI: 10.1117/12.830700.

Nezu I., Nakagawa H., Tokinaga A., et al. (1980) Visual study of large-scale vortical motions in open-channel flows. In: *Annual Conference of JSCE*, Kansai-Branch, 1980, pp. II–10.

Noguchi, K. Nezu, I. Sanjou M. (2008) Turbulence structure and fluid – particle interaction in sediment-laden flows over developing sand dunes. *Environmental Fluid Mechanics* 8: 569–578. DOI: 10.1007/s10652-008-9114-3.

Okada S., Yorozuya A., Koseki H., et al. (2016) Comprehensive measurement techniques of water flow, bedload and suspended sediment in large river using Acoustic Doppler Current Profiler. In: *13th International Symposium on River Sedimentation, ISRS 2016, At Stuttgart, Germany*, 2016, pp. 1274–1280.

Quang N.H., Sasaki J., Higa H., et al. (2017) Spatiotemporal Variation of Turbidity Based on Landsat 8 OLI in Cam Ranh Bay and Thuy Trieu Lagoon, Vietnam. *Water* 9(8). DOI: 10.3390/w9080570.

Rennie C.D., Millar R.G. and Church M.A. (2002) Measurement of Bed Load Velocity using an Acoustic Doppler Current Profiler. *Journal of Hydraulic Engineering* 128(5): 473–483. DOI: 10.1061/(asce)0733-9429(2002)128:5(473).

Rouse H. (1937) Modern Conceptions of the Mechanics of Fluid Turbulence. *Trans. Am. Soc. Civ. Eng.* 102.

Syvitski J.P.M. and Robert Brakenridge G. (2013) Causation and avoidance of catastrophic flooding along the Indus River, Pakistan. *GSA Today* 23(1): 4–10. DOI: 10.1130/GSATG165A.1.

Takebayashi H. (2005) River Configuration in Middle-Lower Reach of River Basin. *Journal of Japan Society of Fluid Mechanics* 24(1): 27–36.

Takebayashi H. and Egashira S. (2001) Formative process and domain of a self-formed stream Channel. *Proceedings of the JSCE* (677): 75–86. DOI: https://doi.org/10.2208/jscej.2001.677_75.

Takebayashi H. and Okabe T. (2009) Numerical modelling of braided streams in unsteady flow. *Proceedings of the Institution of Civil Engineers - Water Management* 162(3): 189–198. DOI: 10.1680/wama.2009.00011.

Teixeira L.C., de Paiva J.B.D., da Silva Pereira J.E., et al. (2016) Relationship between turbidity and suspended sediment concentration from a small hydrographic basin in Santa Maria (Rio Grande do Sul, Brazil). *International Journal of River Basin Management* 14(4). Taylor & Francis: 393–399. DOI: 10.1080/15715124.2016.1198911.

USEPA (1993) *Method 180 . 1 : Determination of Turbidity by Nephelometry*. Available at: https://www.epa.gov/sites/production/files/2015-08/documents/method_180-1_1993.pdf.

Wood M.S. and Teasdale G.N. (2012) *Use of surrogate technologies to estimate suspended sediment in the Clearwater River, Idaho, and Snake River, Washington, 2008-10: Scientific Investigations Report 2013-5052*.

Yorozuya A., Kanno Y., Kazuhiko F., et al. (2010) Bed-load discharge measurement by ADCP in actual rivers. In: *River Flow 2010*, 2010, pp. 1687–1692. Available at: http://vzb.baw.de/e-medien/river-flow-2010/PDF/C5/C5_04.pdf.

Yorozuya A., Motonaga Y. and Iwami Y. (2014) Need to Know how to Conduct ADCP Measurement in Rivers outside of Japan and Preliminary Results. *New phase of river discharge observation* 4: 48–56.

Yorozuya A., Koseki H., Okada S., et al. (2017) Measurement of effective shear velocity and bedload in an actual river. In: *International Symposium and Exhibition on Hydro-Environment Sensors and Software*, 2017, pp. 66–73.

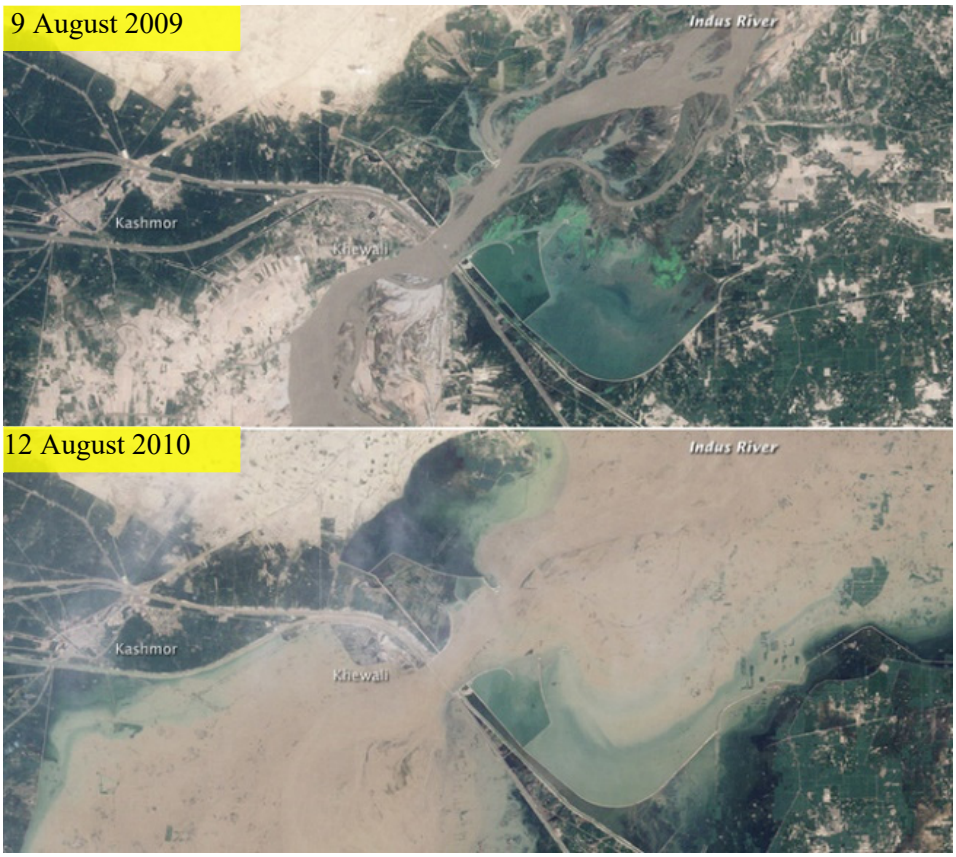

Figure 1.1 Satellite images of Guddu Barrage taken during normal flows (above) and during flood (below). Image Source Landsat-5 NASA.

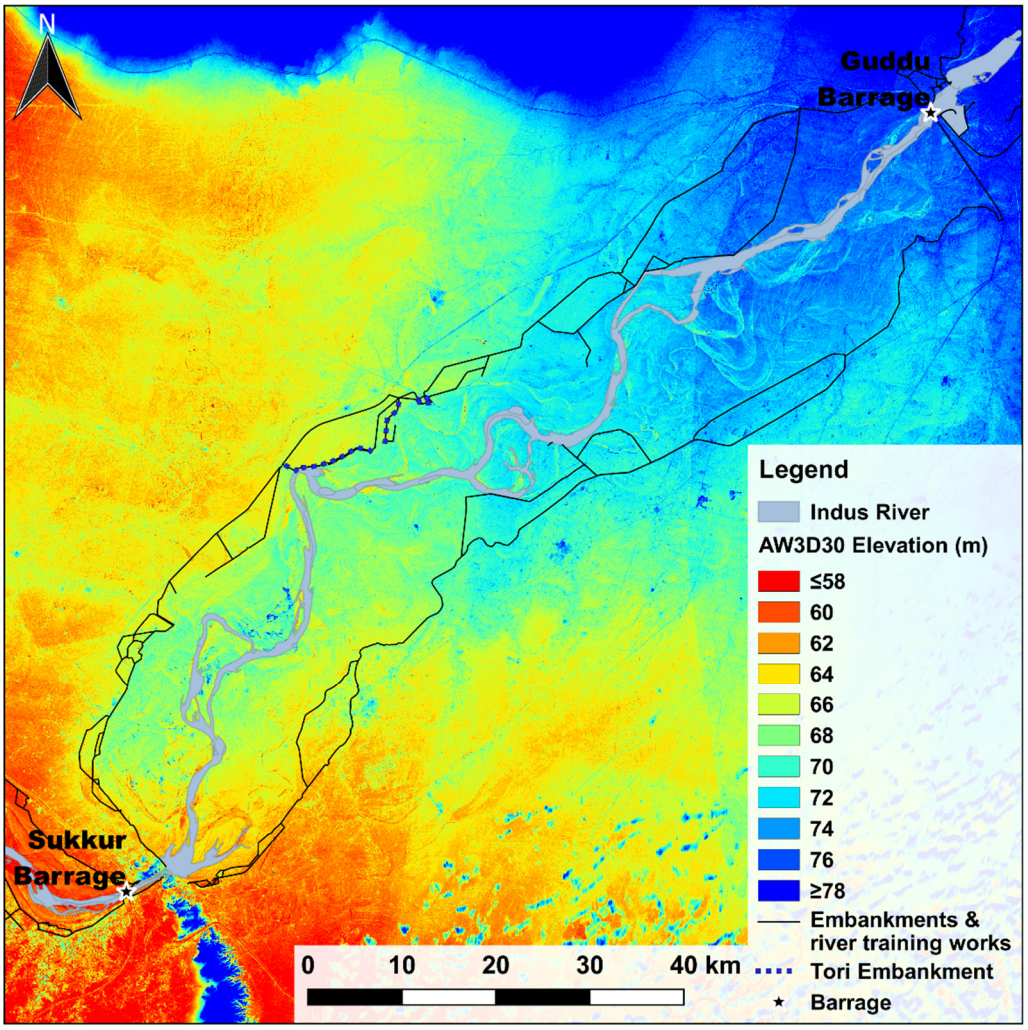

Figure 1.2 Digital Elevation Model (AW3D30, JAXA), showing elevations between Guddu and Sukkur Barrages. Embankments and river training works are also shown.

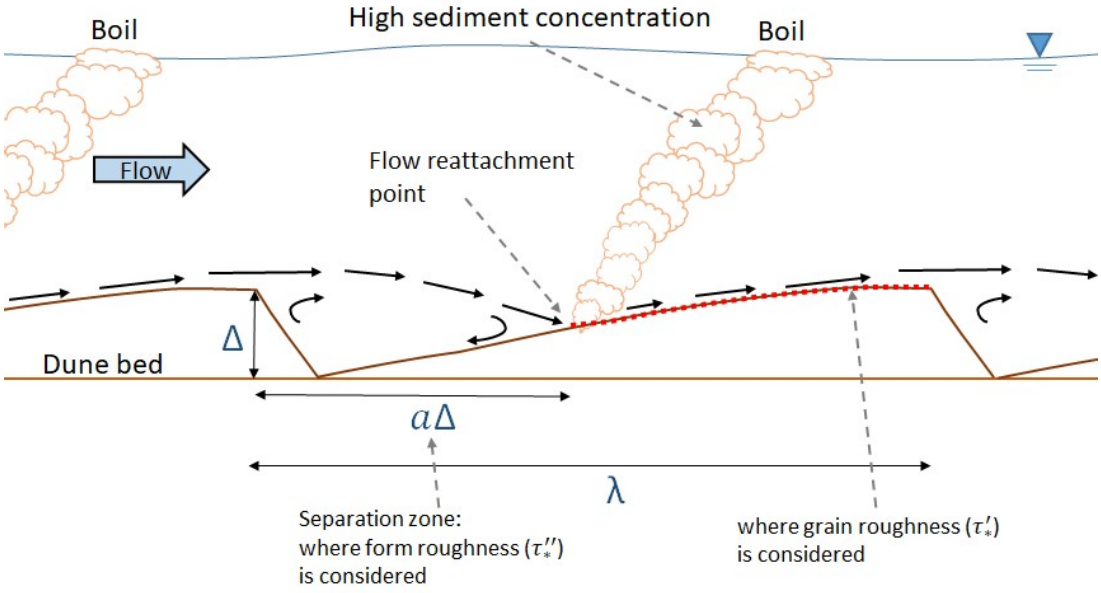

Figure 2.1 Schematic diagram showing 'boil of first kind' forming over a dune bed.

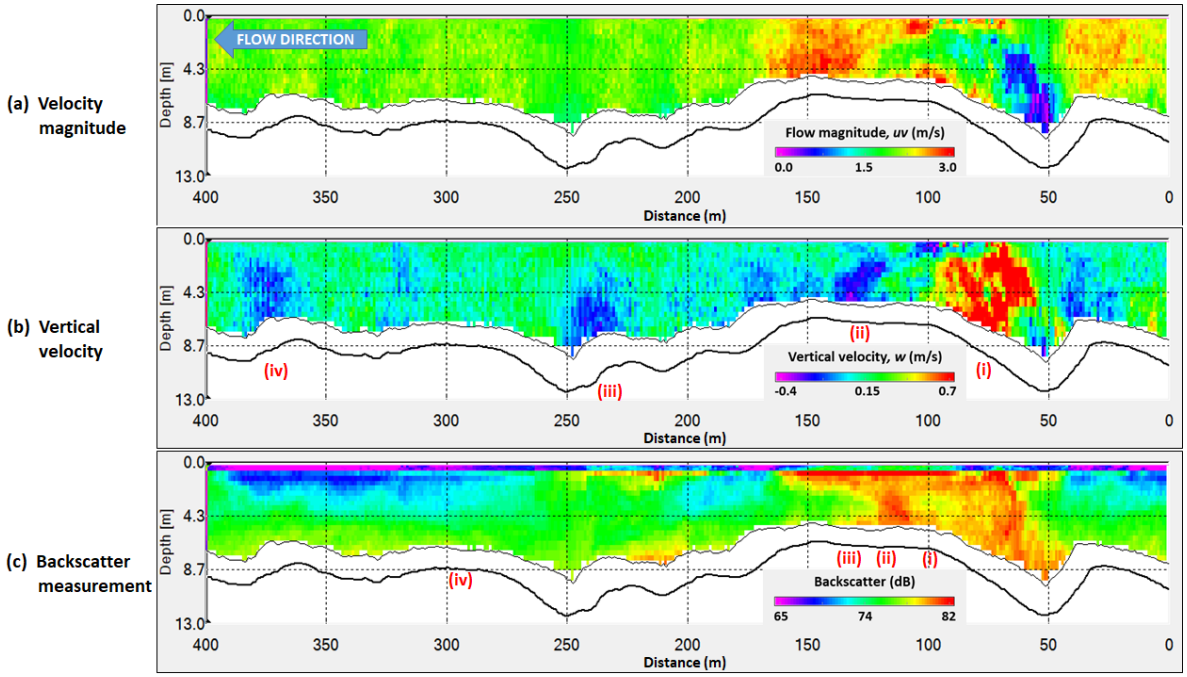

Figure 2.2 Velocity magnitude in the horizontal plane *uv* (m/s), Vertical velocity, *w* (m/s), and Backscatter (dB) measurements by the ADCP during boil observation Gul et al. 2018.

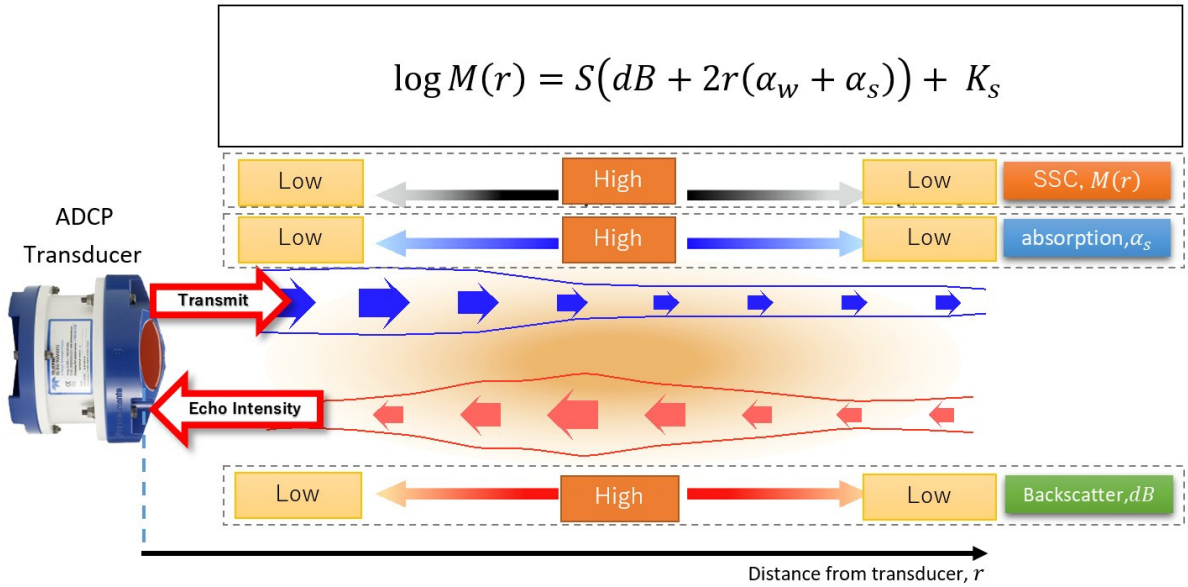

Figure 3.1 Schematic diagram illustrating how suspended sediment can be calculated using the ADCP backscatter, using method proposed by Kitsuda et al. (2006)

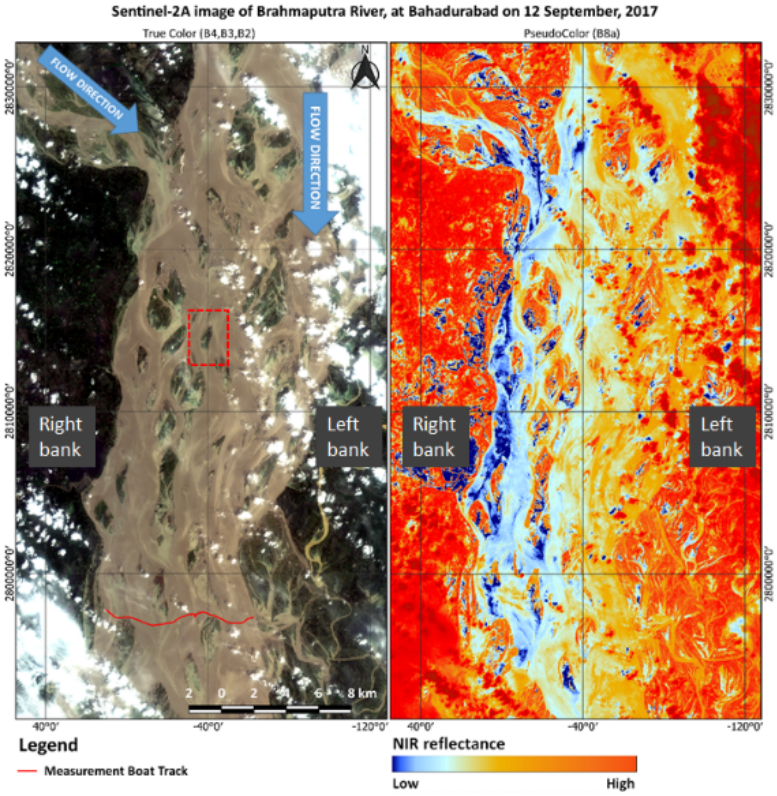

Figure 3.2 Sentinel-2 image acquired on 12 September, 2017 over Brahmaputra River near Bahadurabad shows: RGB True color (Left), NIR reflectance shown in pseudo color (Right)

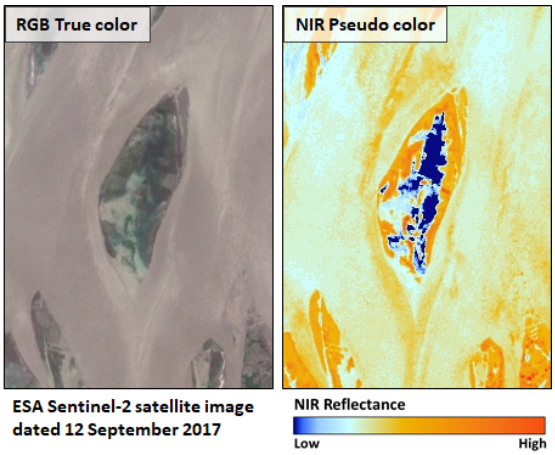

Figure 3.3 NIR reflectance in pseudo color (right) from Sentinel-2 shows turbidity distribution in flow around a sandbar. Flow direction is from top to bottom.

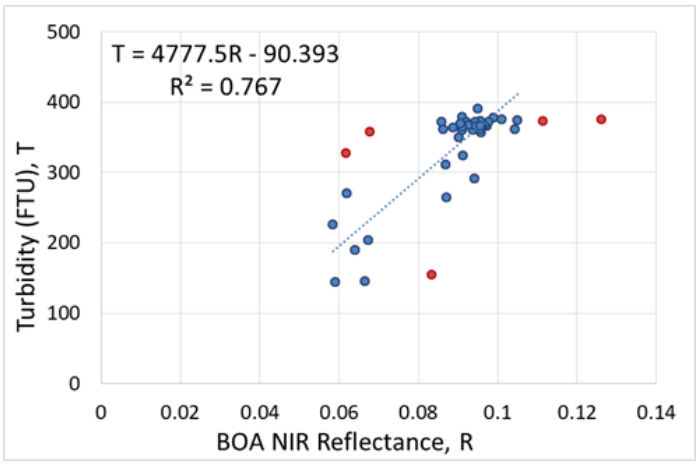

Figure 3.4 The relation between observed Turbidity (FTU) and BOA NIR Reflectance.

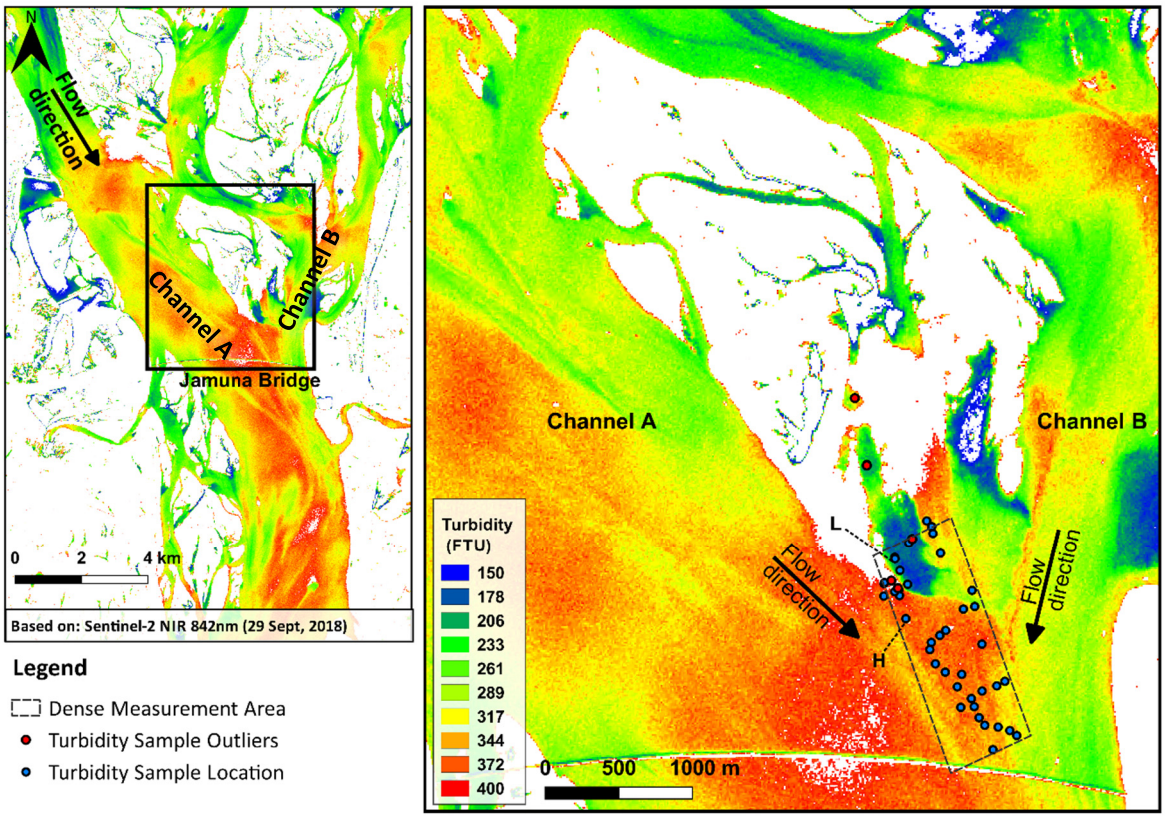

Figure 3.5 Turbidity NIR shown in pseudo color, location of turbidity meter samples shown in Figure 3.4, and the dense measurement area is also highlighted.

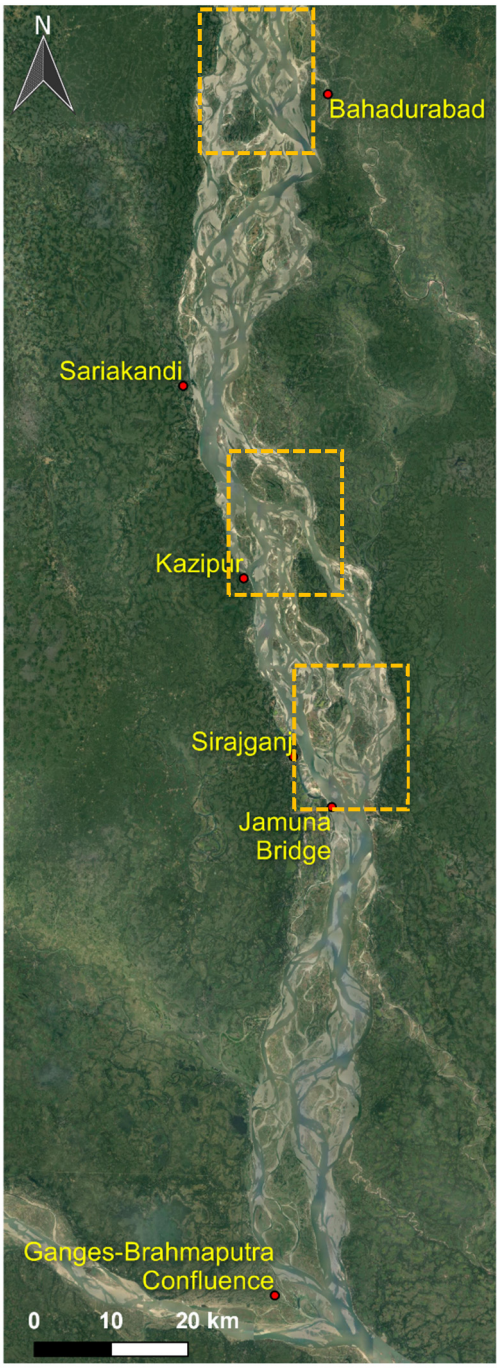

Figure 4.1 Map of Brahmaputra river in Bangladesh, from Bahadurabad to the Ganges –Brahmaputra confluence. Measurements in different flow areas are carried out in three sections of the river, adjacent to Bahadurabad, Kazipur, and Sirajganj, as highlighted.

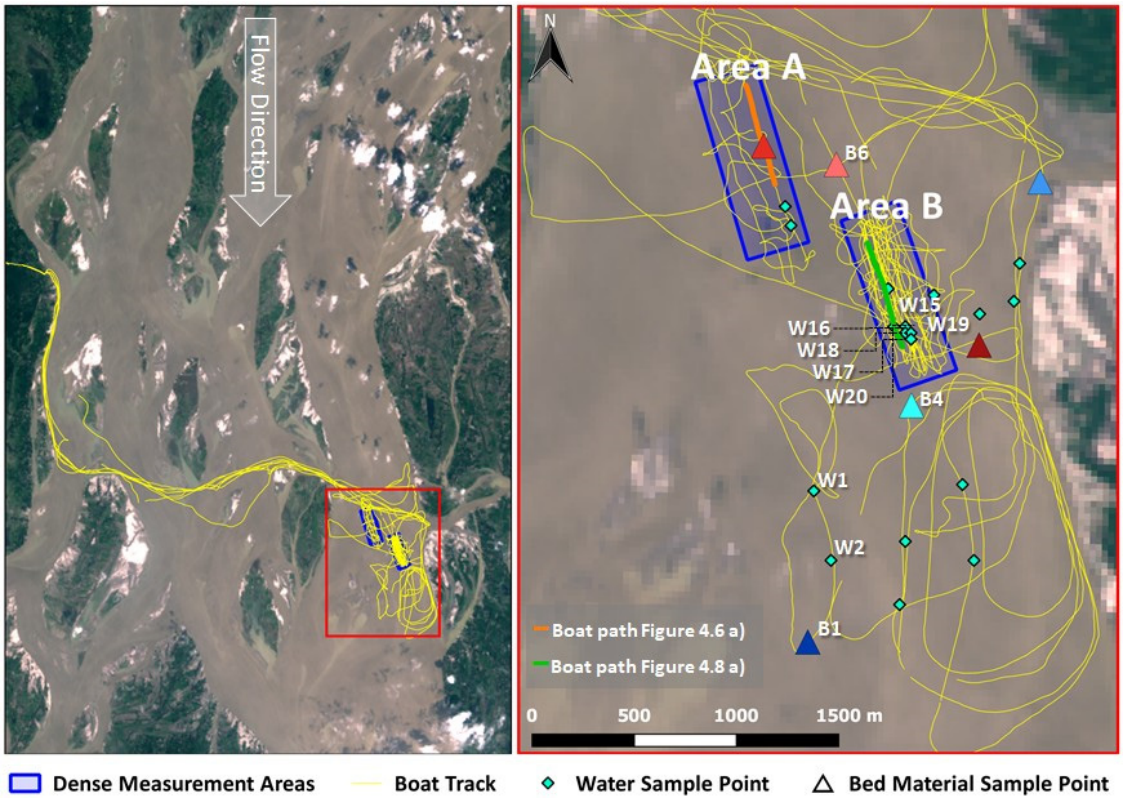

Figure 4.2 Map showing bed material and water sampling points, dense measurement in flow areas with flat bed (area A) & sand-wave (area B) are also highlighted along with Boat path of Figure 4.6 and Figure 4.8

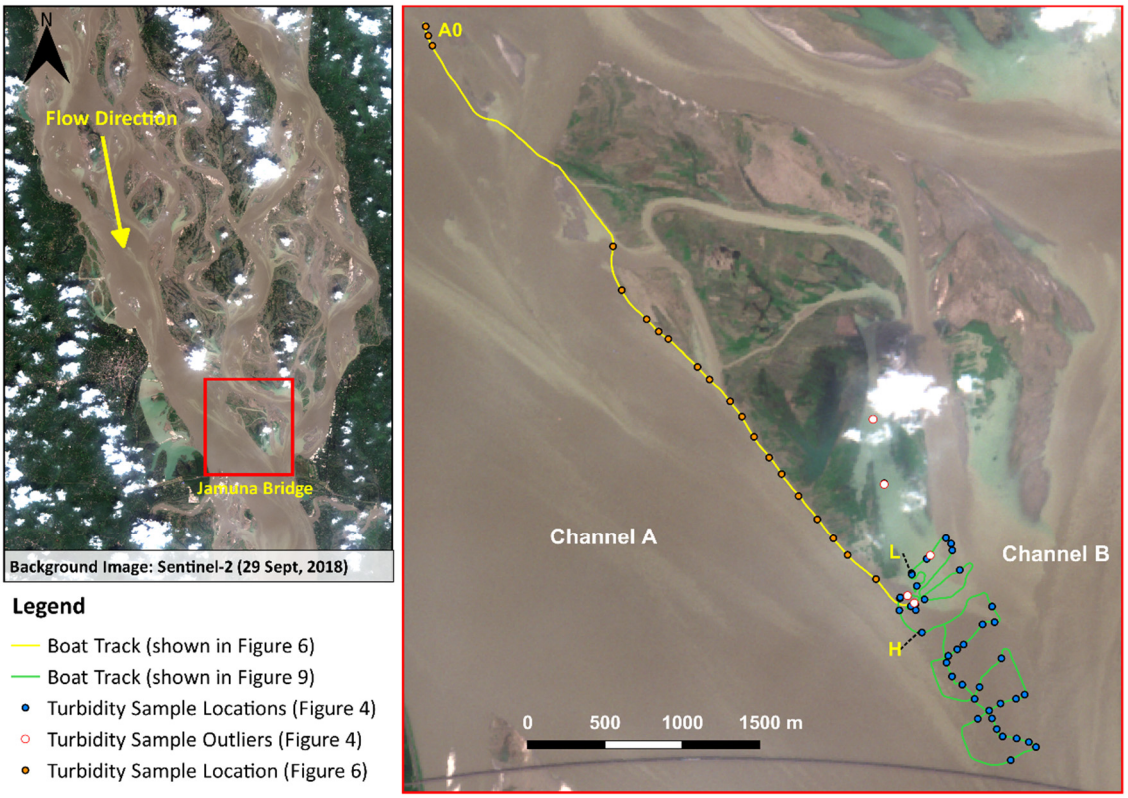

Figure 4.3 Map showing Brahmaputra River, near the Sirajganj and Jamuna Bridge, measurement along the bank and the tail of the sandbar between Channel A and Channel B is shown.

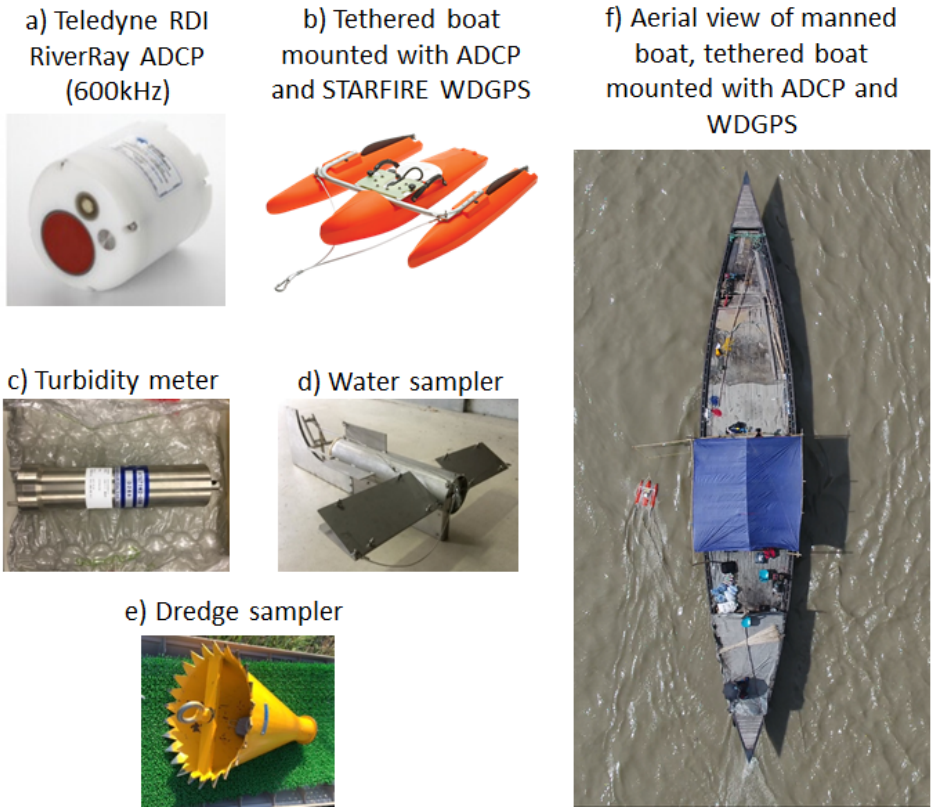

Figure 4.4 Equipment and instruments used to conduct field measurements

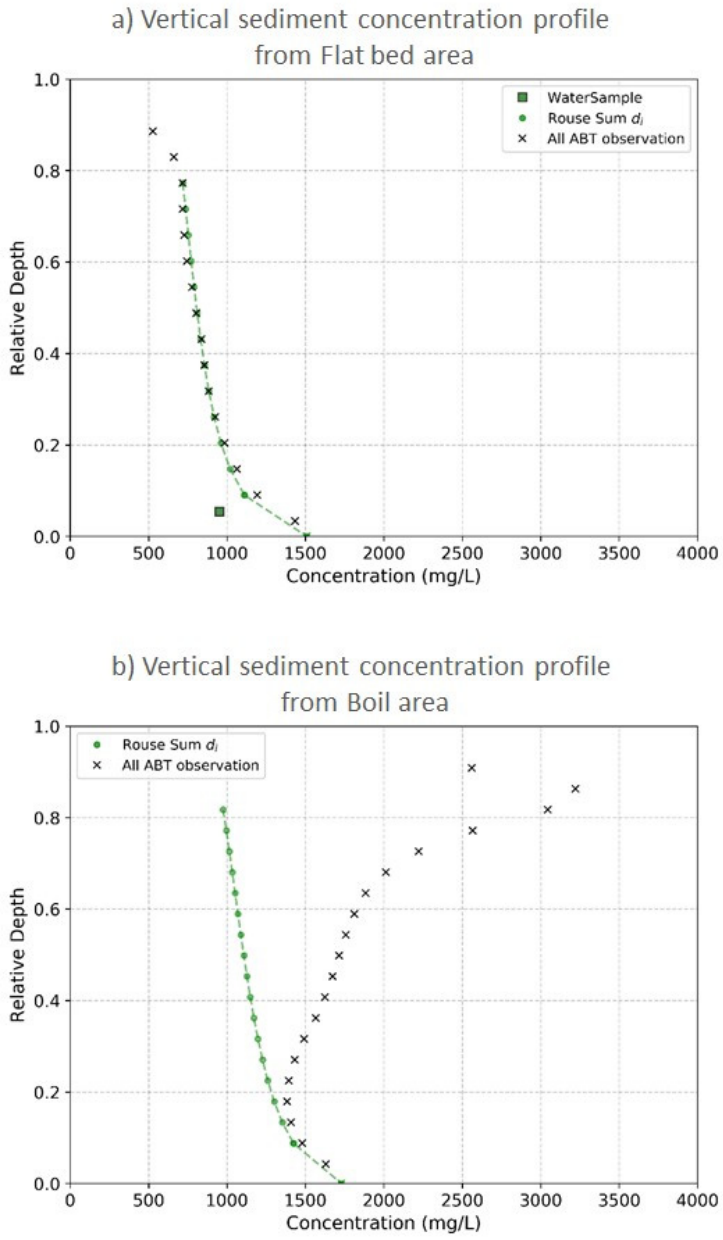

Figure 4.5 Examples of vertical distribution of sediment observed in two different flow areas a) in flat bed area, b) in an area where boil is observed. Concentration profile modelled using equation 2.9 is shown in green.

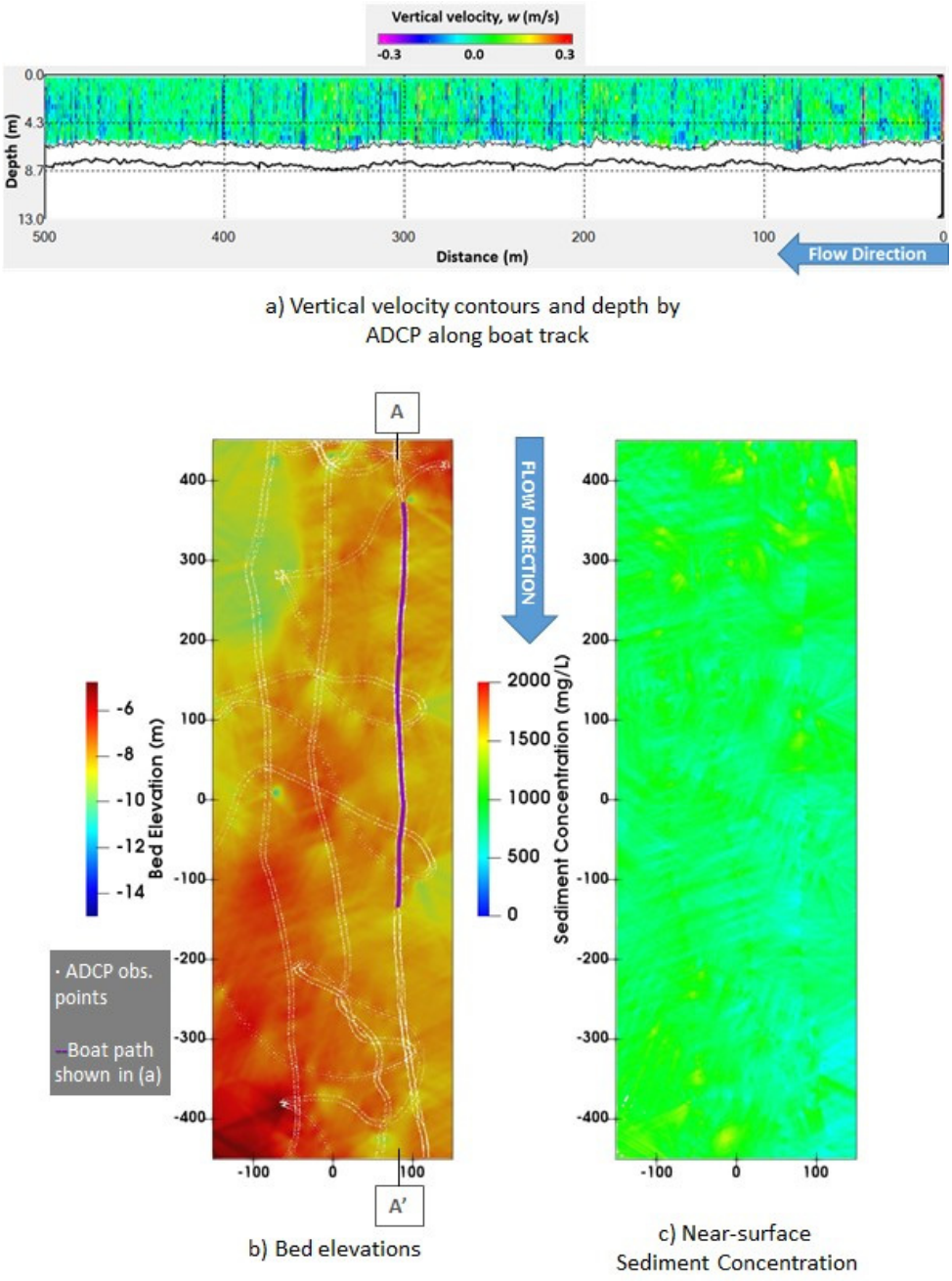

Figure 4.6 Flow area in Bahadurabad where flat-bed conditions are observed a) ADCP transect along the direction of flow showing vertical velocity contours and channel depth, b) Plan view of Bed elevation c) Near surface sediment concentrations using ABT

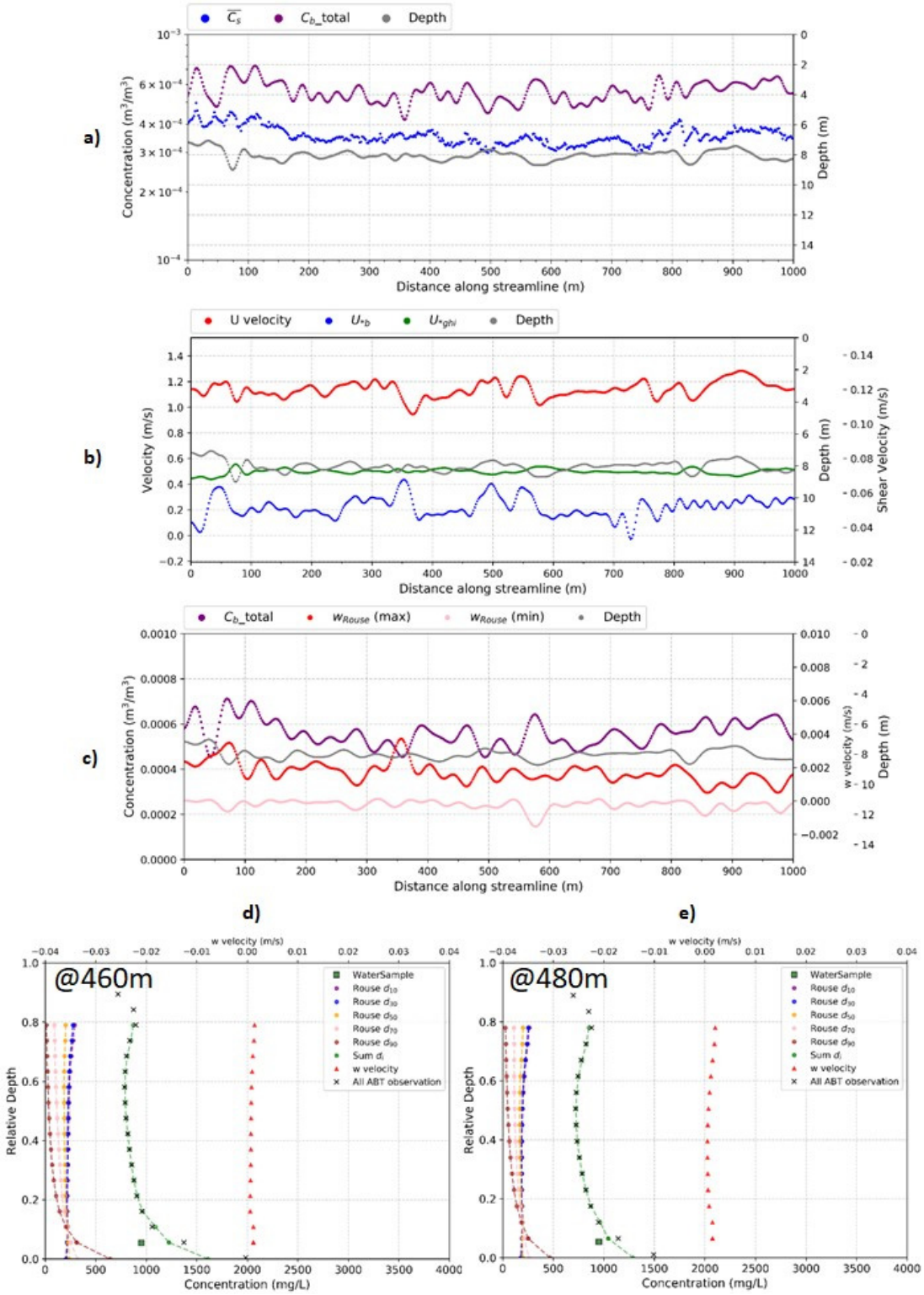

Figure 4.7 Longitudinal profile from A-A', as shown in Figure 4.6

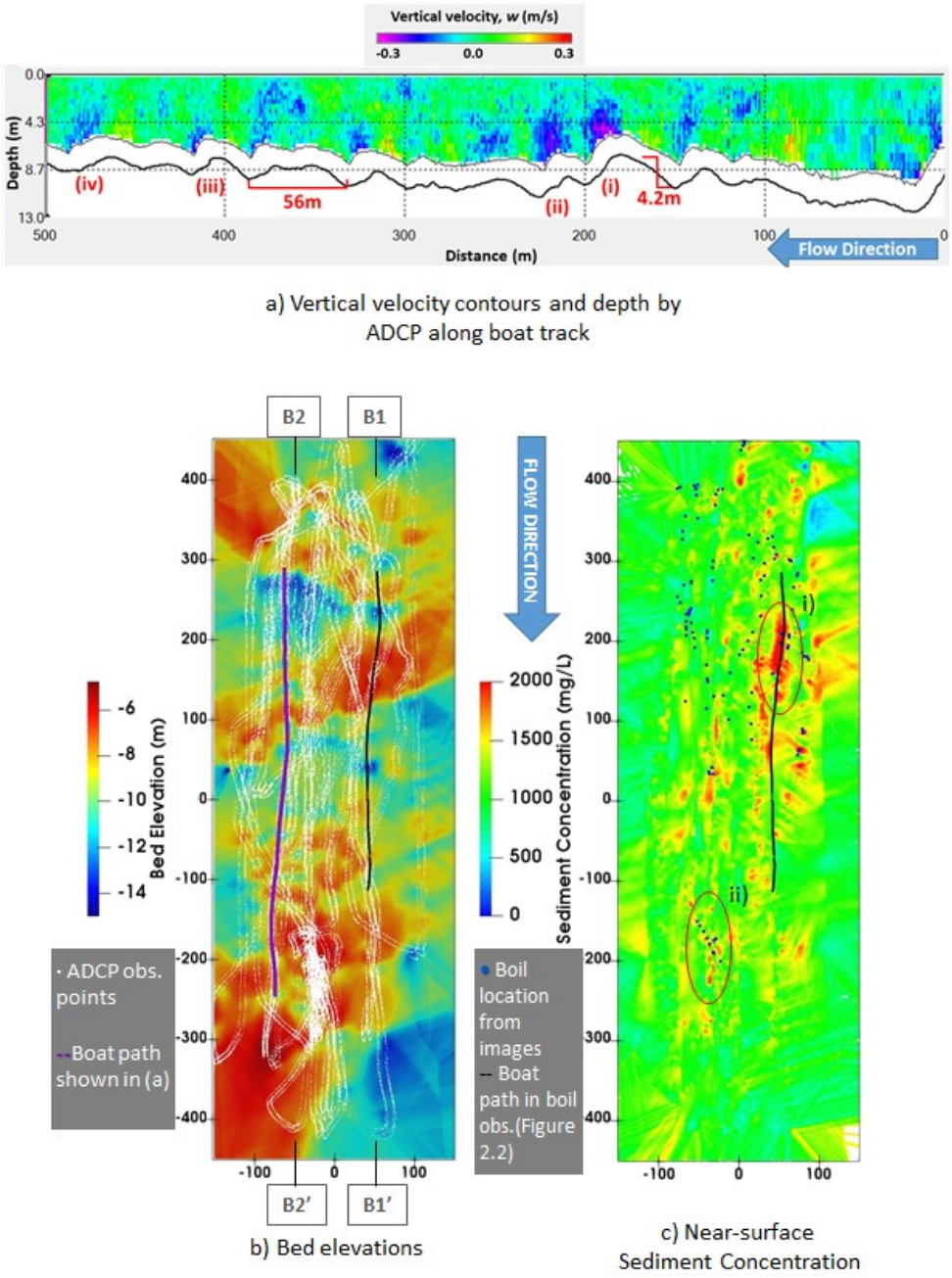

Figure 4.8 Flow area in Bahadurabad where sand-wave bedform is observed a) ADCP transect along the direction of flow showing vertical velocity contours and channel depth, b) Plan view of Bed elevation c) Near surface sediment concentrations using ABT

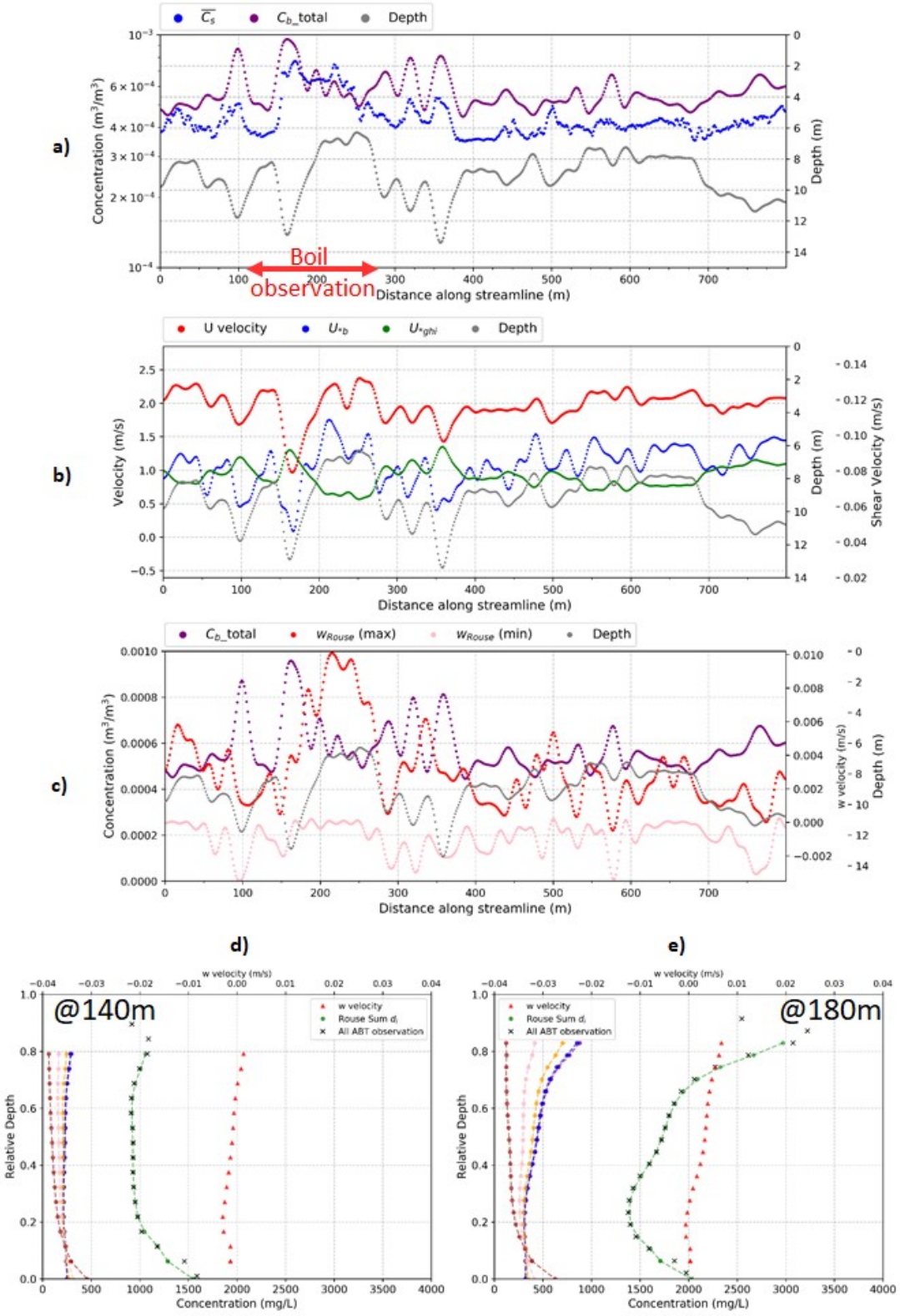

Figure 4.9 Longitudinal profile from B1-B1', as shown in Figure 4.8

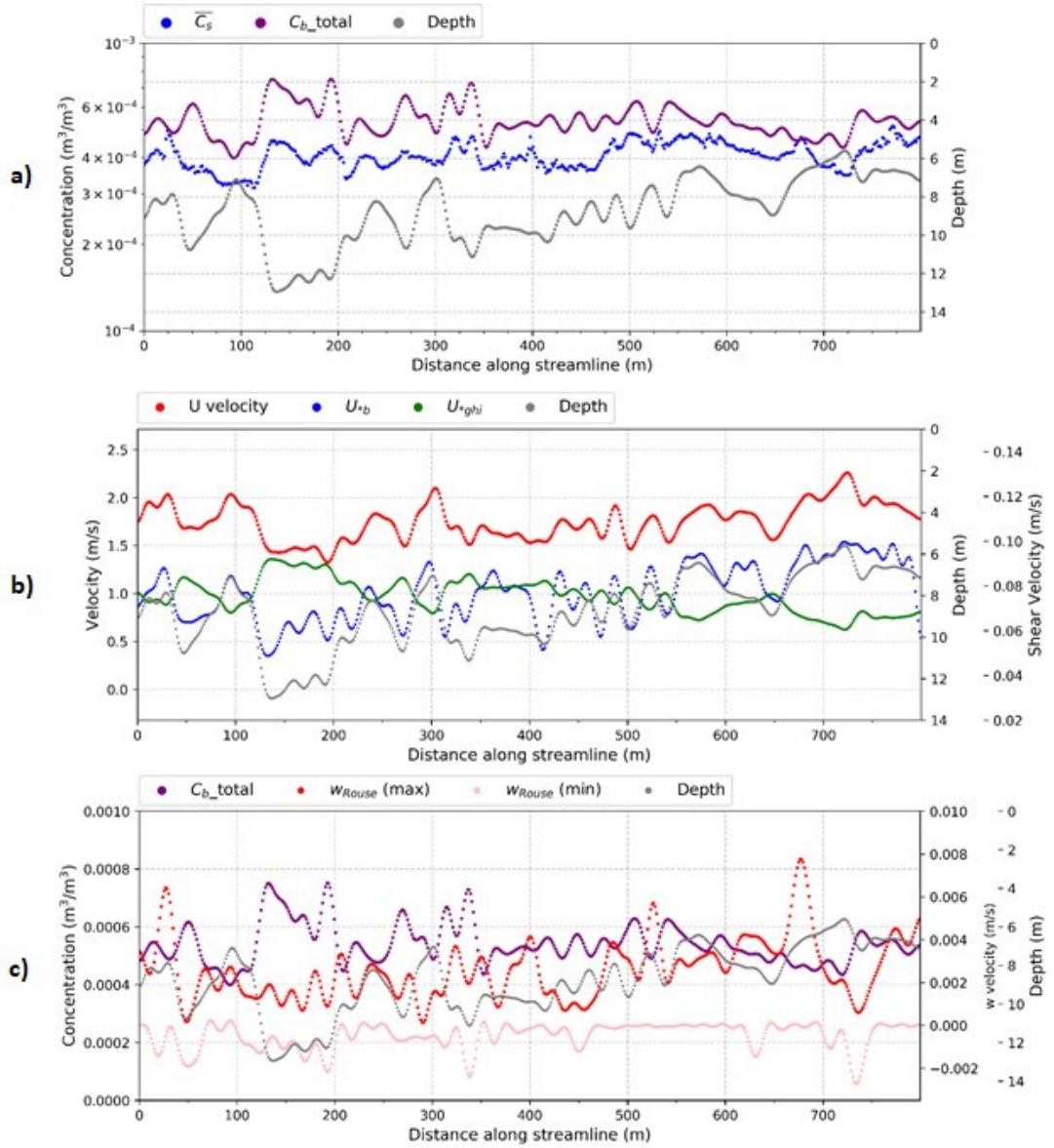

Figure 4.10 Longitudinal profile from B2-B2', as shown in Figure 4.8

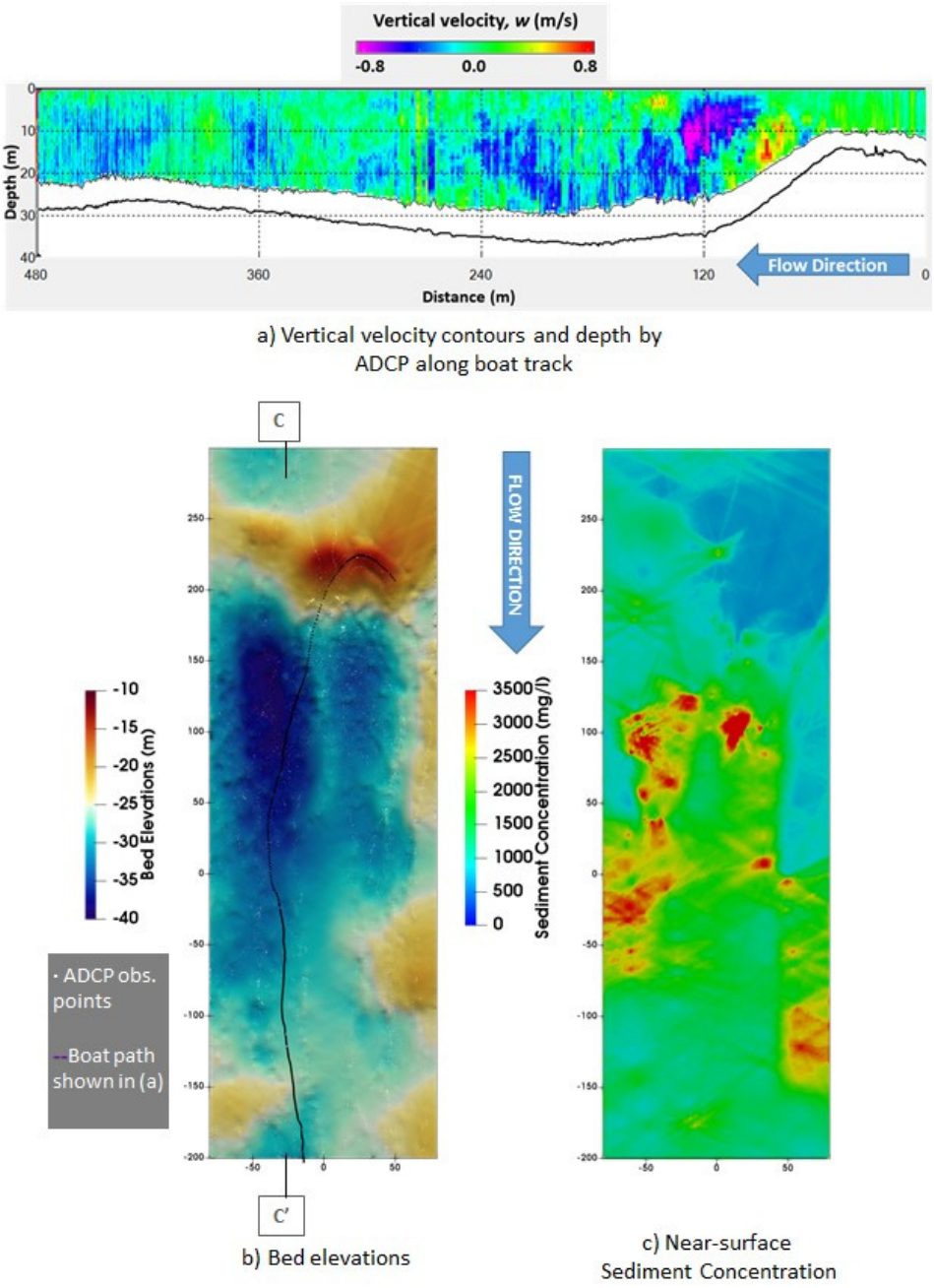

Figure 4.11 Flow area in Kazipur where large scale boil is observed a) ADCP transect along the direction of flow showing vertical velocity contours and channel depth, b) Plan view of Bed elevation c) Near surface sediment concentrations using ABT

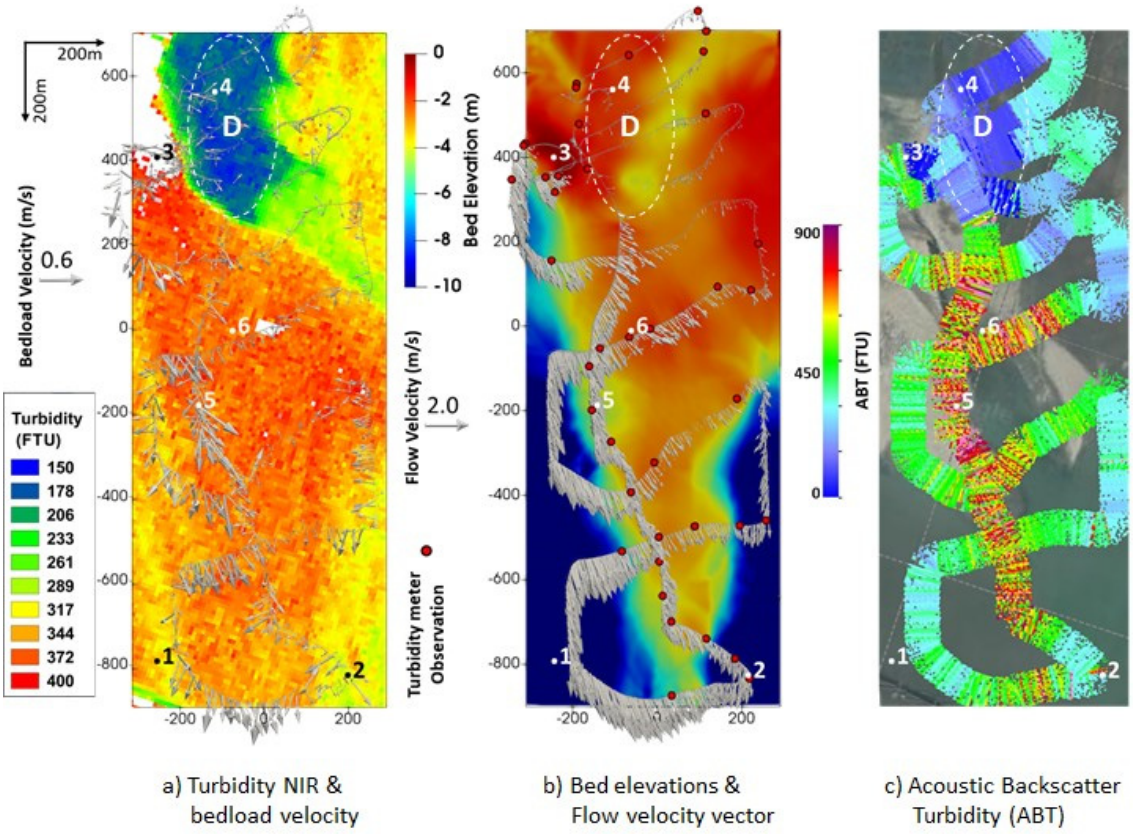

Figure 4.12 a) Turbidity-NIR and bedload velocity, b) Bed elevations and Flow velocity vector, and c) Acoustic Backscatter Turbidity in the dense measurement area immediately downstream of sandbar

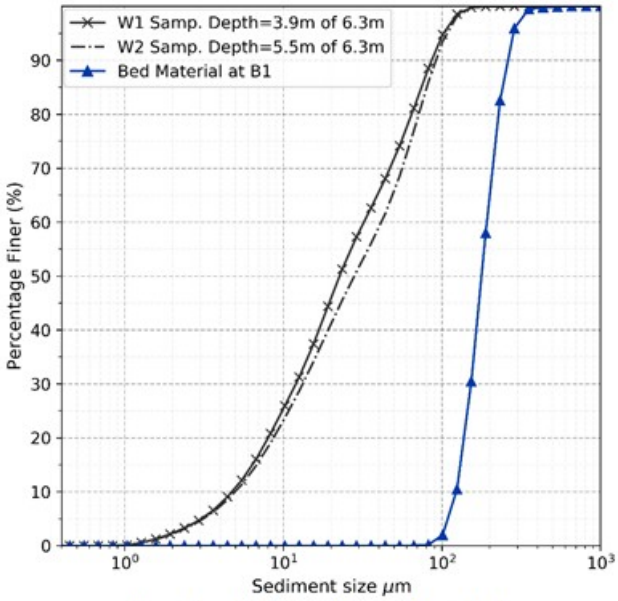

a) Samples from flow without boil

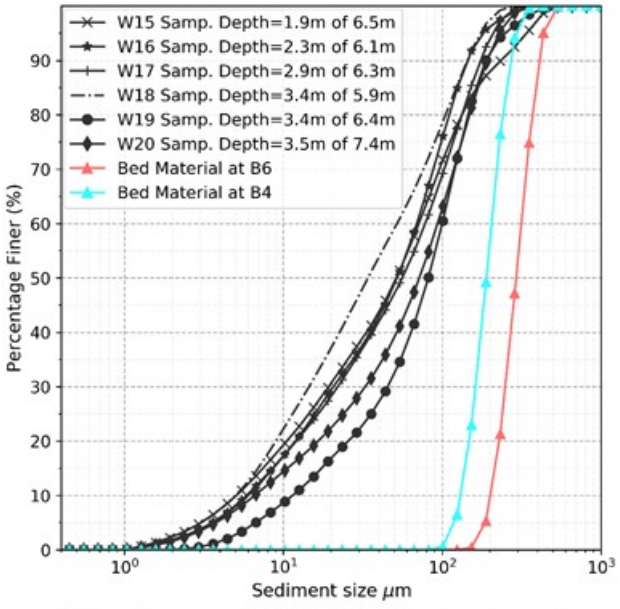

b) Samples from flow area where boil is observed

Figure 4.13 Sediment size distributions from sampling locations shown in Figure 4.2

Water samples *a*m of *b*m denotes sample at depth *a*m where water depth was *b*m.

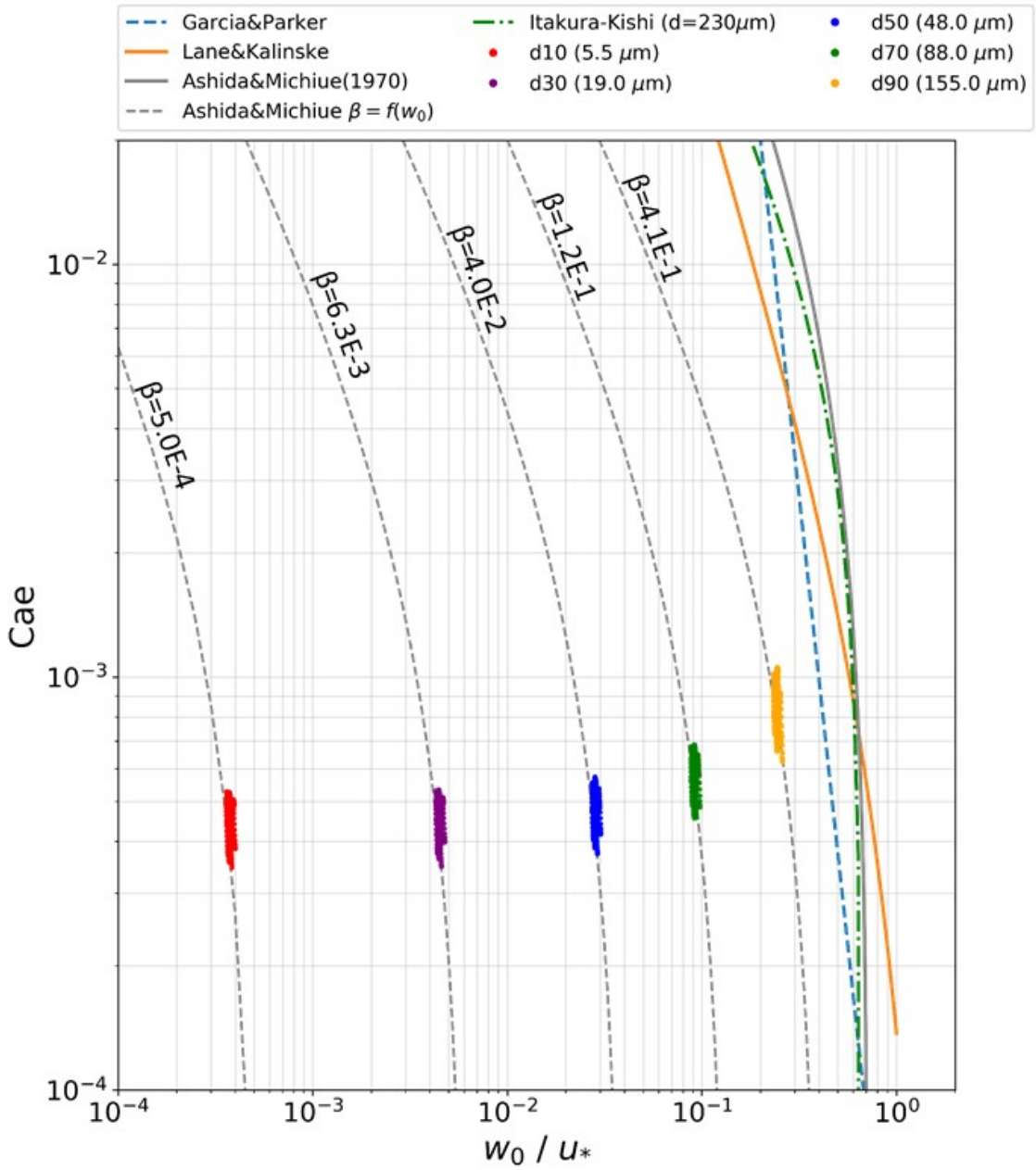

Figure 4.14 The results of C_{ae} - w_0/u_{*b} from Bahadurabad where flat-bed conditions are observed.

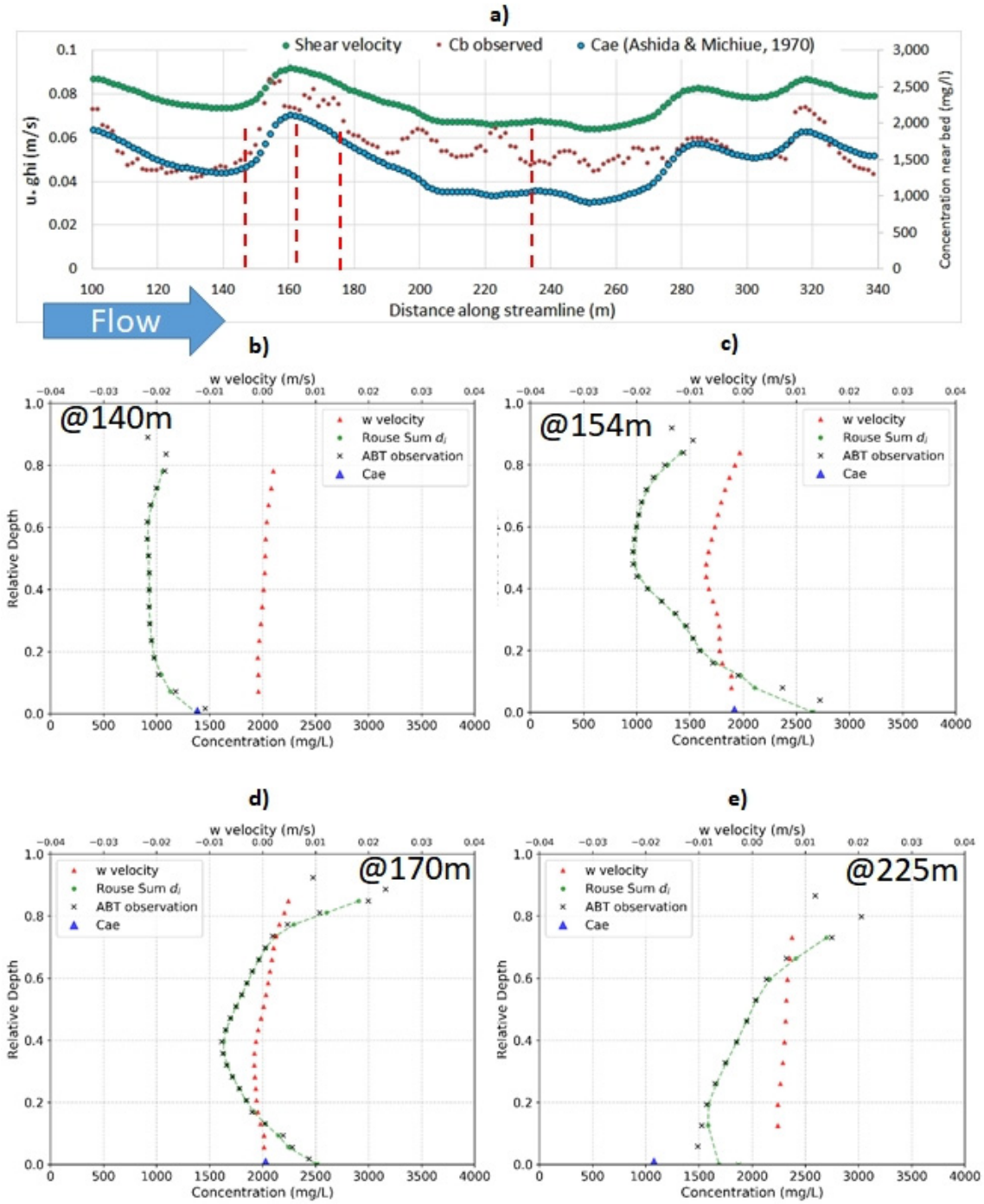

Figure 4.15 100m to 340m distance along streamline B1-B1' where boil is observed, showing depth, shear velocity, depth averaged sediment concentrations and concentration near the bed. Selected vertical sediment concentration profiles along the streampass are also shown.

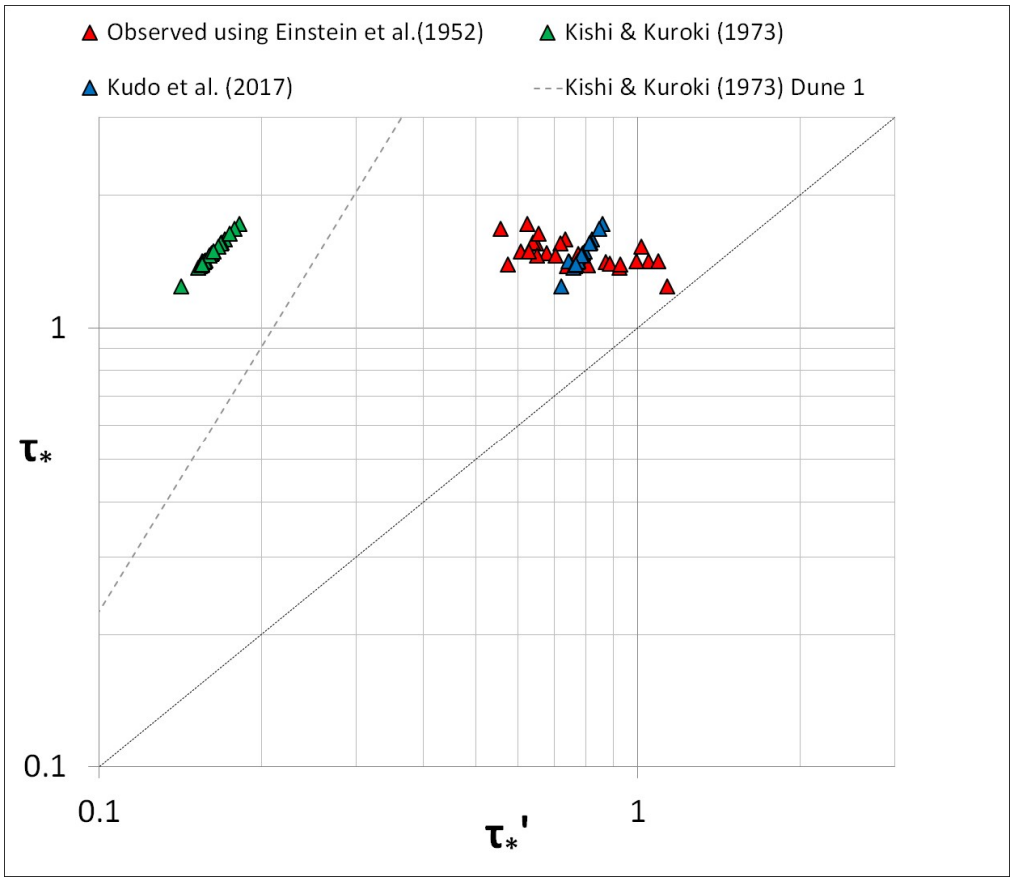

Figure 4.16 The relationship between τ_* and τ_*' where τ_*' is calculated using three methods, 1) observed results based on Einstein and Barbarossa (1952), 2) Kishi & Kuroki (1973), and 3) using Kudo et al. (2017) .

$$\frac{\partial \overline{c_s} \overline{u} h}{\partial x} = \frac{\partial}{\partial x}\left(h\varepsilon_x \frac{\partial \overline{c_s}}{\partial x}\right) + E_s - D_s$$

where boil occurs:

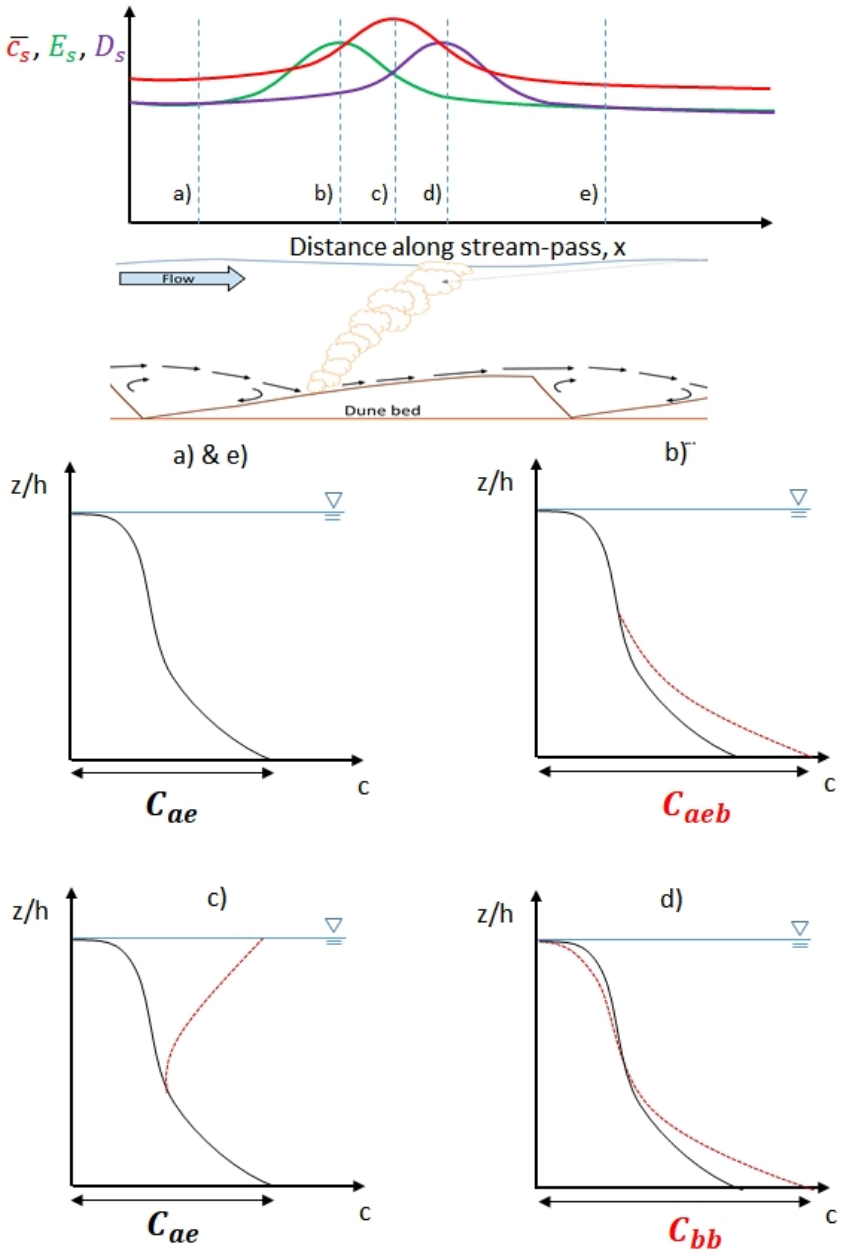

Figure 5.1 Conceptual model of mass conservation of suspended sediment shown in 1-D, in an area where boil exists. Vertical concentration profiles at various sections are highlighted.

$$f(w_p) = \frac{1}{\sqrt{2\pi}\sigma_p} exp\left\{-\frac{1}{2}\left(\frac{w_p}{\sigma_p}\right)^2\right\}$$

Probability of entrainment:

$$G(\xi_0) = \frac{1}{\sqrt{2\pi}}\int_{\xi_0}^{\infty} exp\left\{-\frac{1}{2}(\xi)^2\right\} d\xi$$

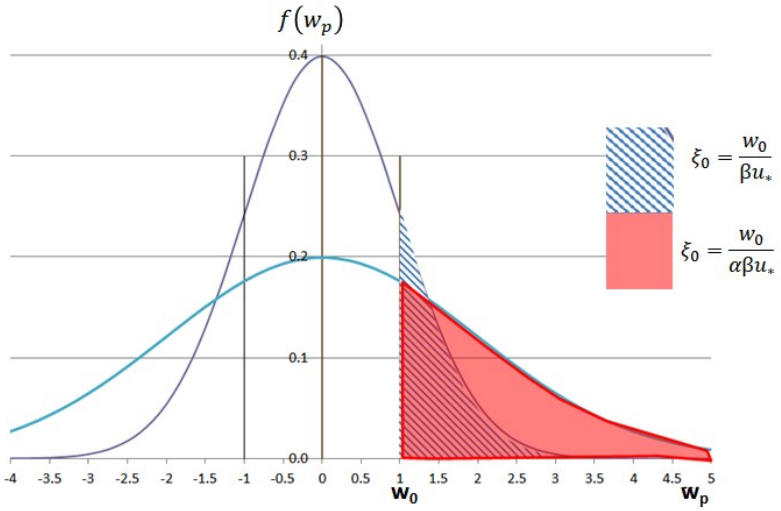

Figure 5.2 Standard normal distribution highlighting probability of entrainment, without boil, and with boil (assuming α=2)

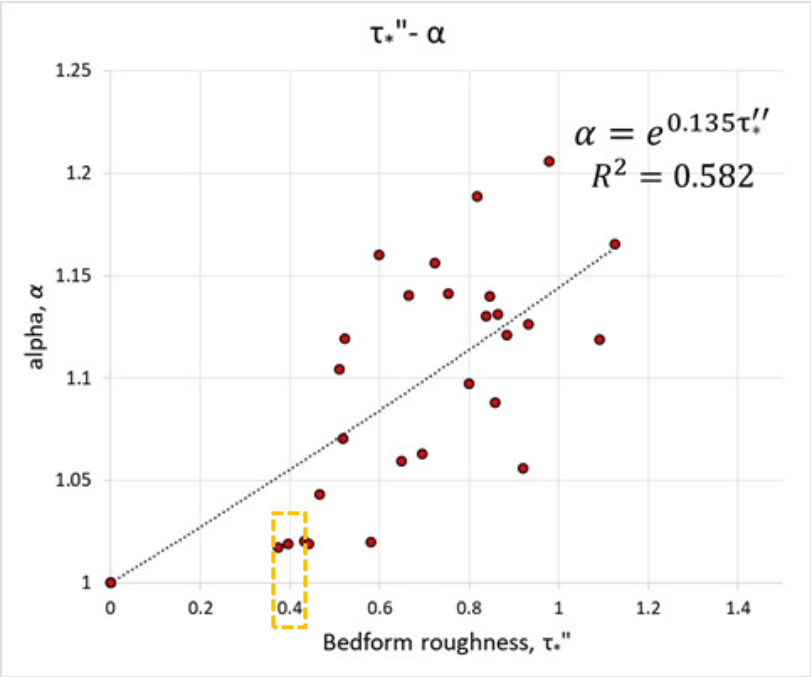

Figure 5.3 Relation between the bedform roughness (τ_*'') and the α based on observations in flow with flatbed conditions, and in flow with bedform and boil

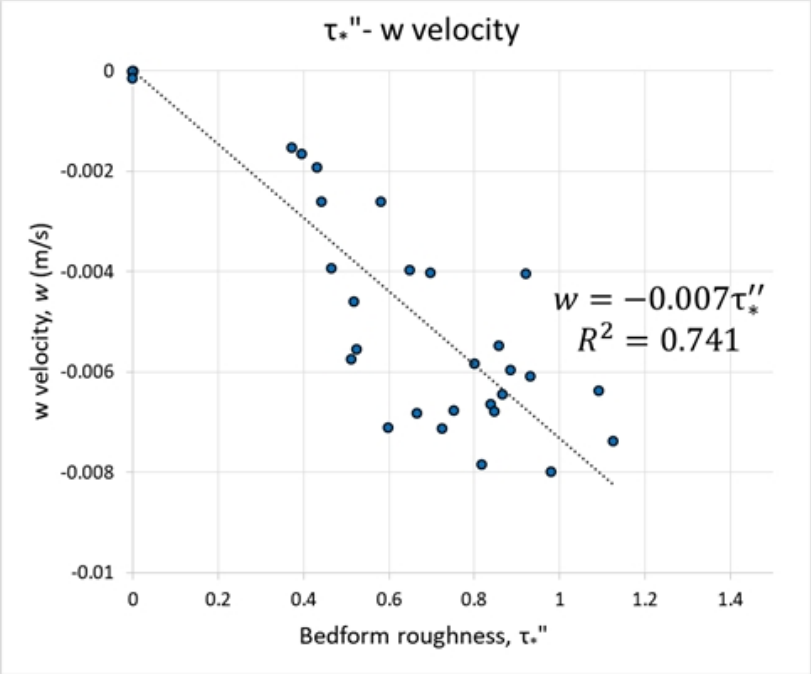

Figure 5.4 Relation between the bedform roughness (τ_*'') and the w velocity based on observations in flow with bedform and boil, and in flow with flatbed conditions.

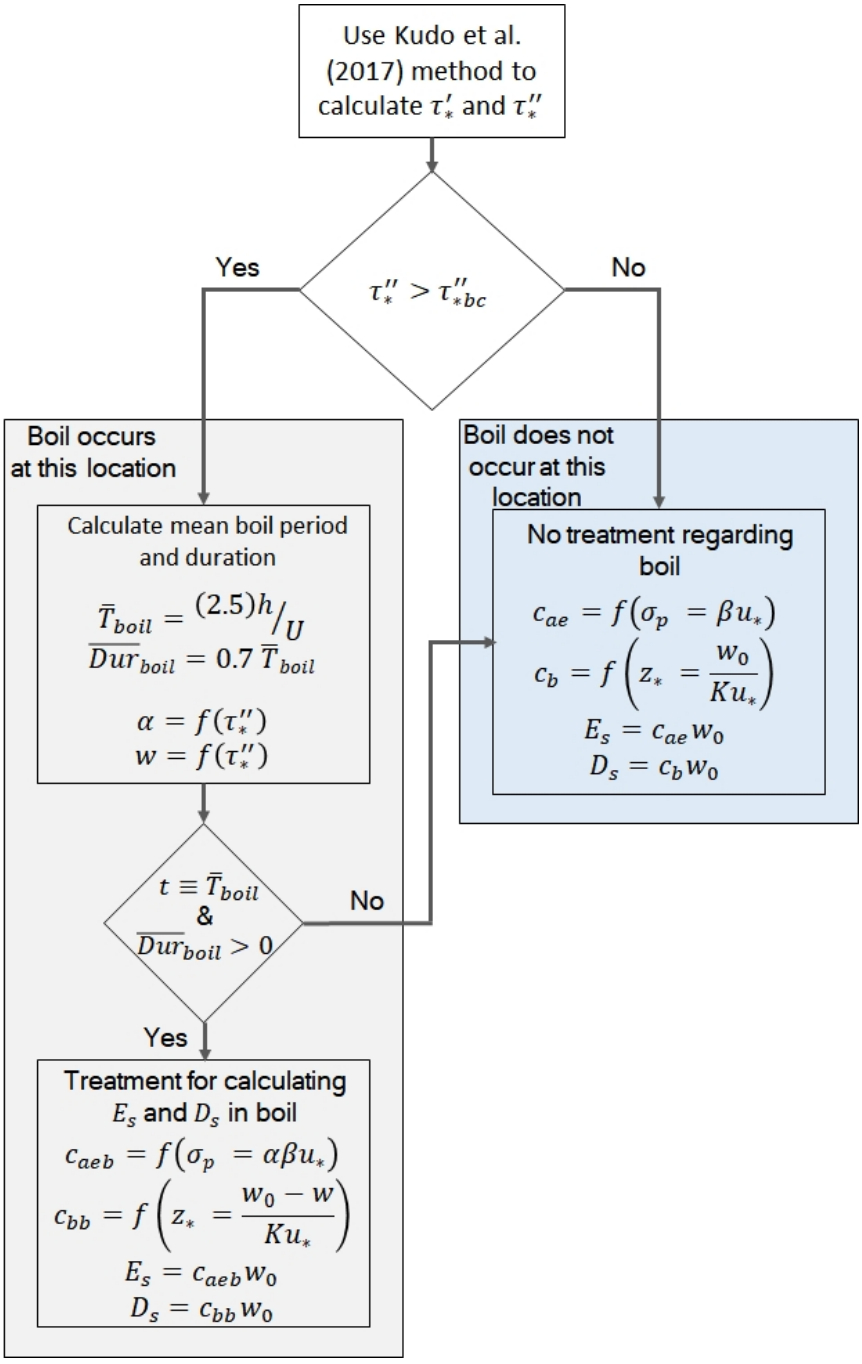

Figure 5.5 Flow chart showing how the modified governing equations to model boil may be used inside the 2-D numerical model

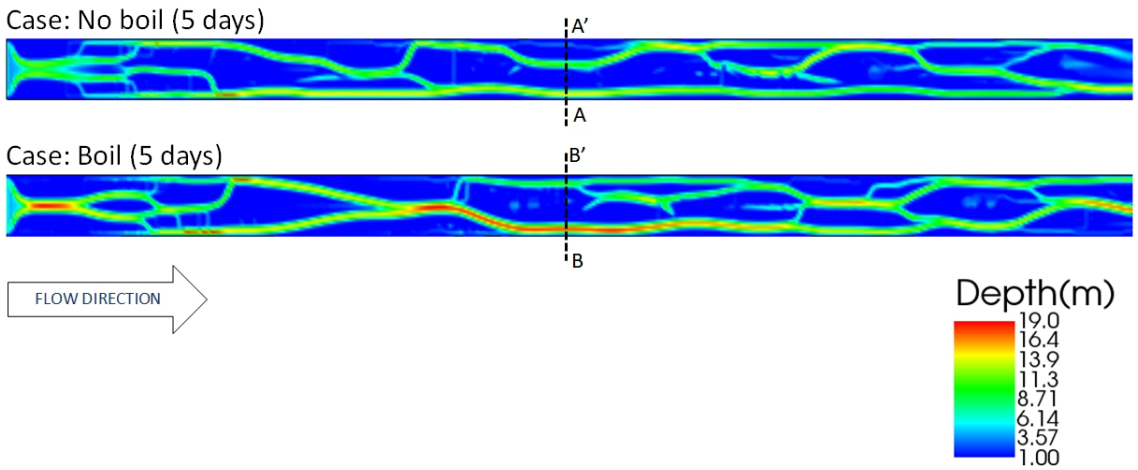

Figure 5.6 Channel depth after 5 days of computation in case without boil treatment (above) and the case where boil treatment is employed (below).

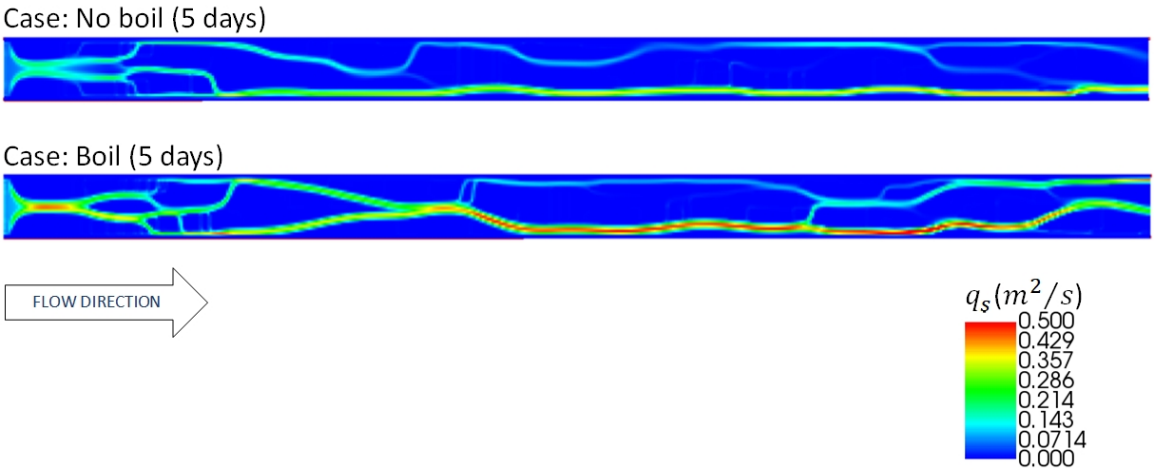

Figure 5.7 Unit suspended sediment discharge, q_s (m^2/s), after 5 days of computation in case without boil treatment (above) and the case where boil treatment is employed (below).

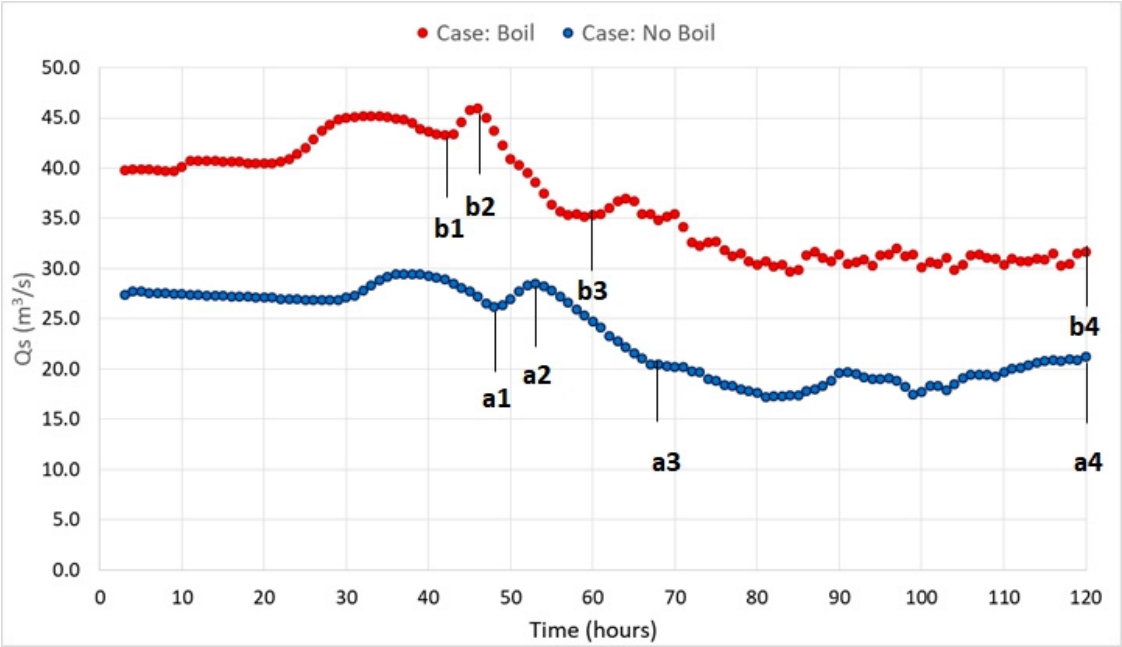

Figure 5.8 Suspended sediment discharge $Q_s(m^3/s)$, with respect to time (hours), shown for the cross sections highlighted A-A' and B-B' in the Figure 5.6, for case with no boil and case with boil respectively.

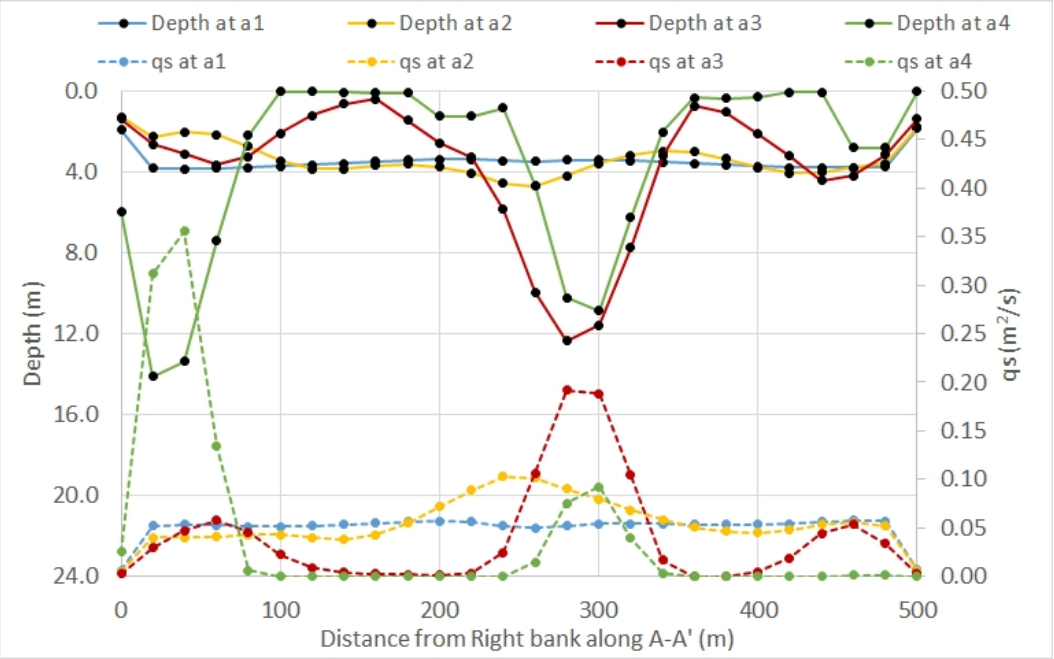

Figure 5.9 Unit suspended sediment discharge $q_s(m^2/s)$ and depth(m), with respect to time (hours), shown for the cross sections highlighted A-A' in the Figure 5.6

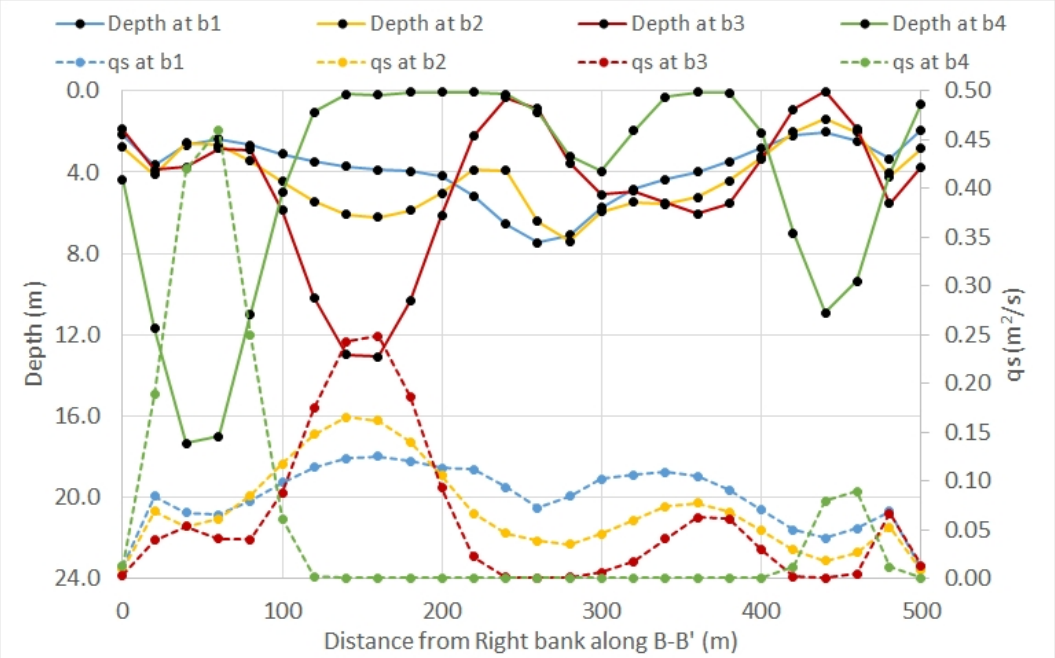

Figure 5.10 Unit suspended sediment discharge $q_s(m^2/s)$ and depth (m), with respect to time (hours), shown for the cross sections highlighted B-B' in the Figure 5.6

Table 5.1 Proposed treatment for erosion and deposition terms in different regions of a bedform, considering the occurrence of boil

Region	**Timing of boil**	**Erosion term**	**Deposition term**	**Percentage Area (%)**
R1	Yes	0	$c_b . w_0$	20
	No			
R2	Yes	$\boldsymbol{c_{aeb} . w_0}$	$c_b . w_0$	15
	No	$c_{ae} . w_0$		
R3	Yes	$c_{ae} . w_0$	$c_b . w_0$	39
	No			
R4	Yes	$c_{ae} . w_0$	$\boldsymbol{c_{bb} . w_0}$	26
	No		$c_b . w_0$	

Table 6.1 Initial condition requirements for 2-D numerical modeling of channel changes in large rivers.

Requirement	**Recommended frequency of measurement**	**Source of measurement**	**Constraints and considerations**
Initial Channel topography	Once per year / after major flood event	High accuracy satellite or aerial DTM	Higher cost for increasing levels of spatial resolution and accuracy.
		Freely available satellite-based DTM	Quality of free DTM may need GCPs or other methods to improve accuracy.
Bed sediment sampling	Once per year / after major flood event	Shovel / scoop	Easy to obtain during field measurements
		Dredge / bed material sampler	Difficult to obtain where flow depth is very large (>30m)
Initial Channel bathymetry	Once per year / after major flood event / more frequent observation near critical infrastructure	ADCP	Simultaneous observation of flow, bathymetry and sediment discharge is an advantage
		Multi-beam sonar	Higher accuracy, high cost, requires specialized human resource

Table 6.2 Boundary condition and validation requirements for 2-D numerical modeling of channel changes in large rivers.

Requirement	**Recommended frequency of measurement**	**Source of measurement**	**Constraints and considerations**
Discharge and water-level boundary condition	3 hourly measurement during 'high flows'	Fixed measurement site e.g. at barrage / weir	Need to estimate uncertainty in the rating curve or measurement method
		ADCP	May incur more operational challenges and human resource for continuous (3 hourly) monitoring
Validation of channel changes	1~3 day intervals	Satellite imagery	Provides spatial distribution of channel changes, at various resolutions (10m~250m) at no cost
	After major flood event / more frequent observation near critical infrastructure	ADCP	Can provide bathymetric information, however covering large areas may require time and human resource.
Validation of sediment concentrations	1~3 day intervals	Satellite imagery (NIR)	Spatial distribution of sediment concentrations, at various resolutions (10m~250m) at no cost
	After major flood event / more frequent observation near critical infrastructure	ADCP + water sampling / turbidity meter	Can provide detailed flow, bathymetry, and sediment concentrations, however covering large areas may require time and human resource.